Part 7
Motion and Relaxation

19 Motion

One of the most important and useful features of NMR is its ability to probe molecular motion, over a wide range of time-scales, ranging from picoseconds (10^{-12} s) to tens of seconds, or even longer in favourable cases.

19.1 Motional Processes

Motional processes may be detected by NMR if they change the nuclear spin Hamiltonian. The nature of these motional effects depends on the type of motion and their time-scale.

19.1.1 Molecular vibrations

Molecules are not rigid objects. They are full of internal dynamics. In general, all nuclei oscillate rapidly around their mean positions. Such motions are called *vibrations*, and typically are on the time-scale of picoseconds (10^{-12} s) or shorter. In general, a vibrational motion is slow if there are many atoms involved, and if those atoms are relatively massive.

Light atoms, such as hydrogen, undergo particularly rapid local oscillations, with a relatively large amplitude. These highly local motions are called *librations*. For example, the typical motion of a C−H group may be depicted as follows:

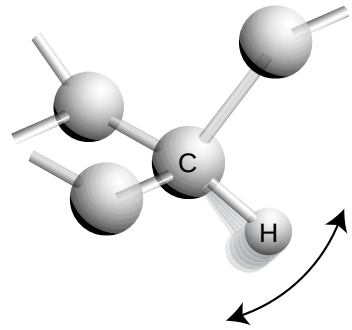

Figure 19.1
Librational motion of a hydrogen atom attached to a heavy atom.

Note that the main direction of the libration is *perpendicular* to the C−H bond direction. Typical libration amplitudes are about $\pm 15^{\circ}$.

Spin Dynamics: Basics of Nuclear Magnetic Resonance, Second Edition Malcolm H. Levitt

19.1.2 Local rotations of molecular groups

Many symmetrical molecular groups rotate rapidly at normal temperatures. For example, methyl groups (CH_3) usually rotate very rapidly around their local threefold axes:

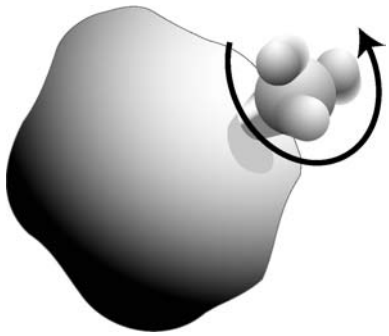

Figure 19.2
Rotational motion of a methyl group.

This motion is typically on the picosecond time-scale at room temperature, but may be as slow as microseconds or milliseconds if the motion is *hindered*, i.e. if the methyl group butts up against something else in the molecule, preventing it from turning around freely.

NH_3^+ groups in proteins and amino acids usually undergo a similar rotational motion about the local threefold axis.

19.1.3 Molecular flexibility

Large molecules, like proteins, have a large degree of internal flexibility, which in some cases is indispensible for their function. One of the most powerful features of NMR is its ability to make such flexibility visible. One example is given in Plate 2.

19.1.4 Chemical exchange

If the motional process involves the making and breaking of chemical bonds, then the molecular motion is called *chemical exchange*.

As a simple example of chemical exchange, consider the following internal cyclization reaction:

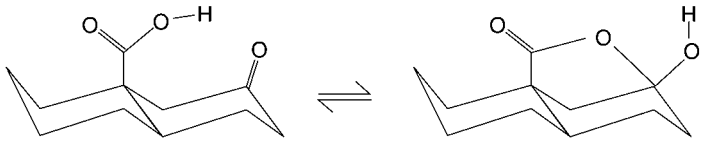

Figure 19.3
A chemical exchange process.

Since the electronic structure is different in the two forms, the chemical shifts and J-couplings change when the exchange process takes place. The formation and breaking of the internal ring, therefore, are detectable by NMR, provided that the process is on an appropriate time-scale.

The term chemical exchange is also used if the conformation of the molecule changes around a relatively rigid entity, such as a double bond or a similar conjugated system. The reaction may even lead to a product that is physically and chemically *identical* to the reactant. An example of this is the slow exchange of the *N*-methyl groups in *N*, *N*′-dimethylformamide:

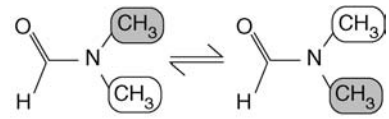

Figure 19.4
N, *N*′-dimethylformamide.

To make the process visible, the above sketch uses grey and white boxes to label the exchanging methyl groups.

Chemical exchange processes occur over a very wide range of time-scales, from nanoseconds (10^{-9} s) to many seconds or longer.

Many methods for detecting chemical reactions require that the concentrations of the two species change as a function of time. For example, if the optical absorption of one of the species is different from the other species, and if the reaction is initially far from equilibrium, then the optical absorption changes as the reaction proceeds, thus allowing the reaction to be followed.

One of the most powerful aspects of NMR is its ability to detect chemical exchange phenomena, *even when the system is in equilibrium*. This is because NMR detects the *molecular motion itself*, rather than the numbers of molecules in different states.

NMR is even capable of detecting the chemical exchange process in *N*, *N*′-dimethylformamide, in which the reactant and the product are indistinguishable.

NMR may detect this type of symmetrical reaction because it involves the individual nuclear spins, which are located at particular sites in the molecule and which act as 'internal spies' reporting on the molecular motion. The two sites are not chemically equivalent, so the chemical shift of a nuclear spin in the 'grey' box changes as the box is transported from one side of the molecule to the other. The change in the chemical shift leads to strong effects on the NMR spectrum, as discussed below. The fact that nuclear spins in the 'white' box experience an exactly symmetrical change in their chemical shifts does not matter.

19.1.5 Molecular rotations

In a *liquid*, the molecules undergo constant random rotations:

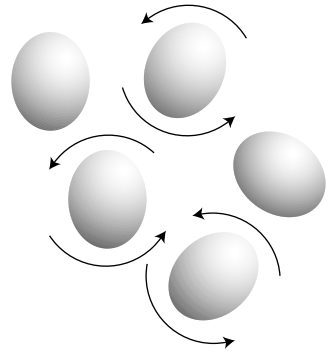

Figure 19.5
Random molecular rotations.

These random rotations are detectable by NMR because they change the anisotropic spin interactions, such as CSA and direct dipole–dipole couplings.

The time-scale of molecular rotations in a liquid depends on the molecular size, and also on other physical parameters such as the viscosity and the temperature. Typically, small molecules rotate in a liquid on the picosecond time-scale, whereas large molecules, such as proteins, rotate in a liquid on the nanosecond time-scale.

In biochemical NMR, a rough estimate of the molecular rotational time-scale (in units of nanoseconds) is obtained by taking the molecular mass (in units of kilodaltons) and dividing by two. For example, the rotational time-scale of a 30 kDa protein molecule in aqueous solution is typically around 15 ns.

The effect of molecular rotations on the motional averaging of nuclear spin interactions was discussed in Section 8.6.

19.1.6 Translational motion

In a liquid, molecules undergo *translations*, i.e. motion of the molecular mass centre through space. Translational motion that is random and uncoordinated is called *diffusion*. Translational motion that is concerted and directed is called *flow*:

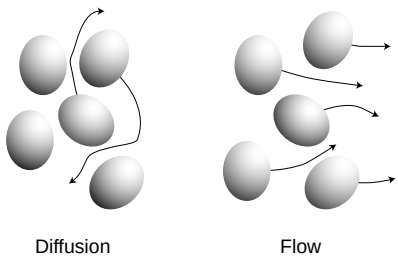

Figure 19.6
Diffusion and flow.

NMR is capable of detecting both kinds of motion, and of distinguishing them.

Molecular translations affect the NMR properties in two different ways:

1. Molecular diffusion on a *microscopic* scale averages out short-range intermolecular spin interactions, as discussed in Section 8.6.
2. Diffusion and flow transport the molecules from one region of space to another, on a *macroscopic* scale. This also affects the behaviour of the spins, if the external magnetic field is *inhomogeneous*.

Detection of *macroscopic* diffusion or flow by NMR is possible in an inhomogeneous magnetic field, because the spin Hamiltonian changes as the molecules move into a different region of space. The inhomogeneous magnetic field may be generated externally, using field gradient coils (see Section 4.7). The motion of the molecules in the direction of the gradient changes the Larmor frequency:

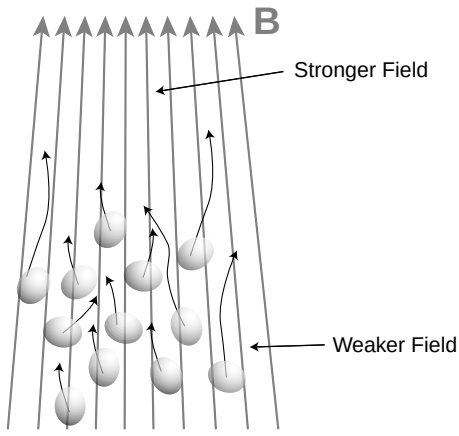

Figure 19.7
Molecules in a flowing liquid, and the application of a magnetic field gradient in the same direction as the flow.

A very important part of NMR is concerned with quantitating molecular diffusion and flow using magnetic field gradients.

In some cases, the inhomogeneous magnetic field is generated by the sample itself. This happens if the sample is grainy and contains particles with different magnetic susceptibility. For example, such effects are important when NMR is used to study the penetration of liquids (such as crude oil) into minerals. Another example is provided by the study of blood flow in the lungs and other body tissues.

Macroscopic diffusion and flow typically change the nuclear spin interactions on the time-scale of milliseconds to seconds.

19.1.7 Mechanical motion

In a *solid*, the thermal molecular rotations are strongly restricted, except in special cases where the molecules are very symmetrical (see the example of fullerene, discussed in Section 1.6.3). Nevertheless, even in a rigid solid, it is possible to influence the nuclear spins by *mechanical rotation of the whole sample* (see Section 19.6).

19.2 Motional Time-Scales

The range of motional time-scales typically encountered for the different motional mechanisms is summarized in the following figure:

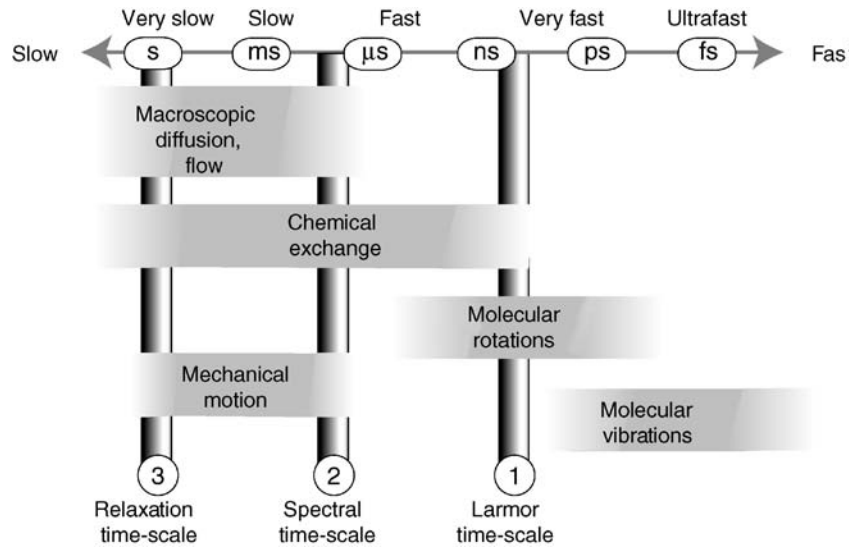

Figure 19.8
Typical motional time-scales for physical processes.

The relevant time-scales run from fractions of a picosecond (for librations), through nanoseconds (for molecular rotations), milliseconds (for many chemical exchange processes and fast mechanical motions), to many seconds (for macroscopic diffusion, flow, slow mechanical motions, and some chemical exchange processes).

The effects of these motional processes on the nuclear spins depend on their relationship to the three characteristic time-scales of the nuclear spin system, indicated by the vertical bars in Figure 19.8.

1. *Larmor time-scale*. Bar ① indicates roughly the time required for the spins to precess through 1 rad in the magnetic field. The characteristic time-scale for bar ① is given by τ^0, where

$$|\omega^0\tau^0| \sim 1$$

For example, if the Larmor frequency of the spins is $\omega^0/2\pi = -500\,\text{MHz}$, then the Larmor time-scale corresponds to $\tau^0 \sim 0.3\,\text{ns}$.

2. *Spectral time-scale*. The characteristic time indicated by bar ② represents the inverse width of the NMR spectrum, measured in frequency units. For example, suppose that the spin system contains two spins, with chemical shift frequencies Ω_1^0 and Ω_2^0. If the chemical shift interactions are dominant, then the spectral time-scale τ_{spec} is given by:

$$|(\Omega_1^0 - \Omega_2^0)\tau_{\text{spec}}| \sim 1$$

If the two spins are both ^{13}C, with a chemical shift difference of 100 ppm, then the time-scale τ_{spec} in a field of 11.74 T is ~13 μs. If the two spins are protons, with a chemical shift difference of 5 ppm, then the time-scale τ_{spec} ~64 μs in the same field.

3. *Relaxation time-scale*. Bar ③ indicates the value of the spin–lattice relaxation time constant T_1. Normally, this is of the order of seconds.

All of these characteristic time-scales depend on the sample, the spin isotope, and physical parameters, such as the magnetic field and the temperature.

19.3 Motional Effects

The effects of motion on the nuclear spin dynamics depend on their time-scale, as summarized by the following diagram:

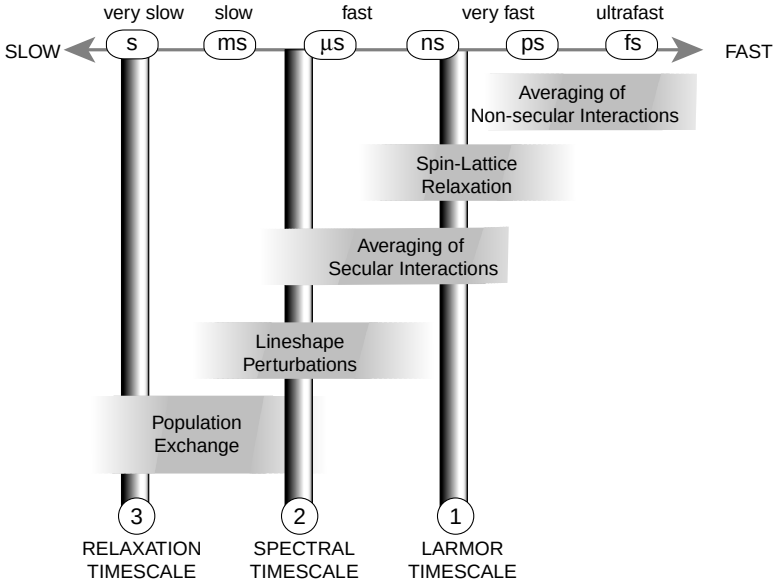

Figure 19.9
Motional time-scales associated with different phenomena.

1. *Averaging of non-secular spin interactions.* Processes that are *faster than the Larmor time-scale* (typically librations and vibrations) average the spin Hamiltonian terms *before* the secular approximation is made (see Section 8.5.2). This process is discussed in Section 19.4.

2. *Spin–lattice relaxation.* Processes that are *on the Larmor time-scale* are responsible for spin–lattice relaxation. Some processes of this type are discussed in Chapter 20.

3. *Averaging of secular spin interactions.* Processes that are *faster than the spectral time-scale but slower than the Larmor time-scale* average the spin Hamiltonian terms *after* the secular approximation is made. This process is also discussed in Section 19.4.

4. *Spectral lineshape perturbations.* Processes that are *on the spectral time-scale* affect the NMR lineshapes strongly. If the motional process is random (such as chemical exchange), such processes typically broaden the spectra, but more complex phenomena may also be observed. A simple case is analysed in Section 19.5. If the motional process is *periodic* (such as mechanical rotation), then the motion generally leads to *sideband* formation. This is discussed in Section 19.6.

5. *Population exchange.* Processes that are *slower than the spectral time-scale* do not significantly affect the NMR lineshapes or relaxation processes. Nevertheless, such slow processes may still be detected by NMR through their influence on the dynamics of spin populations, as long as their time-scale does not greatly exceed T_1 (see Note 1). An example is treated in Section 19.7.

19.4 Motional Averaging

If the motion is rapid (microseconds to femtoseconds), then the nuclear spins experience *motionally averaged* spin interactions, as described in Section 8.6.

An example is the removal of the direct dipole–dipole couplings by molecular rotation and diffusion in an isotropic liquid, as described in Section 9.3.2.

The correct treatment of motional averaging depends on the relative time-scale of the process compared with the Larmor time-scale. Motions that are faster than the Larmor time-scale (typically vibrations) average the spin Hamiltonian *before* the secular approximation is made. Motions that are slower than the Larmor time-scale (typically rotations) average the spin Hamiltonian *after* the secular approximation is made.

The distinction is important because relaxation is caused by *non-secular* Hamiltonian terms, whereas the form of the NMR spectrum is determined by *secular* Hamiltonian terms.

Spin–lattice relaxation is caused by spin interactions that are already averaged over motions that are faster than the Larmor time-scale, but not over slower motions. Typically, this implies that one should correct the values of the spin interaction parameters for rapid vibrational and librational motions, but that one should not correct for rotational or translational motions when treating the spin relaxation.

As an example, consider vibrational averaging of the through-space dipole–dipole coupling. The distance between a ^{13}C nucleus and a directly bonded ^{1}H in a typical C–H group has been determined by neutron diffraction to be 0.109 nm. This corresponds to a direct dipole–dipole coupling of $b_{jk}/2\pi = -23.3$ kHz. In practice, the observed dipole–dipole coupling in a solid is only $b_{jk}/2\pi \sim -20.9$ kHz. The discrepancy is due to the rapid librational motion of the protons. Note that the motion of the protons *perpendicular* to the bond direction is mainly responsible for this reduction in the direct dipole–dipole coupling.[2]

Since the librational motion of CH bonds is much faster than the Larmor time-scale, calculation of dipole–dipole relaxation should use a librationally corrected value for the dipole–dipole coupling constant, i.e. $b_{jk}/2\pi \sim -20.9$ kHz.[3]

It would *not* be appropriate to correct the dipole–dipole coupling for the *rotational* motion of the molecules in a relaxation treatment, since this motion is typically on the Larmor time-scale, or slower.

In the case of calculations of the NMR *spectra* (rather than the relaxation behaviour), it is appropriate to average the spin interactions over all motions that are faster than the spectral time-scale, including both rotations and vibrations. This approach was taken in Chapter 9.

A rather formidable-looking flow chart for motional averaging of the spin Hamiltonian is given below:

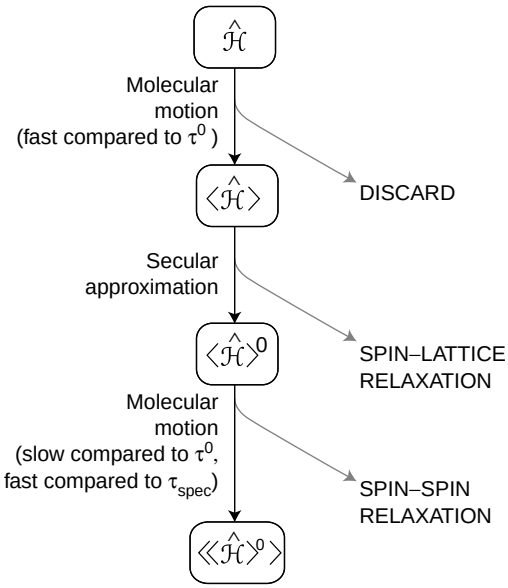

Figure 19.10
A flow diagram for motional averaging.

In the above diagram, angular brackets are used for motional averaging, and the superscript zero is used for the secular part of the spin Hamiltonian. The final result $\langle < \widehat{\mathcal{H}} >^0 \rangle$ is the motionally averaged secular Hamiltonian, whose components are listed in Chapter 9. Such Hamiltonian terms have passed through two stages of motional averaging and one secular approximation.

19.5 Motional Lineshapes and Two-Site Exchange

Motion on the spectral time-scale τ_{spec} causes the NMR lineshapes to change. In this section, the effect of a simple random process is examined.

The example to be discussed now is called *symmetrical two-site exchange*, in which an isolated nuclear spin is transported between two different chemical environments, with different chemical shifts but identical free energies. The process may be depicted thus:

$$A \underset{k}{\overset{k}{\rightleftharpoons}} B$$

where the species A and B have equal probability. The exchange of the *N*-methyl groups in *N*, *N*′-dimethylformamide is a good example of this (see Figure 19.4).

The transition between A and B is considered to be extremely rapid, so that no intermediate states are involved. The *rate constants* for the reactions A → B and B → A are considered to be equal, and are denoted

k. This means that each molecule has a probability $k\tau$ of making a transition to the other state within a short interval τ. The rate constant k is also known as the *transition probability per unit time*.

The trajectories of five different molecules, all starting in the state A, have the following form:

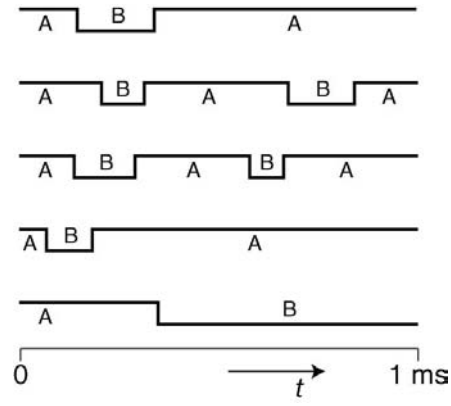

Figure 19.11
A set of trajectories for molecules undergoing two-site exchange.

These examples are consistent with the case $k = 3 \times 10^3\ \mathrm{s}^{-1}$.

The effect of the exchange process on the NMR spectrum depends on the difference in the chemical shift frequencies of the two sites, compared with the exchange rate. Denote the chemical shift frequencies in the two states by Ω_A^0 and Ω_B^0. Define the *chemical shift difference frequency* through:

$$\Omega_\Delta = \Omega_A^0 - \Omega_B^0 \tag{19.1}$$

If the exchange rate constant has roughly the same magnitude as Ω_Δ, then the system is said to be in the *intermediate exchange* regime. This is the regime in which the NMR lineshapes are particularly sensitive to the chemical exchange process.

In the following discussion, we distinguish between two different 'sub-regimes' of intermediate exchange:

1. If the exchange rate constant is smaller than half the magnitude of Ω_Δ (but still comparable in size to Ω_Δ), then the process is said to be in the *slow intermediate exchange* regime:

$$k < |\Omega_\Delta/2| \qquad \text{(slow intermediate exchange)} \tag{19.2}$$

2. If the exchange rate constant is larger than half the magnitude of Ω_Δ (but still comparable in size to Ω_Δ), then the process is said to be in the *fast intermediate exchange* regime:

$$k > |\Omega_\Delta/2| \qquad \text{(fast intermediate exchange)} \tag{19.3}$$

The case $k = |\Omega_\Delta/2|$ is known as the *crossover point*.[4]

These motional regimes may be located on the time-scale diagram as follows:

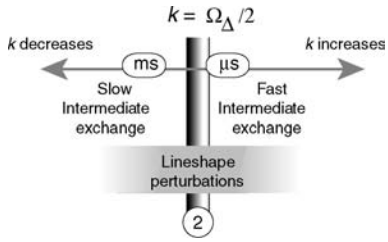

Figure 19.12
The two regimes of intermediate two-site exchange, located on the time-scale diagram.

For two-site exchange, the quantity $|2/\Omega_\Delta|$ corresponds to the 'spectral time-scale' τ_{spec}, mentioned above.

The effect of the chemical exchange on the spectrum is now explored in these two regimes.

19.5.1 Slow intermediate exchange and motional broadening

The term 'slow intermediate exchange' is rather misleading. In fact, the transitions between the two molecular states do not happen very often, but when a transition does occur, it is extremely fast. The term 'infrequent exchange' would be more accurate. For simplicity, I continue to use the common term 'slow intermediate exchange', despite its defects.

When the molecule makes a transition between the two states, the precession frequency of the nucleus changes suddenly. This is depicted for a single molecule in the following diagram:

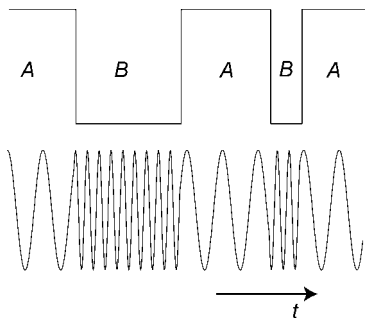

Figure 19.13
Change in the precession frequency on a molecular exchange process.

In the case shown, the precession frequency (relative to the spectrometer reference frequency) is higher for spins in molecules of type B than for molecules of type A (the simulation parameters are $\Omega_A^0/2\pi = 10\,\text{kHz}$, $\Omega_B^0/2\pi = 30\,\text{kHz}$ and $k = 3 \times 10^3\,\text{s}^{-1}$).

The unpredictable jumps in precession frequency cause enhanced dephasing of the transverse magnetization, as shown in the figure below. This shows a superposition of 20 different simulations of the precessing transverse magnetization of spins starting off in molecules of type A but which jump at random intervals between the states A and B:

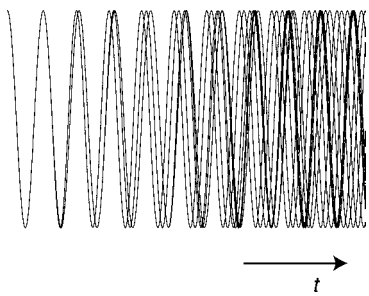

Figure 19.14
Superposition of transverse magnetization oscillations for 20 chemically exchanging molecules, all starting in the same state.

(In this case, the simulation parameters are $\Omega_A^0/2\pi = 10\,\text{kHz}$, $\Omega_B^0/2\pi = 11\,\text{kHz}$ and $k = 500\,\text{s}^{-1}$). The precessing magnetization starts off in phase, but gradually loses coordination as the molecules jump back and forth. This loss of coordination leads to enhanced decay of the total transverse magnetization. The simulation below shows the sum of many such simulations:

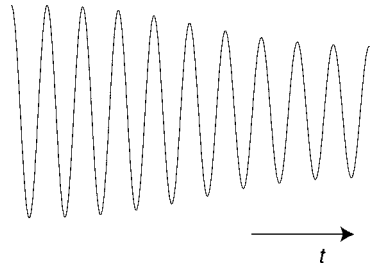

Figure 19.15
Total transverse magnetization for many chemically exchanging molecules, all starting in the same state.

The decay of the transverse magnetization is plain.

Figure 19.16 shows a superposition of precessing transverse magnetization components from many different molecules on the left and the behaviour of the total transverse magnetization on the right for a set of different k values:

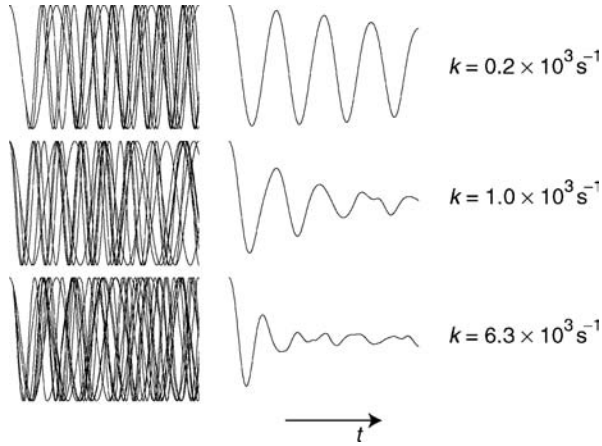

Figure 19.16
Simulations of the precessing transverse magnetization, for three different exchange rate constants in the slow intermediate exchange regime.

(The simulation parameters are $\Omega_A^0/2\pi = 2\,\text{kHz}$ and $\Omega_B^0/2\pi = 4\,\text{kHz}$; each plot spans 1 ms.) If the exchange is faster, then the decay is faster, leading to broader NMR peaks. This is called *motional broadening*.

A formal treatment of the symmetrical two-site exchange spectrum is given in Appendix A.14. In the slow intermediate exchange regime ($k < |\Omega_\Delta/2|$), the spectral lineshape is given by

$$S(\Omega) = \frac{1}{2}\left(1 - \frac{\mathrm{i}k}{R}\right)\mathcal{L}(\Omega; \overline{\Omega} + R, \lambda + k) + \frac{1}{2}\left(1 + \frac{\mathrm{i}k}{R}\right)\mathcal{L}(\Omega; \overline{\Omega} - R, \lambda + k) \tag{19.4}$$

where

$$\overline{\Omega} = \frac{1}{2}(\Omega_A^0 + \Omega_B^0)$$
$$R = \sqrt{|k^2 - (\Omega_\Delta/2)^2|} \tag{19.5}$$

Here, $\mathfrak{L}$ is the complex Lorentzian lineshape specified in Section 5.8.2 and λ is the decay rate constant of the single-quantum coherences, in the absence of the chemical exchange process.

The following plots show how the spectral lineshapes change as the rate constant k increases:

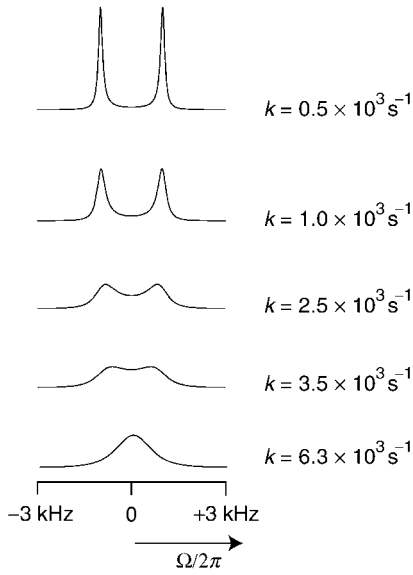

Figure 19.17
Simulated spectra for two-site exchange, in the slow intermediate exchange regime.

The simulation parameters are $\Omega_A^0/2\pi = -1\,\text{kHz}$, $\Omega_B^0/2\pi = +1\,\text{kHz}$, and $\lambda = 0$. Notice how the peaks broaden and come together as k increases. The last plot shows the spectrum at the *crossover point*[4] ($k = |\Omega_\Delta/2|$).

19.5.2 Fast intermediate exchange and motional narrowing

What happens as the exchange rate k increases beyond the crossover point, $k > |\Omega_\Delta/2|$?

Naively, it might be expected that the peaks continue to broaden as k increases, since the jumps in precession frequency occur more often. In fact, the opposite occurs. The left column in Figure 19.18 shows the precessing transverse magnetization components from many different molecules, for a set of different exchange rate constants, in the fast intermediate exchange regime. The right column shows the behaviour of the total transverse magnetization.

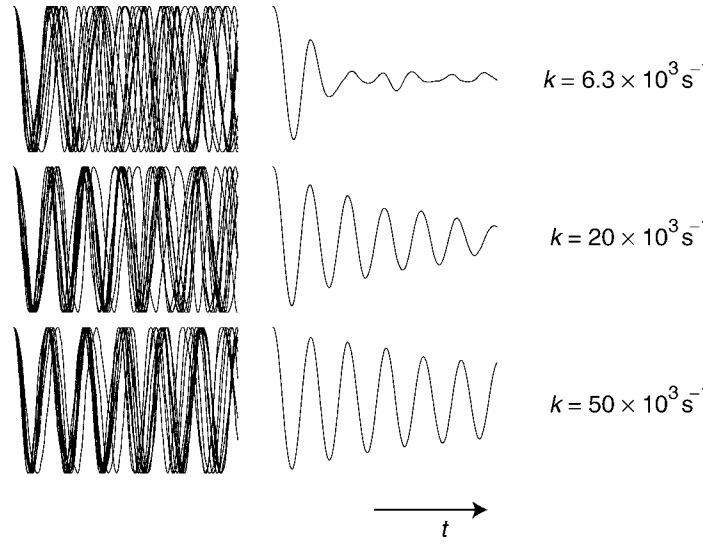

Figure 19.18
Simulations of the precessing transverse magnetization, for three different exchange rate constants in the fast intermediate exchange regime.

(The simulation parameters are $\Omega_A^0/2\pi = 2\,\text{kHz}$ and $\Omega_B^0/2\pi = 4\,\text{kHz}$; each plot spans 1 ms.) Remarkably, the decay of the total transverse magnetization gets *slower* as the exchange rate constant k increases. In the fast exchange regime, the NMR peakwidth is *reduced* by the rapid molecular jumps. This is called *motional narrowing*.

Motional narrowing occurs when the jumps are so frequent that spins in different chemical sites have no time to accumulate a significant phase difference between jumps. Significant precession takes place only after a time interval that corresponds to a large number of site jumps. Since roughly equal amounts of time are spent in the two sites, the *average* precession frequency is rather well defined, even when the precise timing of the individual frequency jumps is unpredictable. In the limit of very fast jumps, the spins experience the average precession frequency of the two sites.

In the fast intermediate exchange regime ($k > |\Omega_\Delta/2|$), the theoretical spectral lineshape is given by the following expression:

$$S(\Omega) = \frac{1}{2}\left(1 + \frac{k}{R}\right)\mathcal{L}(\Omega; \overline{\Omega}, \lambda + k - R) + \frac{1}{2}\left(1 - \frac{k}{R}\right)\mathcal{L}(\Omega; \overline{\Omega}, \lambda + k + R) \tag{19.6}$$

where $\overline{\Omega}$ and R are defined as in Equation 19.5. Some calculated spectra are shown in Figure 19.19 for the case $\Omega_A^0/2\pi = -1\,\text{kHz}$, $\Omega_B^0/2\pi = +1\,\text{kHz}$, and $\lambda = 0$. Notice how the peak gets narrower as k increases beyond the crossover point.

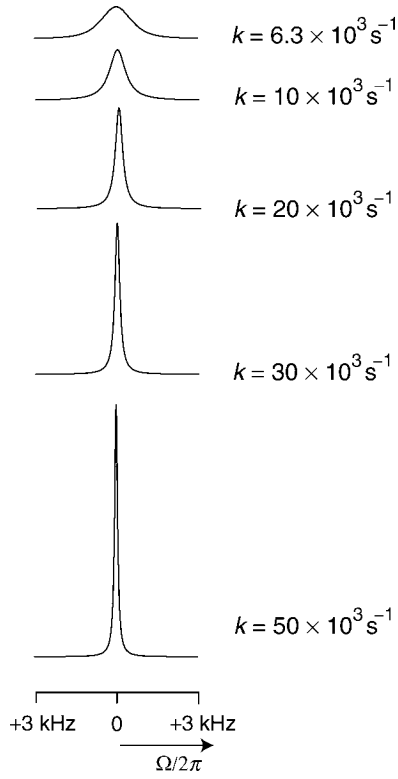

Figure 19.19
Simulated spectra for two-site exchange, in the fast intermediate exchange regime.

The spectral effects of motion may, therefore, be specified exactly for the case of symmetrical two-site exchange. In the slow intermediate exchange regime, the motion causes broadening. As the exchange rate is increased towards the crossover point, the peaks from the distinct chemical sites move together and finally merge. Further increase in the exchange rate causes narrowing of the coalesced peak. In the limit of very fast exchange, the spins only experience the average chemical shift, taken over the motion.

We may now place the case of two-site exchange firmly on the time-scale diagram:

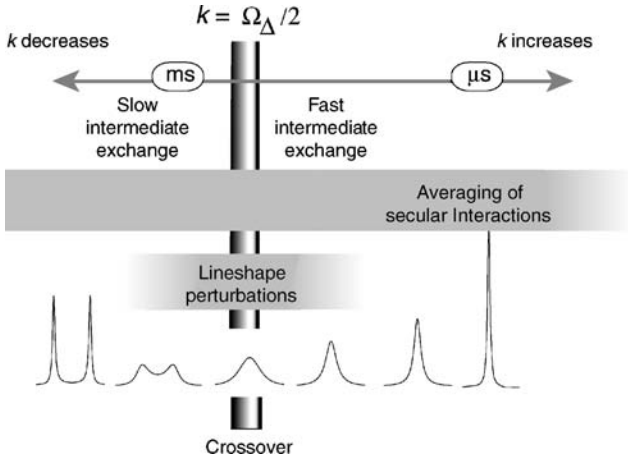

Figure 19.20
Intermediate two-site exchange located on the time-scale diagram.

In the intermediate exchange regime $k \cong |\Omega_\Delta/2|$, experimental spectra are very sensitive to the dynamics and may be used to obtain an accurate estimate of the exchange rate constant.

Some experimental ^{13}C spectra of ^{13}C-enriched *N*, *N*′-dimethylformamide, taken at a variety of temperatures in the gas phase, are shown in Figure 19.21. The rate constant k was determined at each temperature by fitting the experimental spectrum to the theoretical lineshape of Equations 19.4 and 19.6, and is shown on each plot.[5] In this case, the temperature-dependent rate constants $k(T)$ fit well to an *Arrhenius equation* of the form

$$k(T) = A \exp\{-E_{\text{act}}/\mathbb{N}_A k_B T\}$$

where $\mathbb{N}_A = 6.022 \times 10^{23}$ mol^{-1} denotes the Avogadro constant (number of molecules in a mole of substance). The determined values of the Arrhenius activation energy and the pre-exponential factor are $E_{\text{act}} = 90.1$ kJ mol^{-1} and $A = 1.16 \times 10^{14}$ s^{-1} respectively.

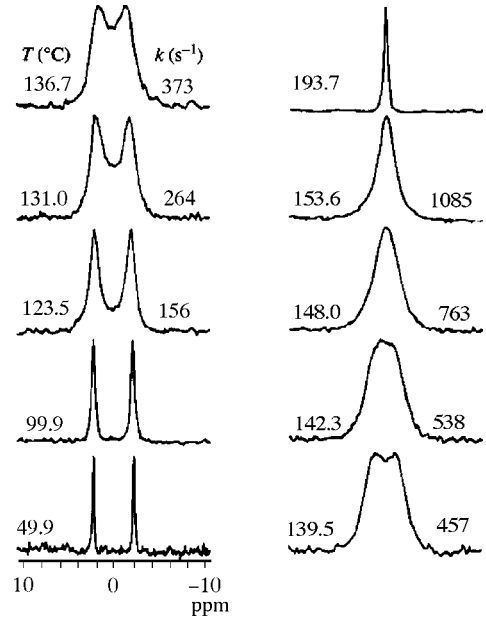

Figure 19.21 Experimental ^{13}C spectra of ^{13}C-enriched *N*, *N*′-dimethylformamide gas at a set of different temperatures in a field of 4.7 T. Taken from B. D. Ross and N. S. True, *J. Am. Chem. Soc.* **106**, 2451 (1984). (Reproduced by permission of the American Chemical Society.)

19.5.3 Averaging of *J*-splittings

Consider a heteronuclear two-spin-1/2 system, consisting of an *I*-spin coupled to an *S*-spin, with coupling constant J_{IS}. As described in Chapter 15, the *S*-spin spectrum consists of two peaks, separated in frequency by $2\pi J_{IS}$ (in radians per second). One of the peaks is associated with the $\rho_{\boxed{\alpha-}}$ (-1)-quantum coherence, and the other peak is associated with the $\rho_{\boxed{\beta-}}$ (-1)-quantum coherence.

Now suppose that the *I*-spin has a short spin–lattice relaxation time constant T_1. In Section 20.3.6 it is shown that the spin–lattice relaxation process may be modelled as a kinetic exchange of the *I*-spin states $|\alpha\rangle$ and $|\beta\rangle$ with rate constant $k = \frac{1}{2}{T_1}^{-1}$. The *S*-spin lineshapes correspond to the equations given above for two-site chemical exchange (Equations 19.4 and 19.6), if the following substitutions are made:

$$k \Rightarrow \frac{1}{2}{T_1}^{-1}$$

$$\Omega_\Delta \Rightarrow 2\pi J_{IS}$$

In the slow exchange limit ($T_1^{-1} << 2\pi|J_{IS}|$), the T_1 process broadens each doublet component by $\frac{1}{2}T_1^{-1}$ rad s^{-1}. In the fast exchange limit ($T_1^{-1} >> 2\pi|J_{IS}|$), the doublet splitting disappears and the S-spin spectrum has the form of a single peak at the Sspin chemical shift:

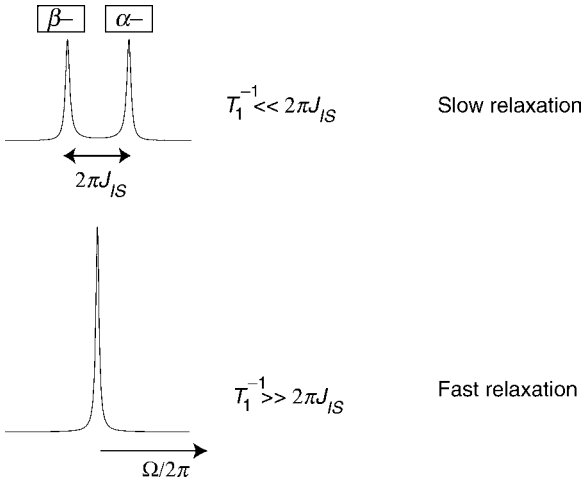

Figure 19.22
Averaging of a heteronuclear J-splitting by spin–lattice relaxation of the coupled spin.

Essentially the same conclusions apply if the rapidly relaxing I-spin has spin > 1/2. This is the most common case, since the quadrupole couplings of spins > 1/2 provide a powerful relaxation mechanism. The averaging of J-splittings by rapid longitudinal relaxation was exploited in Section 17.3.

19.5.4 Asymmetric two-site exchange

Consider again the case of chemical exchange between two molecular species, A and B. In general, the rate constant from A to B is different from the rate constant from B to A:

$$A \underset{k'}{\overset{k}{\rightleftharpoons}} B$$

For example, the exchange could represent a reversible reaction that favours one side. The reaction A → B runs faster than the reaction B → A, because of an asymmetric energy barrier:

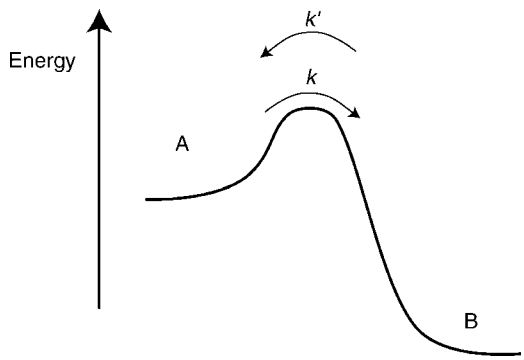

Figure 19.23
An asymmetric chemical reaction.

The ratio of rate constants $K = k/k'$ is called the *equilibrium constant* of the reaction; it is equal to the ratio of species concentrations $[\mathrm{B}]_{\mathrm{eq}} / [\mathrm{A}]_{\mathrm{eq}}$ when the reaction is in equilibrium.[6]

The full expressions for the lineshapes in the case of asymmetric two-site exchange will not be given here. The most important conclusion is that, in the fast exchange limit $k >> |\Omega_\Delta/2|$, the spectrum collapses to a single peak whose position is given by the mean of the two chemical shifts, *weighted by the equilibrium concentrations of the two species* (see Figure 19.24):[6]

$$\Omega_{\mathrm{peak}} = \frac{[A]_{\mathrm{eq}}\,\Omega_{\mathrm{A}}^0 + [B]_{\mathrm{eq}}\,\Omega_{\mathrm{B}}^0}{[A]_{\mathrm{eq}} + [B]_{\mathrm{eq}}} = \frac{\Omega_{\mathrm{A}}^0 + K\Omega_{\mathrm{B}}^0}{1+K}$$

If the chemical shifts of the two species are known, then the position of the peak in the rapid-exchange spectrum may be used to derive the equilibrium constant of the reaction. This is a very useful property that is widely applied in many branches of chemistry.

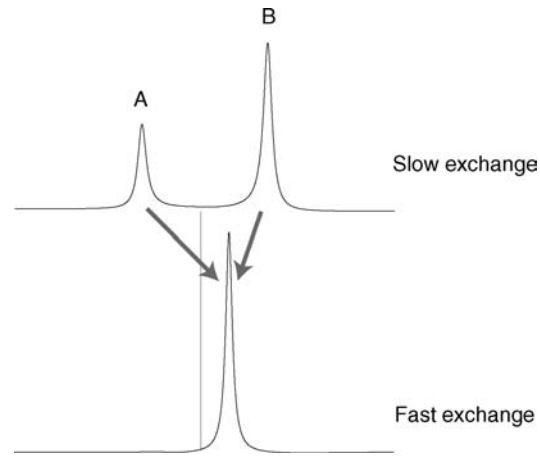

Figure 19.24
NMR spectrum for an asymmetric two-site exchange process.

Sometimes, the spectral frequency of an NMR peak is found to have a strong temperature dependence. Very often, this is because of a rapid asymmetric exchange process; since the equilibrium constant depends on temperature, so does the peak position.

19.5.5 Knight shift

An interesting example of rapid asymmetric exchange is encountered in the NMR of metals.

Nuclear spins in metals are coupled to unpaired conduction electrons, through a mechanism called the *hyperfine coupling* (this resembles the J-coupling, but has a much larger magnitude, often many megahertz). In practice, each nucleus is coupled to a large number of electrons, but, in order to simplify the discussion, let us consider only one electron. The NMR spectrum of the nucleus would be expected to display the usual doublet structure, since the electron has spin-1/2:

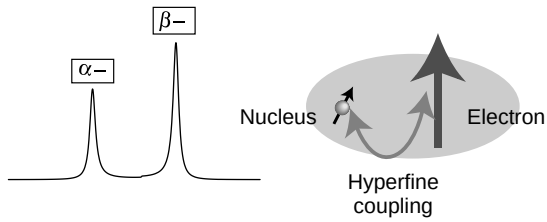

Figure 19.25
Hyperfine doublet of a nucleus coupled to an electron.

In this diagram, the $\rho_{\boxed{\beta-}}$ peak is shown as being more intense than the $\rho_{\boxed{\alpha-}}$ peak, since the Boltzmann distribution leads to a higher population in the electronic $|\beta\rangle$ states than in the electronic $|\alpha\rangle$ states, because of the Zeeman splitting of the electron in the magnetic field, and the fact that the electron has negative gyromagnetic ratio.

In the case of nuclear spins, this population difference is negligible, because the Zeeman energy is at least five orders of magnitude smaller than the available thermal energy, at room temperature. For electrons, on the other hand, the Zeeman splitting is three orders of magnitude larger, and the Boltzmann population differential may no longer be ignored.

As a result, the case of a nucleus coupled to an electron corresponds to the asymmetric two-site exchange problem. The asymmetry is caused by the different energies of the electronic $|\alpha\rangle$ and $|\beta\rangle$ states.

If the electrons have a very short T_1 (which is almost always the case), then the NMR spectrum collapses to a single peak, as described in Section 19.5.4. The position of the peak depends on the relative populations of the electronic states and is therefore shifted, since these states are not equally populated:

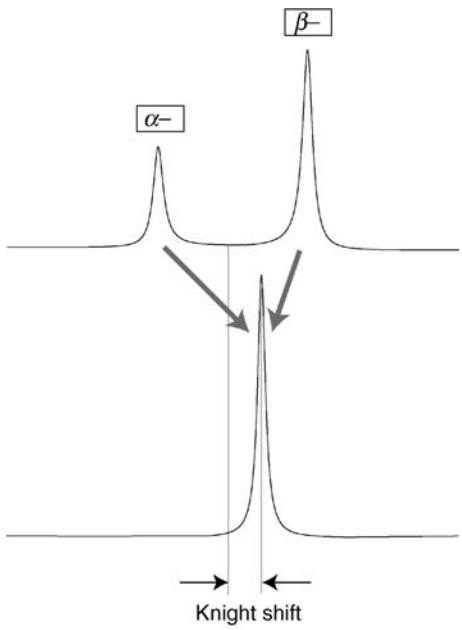

Figure 19.26
Origin of the Knight shift.

This is called the *Knight shift* (after its discoverer), and is widely used to probe the electronic structures of metals, semiconductors, and superconductors.[7]

The Knight shift depends linearly on the magnetic field and is inversely proportional to the absolute temperature, as may easily be deduced from the rough mechanistic sketch given above.

If a metal is cooled, the Knight shift increases, since the difference in Boltzmann populations between the electronic states increases. However, if the metal is cooled so much that it makes a transition into a

superconductor, then the Knight shift suddenly becomes much smaller, since the electron spins pair up to form the spin-pair bosons, which are characteristic of the superconducting state.[7]

19.5.6 Paramagnetic shifts

The nuclear spin resonances of paramagnetic materials are shifted in frequency for exactly the same reason as for the Knight shift. Paramagnetic substances contain localized unpaired electrons, which couple to surrounding nuclei through the hyperfine interactions. Since the electron Zeeman states are unequally populated, and the electron relaxation is very fast, the overall effect is to shift the nuclear spin resonances.

For example, it is possible to add *paramagnetic shift reagents* to a solution in order to shift selectively the resonances of those nuclear spins that are relatively exposed to the solvent.

19.6 Sample Spinning

Mechanical sample rotation is typically on the spectral time-scale and influences the NMR spectra of solids strongly, since it modulates the anisotropic spin interactions (quadrupole couplings, chemical shift anisotropies and direct dipole–dipole couplings). In some circumstances, it is possible to use rapid sample spinning to average out anisotropic spin interactions completely. Typical rotation frequencies range from a few hundreds of hertz up to around 70 kHz. In favourable cases, fast sample spinning provides a solid-state NMR spectrum that resembles that of a liquid sample.

In *magic-angle spinning* (MAS), the solid sample is rotated rapidly around an axis which subtends the 'magic angle' ($\Theta_{\text{magic}} = \arctan\sqrt{2} = 54.74^\circ$; see Section 9.3) with respect to the static field:

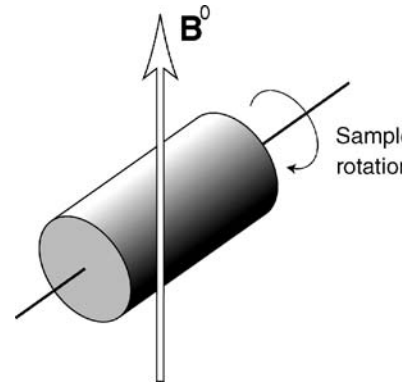

Figure 19.27
Magic-angle sample spinning.

This process averages out the secular parts of the CSA and dipolar interactions. If the spinning frequency is large enough, this leads to spin-1/2 spectra with peaks at the isotropic chemical shifts, and a resolution approaching that of a liquid sample (see Figure 19.28).

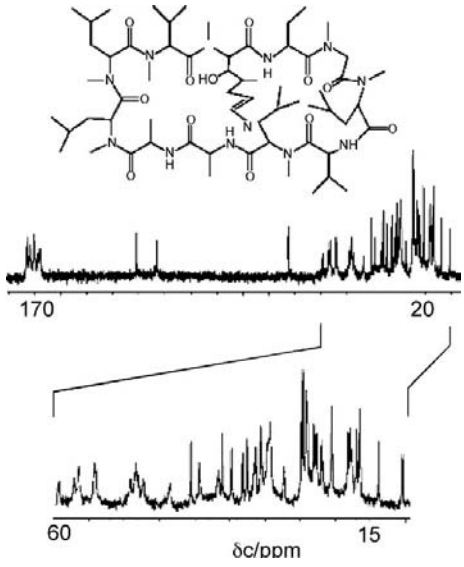

Figure 19.28
^{1}H-decoupled solid-state ^{13}C spectra of cyclosporin A (see inset), in a magnetic field of 11.74 T, at a magic-angle spinning frequency of $\omega_r/2\pi = 33.3$ kHz. Adapted from D. D. Laws, H.-M. L. Bitter and A. Jerschow, *Angew. Chem. Int. Ed.* **41**, 3096–3129 (2002).

If the magic-angle-spinning frequency is not sufficiently large compared with shift anisotropies, the spectrum contains extra peaks called *spinning sidebands*. These appear at frequencies given by $\omega_j^{\text{iso}} + k\omega_r$, where ω_r is the spinning frequency and k is an integer. A set of experimental spectra displaying spinning sidebands is shown in Figure 19.29. A variety of methods exist for separating or suppressing spinning sidebands, even at low spinning frequencies (see *Further Reading*).

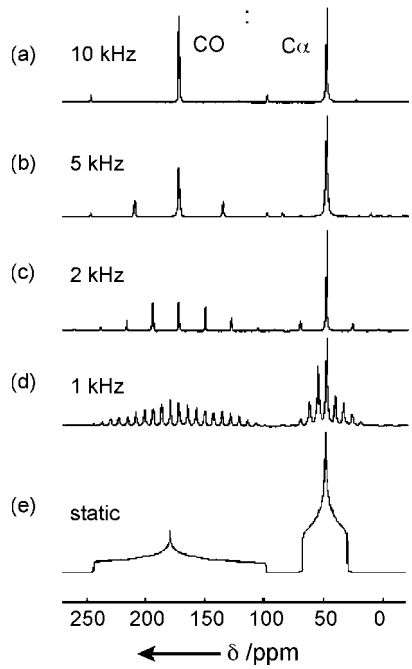

Figure 19.29
^{1}H-decoupled solid-state ^{13}C spectra of $^{13}C_2$-glycine powder, in a magnetic field of 11.74 T, at a variety of magic-angle spinning frequencies. Spectrum (e) is a simulated static spectrum. Adapted from D. D. Laws, H.-M. L. Bitter and A. Jerschow, *Angew. Chem. Int. Ed.* **41**, 3096–3129 (2002).

In most commercial magic-angle-spinning NMR probes, the r.f. coil is wound about the sample rotation axis ($\theta_{RF} = \Theta_{magic}$, see Figure 8.10). This leads to the simplest mechanical construction, but reduces the nutation frequency generated by a given r.f. field. The nutation frequency scaling factor for a coil at the magic angle is $\sin\theta_{RF} = \sin(\arctan\sqrt{2}) = \sqrt{2/3} = 0.816$.

The central transition peaks of half-integer quadrupolar nuclei are broadened by second-order quadrupolar interactions, which cannot be eliminated by magic-angle spinning alone. A variety of methods are available for eliminating second-order quadrupolar broadening, including rotation of the sample about two axes at the same time, and combinations of magic-angle spinning and r.f. pulses (see the *Further Reading* to Chapter 13).

19.7 Longitudinal Magnetization Exchange

Let us now return to the symmetrical two-site exchange process between species A and B:

$$A \underset{k}{\overset{k}{\rightleftharpoons}} B$$

Suppose now that the exchange process occurs infrequently, so that $k << |\Omega_\Delta/2|$. In this regime of *very slow exchange*, the effect on the NMR spectrum is minor. The exchange process merely broadens the NMR peaks slightly. According to Equation 19.4, the widths of the two peaks are given by $2(\lambda + k)$ rad s^{-1}, rather than 2λ rad s^{-1}, which would be the peak widths if there were no exchange. If the natural decay constant λ is larger than k, then the lineshapes are insensitive to the exchange process.

In this regime, it is very difficult to study the slow exchange process using the peak broadening, which is neither strong nor particularly specific. A different approach is therefore necessary for studying dynamic processes in the slow exchange regime.

19.7.1 Two-dimensional exchange spectroscopy

Slow exchange may be studied by using the *exchange of longitudinal magnetization* between the two chemical sites. This may be done by performing two-dimensional spectroscopy with a sequence of three $\pi/2$ pulses:

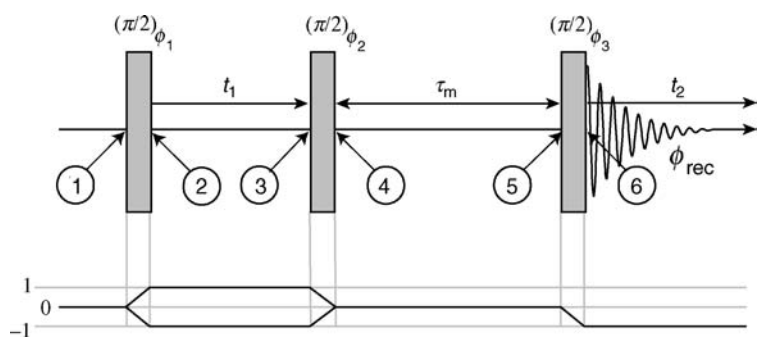

Figure 19.30
Pulse sequence for two-dimensional exchange spectroscopy.

Table 19.1 An eight-step phase cycle ($\mathfrak{n} = 8$) appropriate for the 2D-exchange experiment[8]. The phase Ψ is used in the States scheme for generating pure absorption 2D lineshapes, with discrimination of positive and negative Ω_1-frequencies (see Section 5.9.4). For the "cosine" data set, $\Psi = 0$. For the "sine" data set, $\Psi = -\pi/2$ (see Note 9).

Cycle counter $\mathfrak{m}$	ϕ_1	ϕ_2	ϕ_3	ϕ_{rec}
0	Ψ	π	0	0
1	$\Psi + \pi$	π	0	π
2	Ψ	π	$\pi/2$	$\pi/2$
3	$\Psi + \pi$	π	$\pi/2$	$3\pi/2$
4	Ψ	π	π	π
5	$\Psi + \pi$	π	π	0
6	Ψ	π	$3\pi/2$	$3\pi/2$
7	$\Psi + \pi$	π	$3\pi/2$	$\pi/2$

As usual, the single-headed arrow labelled t_1 implies arrayed signal acquisition with variation of this time delay. The double-headed arrow marked τ_{m} implies that this interval is kept fixed during the acquisition of the two-dimensional data matrix $s(t_1, t_2)$.

The fixed interval τ_{m} plays a central role in this experiment and is called the *mixing interval*.

The diagram shows the coherence transfer pathways for this pulse sequence: the desired signals pass through (± 1)-quantum coherence during the interval between the first $\pi/2$ pulses, have coherence order zero during the mixing interval τ_{m}, and are converted into observable (-1)-quantum coherences by the last $\pi/2$ pulse. An eight-step phase cycle for selecting this signal pathway is given in Table 19.1. This phase table also includes the implementation of the States scheme for generating pure absorption two-dimensional lineshapes (see Section 5.9.4). The phase cycle may be treated using the principles in Appendix A.11.

Consider the simplest possible case, in which each molecule contains a single, isolated, nuclear spin-1/2. The chemical exchange process changes the chemical shift of the spin. In the case of slow symmetrical two-site exchange, the two-dimensional spectrum has the following form:

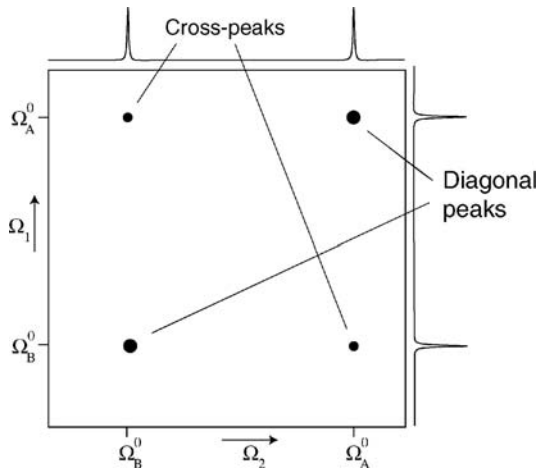

Figure 19.31 Schematic form of a two-dimensional exchange spectrum.

There are two *diagonal peaks*, at frequency coordinates $(\Omega_1, \Omega_2) = \left(\Omega_{\text{A}}^0, \Omega_{\text{A}}^0\right)$ and $(\Omega_1, \Omega_2) = \left(\Omega_{\text{B}}^0, \Omega_{\text{B}}^0\right)$, and two *cross-peaks*, at frequency coordinates $(\Omega_1, \Omega_2) = \left(\Omega_{\text{A}}^0, \Omega_{\text{B}}^0\right)$ and $(\Omega_1, \Omega_2) = \left(\Omega_{\text{B}}^0, \Omega_{\text{A}}^0\right)$. The existence of the

cross-peaks is a signature of the dynamic exchange process between the two sites. The cross-peak amplitudes provide a quantitative estimate of the exchange rate constant.

At short mixing intervals $\tau_m < k^{-1}$, the cross-peaks are absent and the spectrum contains only diagonal peaks. As the mixing interval increases, the cross-peaks become more intense and the diagonal peaks weaker. If the mixing interval is longer than around $2k^{-1}$, the cross-peaks and diagonal peaks have approximately equal intensity. Further increase in τ_m causes both cross-peaks and diagonal peaks to decrease:

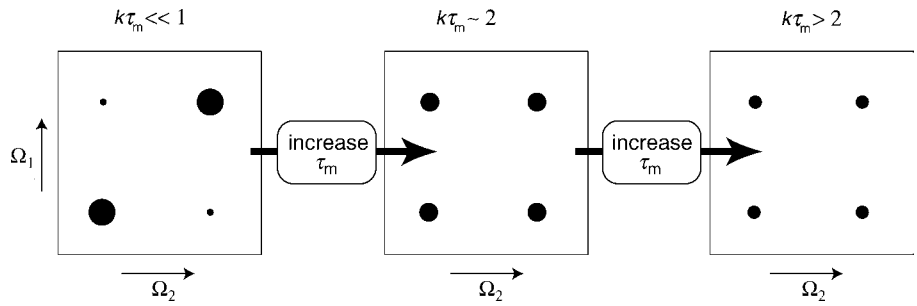

Figure 19.32 Change in the two-dimensional exchange spectrum as the mixing interval τ_m increases, for the case of symmetrical two-site exchange.

A derivation of the theoretical peak amplitudes is given in Appendix A.14.4. If the spin–lattice relaxation times of the two sites are the same ($T_1^A = T_1^B = T_1$), then the amplitudes of the diagonal and cross-peaks are given by

$$a_{diag}(\tau_m) = \cosh(k\tau_m)\exp\{-(k + T_1{}^{-1})\tau_m\}$$
$$a_{cross}(\tau_m) = \sinh(k\tau_m)\exp\{-(k + T_1{}^{-1})\tau_m\} \qquad (19.7)$$

where the hyperbolic cosine and sine functions are defined as:

$$\cosh x = \frac{1}{2}(e^x + e^{-x})$$
$$\sinh x = \frac{1}{2}(e^x - e^{-x})$$

The peak amplitudes are shown below for the case $k = 10\,s^{-1}$ and $T_1^A = T_1^B = T_1 = 1\,s$:

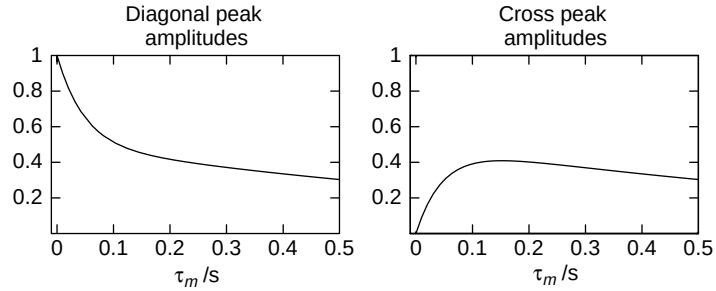

Figure 19.33 Diagonal and cross-peak amplitudes as a function of τ_m.

The *ratio* of the cross-peak and diagonal-peak amplitudes is independent of the spin–lattice relaxation time T_1, and is given by

$$\frac{a_{\text{cross}}}{a_{\text{diag}}}(\tau_{\text{m}}) = \frac{\sinh(k\tau_{\text{m}})}{\cosh(k\tau_{\text{m}})} = \tanh k\tau_{\text{m}} \tag{19.8}$$

where the hyperbolic tangent is defined as

$$\tanh x = \sinh x / \cosh x$$

The behaviour of the cross-peak/diagonal-peak ratio is shown below for the case $k = 10\,\text{s}^{-1}$ and $T_1^{\text{A}} = T_1^{\text{B}} = T_1 = 1\,\text{s}$:

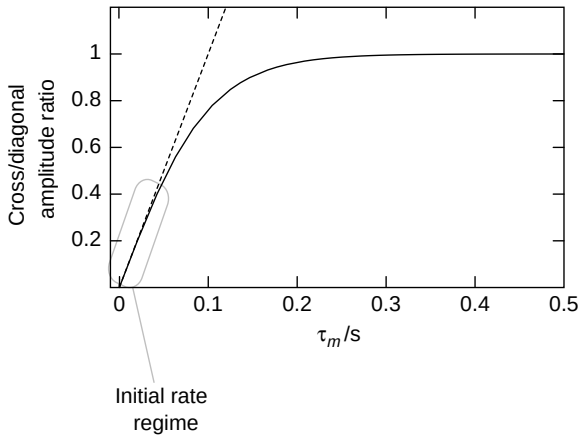

Figure 19.34
Ratio of the cross-peak amplitude to the diagonal-peak amplitude as a function of τ_{m}.

At short mixing intervals ($k\tau_{\text{m}} < 1$), the cross-peak to diagonal-peak ratio is approximately linearly dependent on τ_{m}, according to

$$\frac{a_{\text{cross}}}{a_{\text{diag}}}(\tau_{\text{m}}) \cong k\tau_{\text{m}} \tag{19.9}$$

as shown by the dotted line in the plot. This is called the *initial rate regime*.

The rate constant k of the exchange process may be estimated by repeating the two-dimensional experiment with several values of the mixing interval τ_{m}, followed by fitting the experimental cross-peak/diagonal-peak ratios to Equation 19.8 (in the general case), or to Equation 19.9 (in the initial rate regime).

19.7.2 Theory

I now give a theoretical description of the two-dimensional exchange experiment using the density operator formalism. We must take into account the fact that the spins are transported between two different sorts of molecules, A and B, in a dynamic exchange process.

As discussed in Appendix A.14, it is possible to write the spin density operator as

$$\hat{\rho} = \frac{1}{2}\hat{\rho}^A + \frac{1}{2}\hat{\rho}^B$$

for the case of two-site exchange. The density operator of spins in molecules of type A is given by

$$\hat{\rho}^A = \overline{|\psi\rangle\langle\psi|}^A$$

where the overbar indicates averaging over all type-A molecules. Similarly, the density operator of spins in molecules B is given by

$$\hat{\rho}^B = \overline{|\psi\rangle\langle\psi|}^B$$

where the overbar indicates averaging over all type-B molecules.

The spin density operator components at the beginning of the pulse sequence are given by

$$\hat{\rho}^A_{①} \sim I_z\,; \qquad \hat{\rho}^B_{①} \sim I_z$$

ignoring the unity operator and the usual numerical factors. This describes a state in which the spins of both types of molecule are weakly polarized along the z-axis by the external magnetic field.

In the case of very slow exchange ($k << |\Omega_\Delta/2|$), the evolution of the spin density operator components up to time point ④ may be calculated independently, using the geometrical arguments developed in Chapters 11 and 12. For spins in molecules of type A, the first two $\pi/2$ pulses and the variable interval t_1 lead to the following transformation:

$$\begin{aligned}
\hat{\rho}^A_{①} &= I_z \\
&\downarrow\ (\pi/2)_x \\
\hat{\rho}^A_{②} &= -I_y \\
&\downarrow\ t_1 \\
\hat{\rho}^A_{③} &= \left(-I_y \cos(\Omega^0_{\mathrm{A}} t_1) + I_x \sin(\Omega^0_{\mathrm{A}} t_1)\right)\ \exp\{-\lambda' t_1\} \\
&\downarrow\ (\pi/2)_{\bar{x}} \\
\hat{\rho}^A_{④} &= \left(+I_z \cos(\Omega^0_{\mathrm{A}} t_1) + I_x \sin(\Omega^0_{\mathrm{A}} t_1)\right)\ \exp\{-\lambda' t_1\}
\end{aligned}$$

(The phases of the pulses correspond to the first row of Table 19.1, with $\Psi = 0$.) These transformations are depicted in the following diagrams:

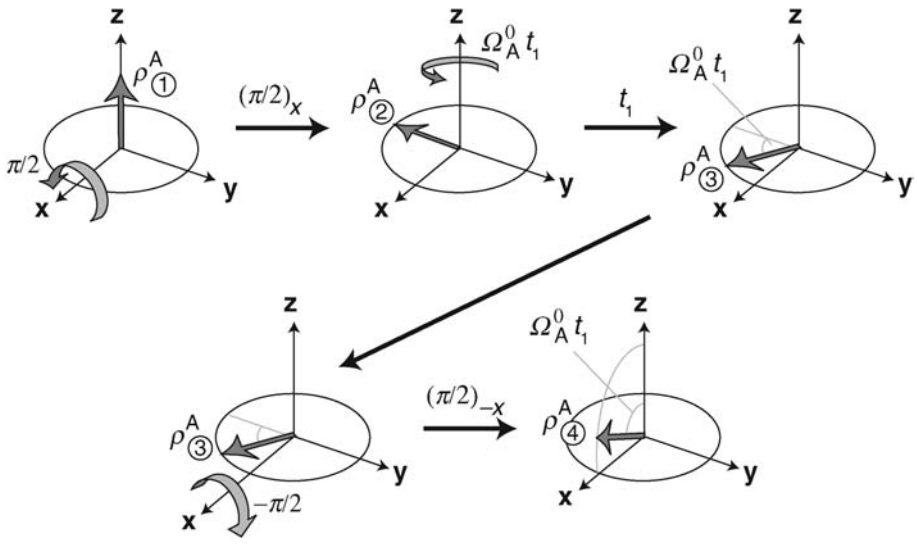

Figure 19.35
Transformations of the density operator of spins in type-A molecules, during the first part of a two-dimensional exchange pulse sequence.

Equation 19.10 includes a damping factor $\exp\{-\lambda' t_1\}$ for the decay of transverse relaxation during the evolution interval t_1. According to Equation 19.4, the decay rate constant is given by

$$\lambda' = \lambda + k$$

where the contribution k takes into account the peak broadening from the slow exchange process and λ takes into account any other coherence decay mechanisms. The overall transverse relaxation time is $T_2 = 1/\lambda'$.

Similarly, the density operator for spins in molecules of type B at time point ④ is given by

$$\hat{\rho}^B_{④} = \left(+I_z \cos(\Omega^0_B t_1) + I_x \sin(\Omega^0_B t_1)\right) \exp\{-\lambda' t_1\}$$

As shown in Appendix A.11, the phase cycle specified in Table 19.1 has the effect of suppressing all signal contributions that do not pass through longitudinal magnetization under the mixing interval. As a result, only the longitudinal spin density operator components at time point ④ need be taken into account. These are

$$\hat{\rho}^A_{④} = I_z \cos(\Omega^0_A t_1) \exp\{-\lambda' t_1\} + \ldots$$
$$\hat{\rho}^B_{④} = I_z \cos(\Omega^0_B t_1) \exp\{-\lambda' t_1\} + \ldots$$

In the two-dimensional experiment, data are collected with a large number of values of the evolution interval t_1. As t_1 increases, the longitudinal magnetization of spins in molecules A oscillates at the frequency Ω^0_A. Similarly, the longitudinal magnetization of spins in molecules B oscillates at the frequency Ω^0_B. These characterisitic t_1 modulations provide *frequency labels* that reveal the origin of the longitudinal magnetization components at time point ④.

Consider now the evolution of the density operator in the mixing interval τ_m. The exchange process leads to a transport of longitudinal magnetization between the two components of the spin density operator, $\hat{\rho}^A$ and $\hat{\rho}^B$, at the same time as the magnetization components decay, due to spin–lattice relaxation. The fate of the A-type spin magnetization during the mixing interval is sketched below:

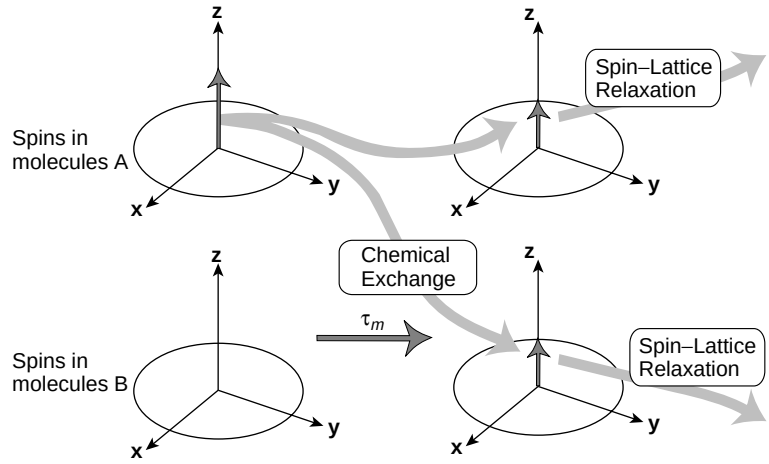

Figure 19.36
Physical processes during the mixing interval of a two-dimensional exchange experiment.

An accurate treatment of the magnetization dynamics is given in Appendix A.14.4. The spin density operator at time ⑤ is given by

$$\hat{\rho}^{\mathrm{A}}_{⑤} = I_z \left\{ a_{\mathrm{A}\to\mathrm{A}}(\tau_\mathrm{m}) \cos(\Omega^0_\mathrm{A} t_1) + a_{\mathrm{B}\to\mathrm{A}}(\tau_\mathrm{m}) \cos(\Omega^0_\mathrm{B} t_1) \right\} \exp\{-\lambda' t_1\} + \ldots$$
$$\hat{\rho}^{\mathrm{B}}_{⑤} = I_z \left\{ a_{\mathrm{B}\to\mathrm{B}}(\tau_\mathrm{m}) \cos(\Omega^0_\mathrm{B} t_1) + a_{\mathrm{A}\to\mathrm{B}}(\tau_\mathrm{m}) \cos(\Omega^0_\mathrm{A} t_1) \right\} \exp\{-\lambda' t_1\} + \ldots$$

where the diagonal- and cross-magnetization transfer amplitudes are given in Equation 19.7.

The final $\pi/2$ pulse performs the usual conversion of longitudinal magnetization into transverse magnetization:

$$\hat{\rho}^{\mathrm{A}}_{⑥} = -I_y \left\{ a_{\mathrm{A}\to\mathrm{A}}(\tau_\mathrm{m}) \cos(\Omega^0_\mathrm{A} t_1) + a_{\mathrm{B}\to\mathrm{A}}(\tau_\mathrm{m}) \cos(\Omega^0_\mathrm{B} t_1) \right\} \exp\{-\lambda' t_1\} + \ldots$$
$$\hat{\rho}^{\mathrm{B}}_{⑥} = -I_y \left\{ a_{\mathrm{B}\to\mathrm{B}}(\tau_\mathrm{m}) \cos(\Omega^0_\mathrm{B} t_1) + a_{\mathrm{A}\to\mathrm{B}}(\tau_\mathrm{m}) \cos(\Omega^0_\mathrm{A} t_1) \right\} \exp\{-\lambda' t_1\} + \ldots$$

The (-1)-quantum coherences at the beginning of the detection interval, therefore, are

$$\hat{\rho}^{\mathrm{A}}_{\boxed{-}⑥} = \frac{1}{2\mathrm{i}} \left\{ a_{\mathrm{A}\to\mathrm{A}}(\tau_\mathrm{m}) \cos(\Omega^0_\mathrm{A} t_1) + a_{\mathrm{B}\to\mathrm{A}}(\tau_\mathrm{m}) \cos(\Omega^0_\mathrm{B} t_1) \right\} \exp\{-\lambda' t_1\}$$
$$\hat{\rho}^{\mathrm{B}}_{\boxed{-}⑥} = \frac{1}{2\mathrm{i}} \left\{ a_{\mathrm{B}\to\mathrm{B}}(\tau_\mathrm{m}) \cos(\Omega^0_\mathrm{B} t_1) + a_{\mathrm{A}\to\mathrm{B}}(\tau_\mathrm{m}) \cos(\Omega^0_\mathrm{A} t_1) \right\} \exp\{-\lambda' t_1\}$$

The transverse magnetization precesses during the subsequent detection interval at the appropriate chemical

shift frequency and induces a quadrature NMR signal in the usual way. For spins in molecules A during the detection interval, the signal is given by

$$s_A^{\cos}(t_1, t_2) = 2\mathrm{i}\hat{\rho}^A_{\boxed{-}}\textcircled{6}\ \exp\{(\mathrm{i}\Omega_A^0 - \lambda')t_2\}$$

(The superscript 'cos' indicates the 'cosine' data set in the States procedure, generated with phase $\Psi = 0$.) For spins in molecules B during the detection interval, the signal is given by

$$s_B^{\cos}(t_1, t_2) = 2\mathrm{i}\hat{\rho}^B_{\boxed{-}}\textcircled{6}\ \exp\{(\mathrm{i}\Omega_B^0 - \lambda')t_2\}$$

These results may be combined to obtain the full two-dimensional signal for the 'cosine' data set ($\Psi = 0$):

$$s^{\cos}(t_1, t_2) = s^{\cos}_{\mathrm{A}\to\mathrm{A}}(t_1, t_2) + s^{\cos}_{\mathrm{A}\to\mathrm{B}}(t_1, t_2) + s^{\cos}_{\mathrm{B}\to\mathrm{A}}(t_1, t_2) + s^{\cos}_{\mathrm{B}\to\mathrm{B}}(t_1, t_2)$$

with

$$\begin{aligned}
s^{\cos}_{\mathrm{A}\to\mathrm{A}}(t_1, t_2) &= a_{\mathrm{A}\to\mathrm{A}}(\tau_\mathrm{m})\cos(\Omega^0_\mathrm{A} t_1)\exp\{-\lambda' t_1\}\exp\{(\mathrm{i}\Omega^0_\mathrm{A} - \lambda')t_2\}\\
s^{\cos}_{\mathrm{A}\to\mathrm{B}}(t_1, t_2) &= a_{A\to B}(\tau_\mathrm{m})\cos(\Omega^0_\mathrm{A} t_1)\exp\{-\lambda' t_1\}\exp\{(\mathrm{i}\Omega^0_\mathrm{B} - \lambda')t_2\}\\
s^{\cos}_{\mathrm{B}\to\mathrm{A}}(t_1, t_2) &= a_{\mathrm{B}\to\mathrm{A}}(\tau_\mathrm{m})\cos(\Omega^0_\mathrm{B} t_1)\exp\{-\lambda' t_1\}\exp\{(\mathrm{i}\Omega^0_\mathrm{A} - \lambda')t_2\}\\
s^{\cos}_{\mathrm{B}\to\mathrm{B}}(t_1, t_2) &= a_{\mathrm{B}\to\mathrm{B}}(\tau_\mathrm{m})\cos(\Omega^0_\mathrm{B} t_1)\exp\{-\lambda' t_1\}\exp\{(\mathrm{i}\Omega^0_\mathrm{B} - \lambda')t_2\}
\end{aligned}$$

The terms $s^{\cos}_{A\to A}$ and $s^{\cos}_{B\to B}$ generate the two diagonal peaks in the two-dimensional spectrum. The terms $s^{\cos}_{A\to B}$ and $s^{\cos}_{B\to A}$ generate the two cross-peaks.

Note that all four signals display cosine modulations with respect to t_1, as required for the 'cosine' data set in the States data acquisition scheme.

If the derivation is repeated for the 'sine' data set ($\Psi = -\pi/2$),[9] we get

$$s^{\sin}(t_1, t_2) = s^{\sin}_{\mathrm{A}\to\mathrm{A}}(t_1, t_2) + s^{\sin}_{A\to B}(t_1, t_2) + s^{\sin}_{\mathrm{B}\to\mathrm{A}}(t_1, t_2) + s^{\sin}_{B\to B}(t_1, t_2)$$

with

$$\begin{aligned}
s^{\sin}_{\mathrm{A}\to\mathrm{A}}(t_1, t_2) &= a_{\mathrm{A}\to\mathrm{A}}(\tau_\mathrm{m})\sin(\Omega^0_\mathrm{A} t_1)\exp\{-\lambda' t_1\}\exp\{(\mathrm{i}\Omega^0_\mathrm{A} - \lambda')t_2\}\\
s^{\sin}_{\mathrm{A}\to\mathrm{B}}(t_1, t_2) &= a_{\mathrm{A}\to\mathrm{B}}(\tau_\mathrm{m})\sin(\Omega^0_\mathrm{A} t_1)\exp\{-\lambda' t_1\}\exp\{(\mathrm{i}\Omega^0_\mathrm{B} - \lambda')t_2\}\\
s^{\sin}_{\mathrm{B}\to\mathrm{A}}(t_1, t_2) &= a_{\mathrm{B}\to\mathrm{A}}(\tau_\mathrm{m})\sin(\Omega^0_\mathrm{B} t_1)\exp\{-\lambda' t_1\}\exp\{(\mathrm{i}\Omega^0_\mathrm{A} - \lambda')t_2\}\\
s^{\sin}_{\mathrm{B}\to\mathrm{B}}(t_1, t_2) &= a_{\mathrm{B}\to\mathrm{B}}(\tau_\mathrm{m})\sin(\Omega^0_\mathrm{B} t_1)\exp\{-\lambda' t_1\}\exp\{(\mathrm{i}\Omega^0_\mathrm{B} - \lambda')t_2\}
\end{aligned}$$

All terms have sine modulations with respect to t_1, as required by the States scheme.

The data sets $s^{\cos}(t_1, t_2)$ and $s^{\sin}(t_1, t_2)$ are combined and processed as described in Section 5.9.4 to obtain the two-dimensional spectrum:

$$S(\Omega_1, \Omega_2) = S_{\mathrm{A}\to\mathrm{A}}(\Omega_1, \Omega_2) + S_{\mathrm{A}\to\mathrm{B}}(\Omega_1, \Omega_2) + S_{\mathrm{B}\to\mathrm{A}}(\Omega_1, \Omega_2) + S_{\mathrm{B}\to\mathrm{B}}(\Omega_1, \Omega_2)$$

where

$$\begin{aligned}
\mathrm{Re}\{S_{\mathrm{A}\to\mathrm{A}}(\Omega_1, \Omega_2)\} &= a_{\mathrm{diag}}(\tau_{\mathrm{m}})\, \mathcal{A}(\Omega_1, \Omega_2;\ \Omega_{\mathrm{A}}^0, \lambda', \Omega_{\mathrm{A}}^0, \lambda') \\
\mathrm{Re}\{S_{\mathrm{A}\to\mathrm{B}}(\Omega_1, \Omega_2)\} &= a_{\mathrm{cross}}(\tau_{\mathrm{m}})\, \mathcal{A}(\Omega_1, \Omega_2;\ \Omega_{\mathrm{A}}^0, \lambda', \Omega_{\mathrm{B}}^0, \lambda') \\
\mathrm{Re}\{S_{\mathrm{B}\to\mathrm{A}}(\Omega_1, \Omega_2)\} &= a_{\mathrm{cross}}(\tau_{\mathrm{m}})\, \mathcal{A}(\Omega_1, \Omega_2;\ \Omega_{\mathrm{B}}^0, \lambda', \Omega_{\mathrm{A}}^0, \lambda') \\
\mathrm{Re}\{S_{\mathrm{B}\to\mathrm{B}}(\Omega_1, \Omega_2)\} &= a_{\mathrm{diag}}(\tau_{\mathrm{m}})\, \mathcal{A}(\Omega_1, \Omega_2;\ \Omega_{\mathrm{B}}^0, \lambda', \Omega_{\mathrm{B}}^0, \lambda')
\end{aligned}$$

and

$$\begin{aligned}
a_{\mathrm{diag}} &= a_{A\to A} = a_{B\to B} \\
a_{\mathrm{cross}} &= a_{A\to B} = a_{B\to A}
\end{aligned}$$

The two-dimensional absorption lineshape $\mathcal{A}$ is defined in Equation 5.26.

The result is a two-dimensional spectrum containing two absorption diagonal peaks with amplitudes a_{diag} and two absorption cross-peaks with amplitudes a_{cross}:

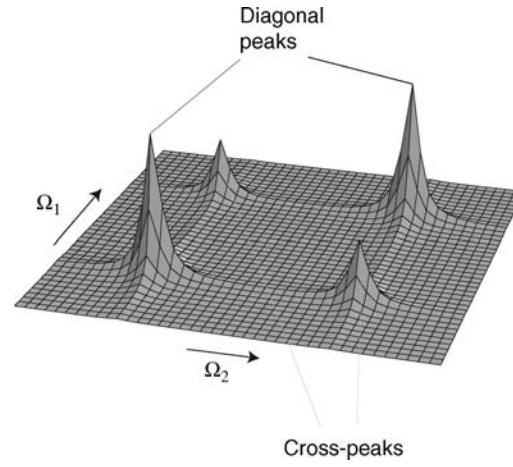

Figure 19.37
Form of the two-dimensional exchange spectrum.

An experimental application of two-dimensional exchange spectroscopy is shown in Figure 19.38.

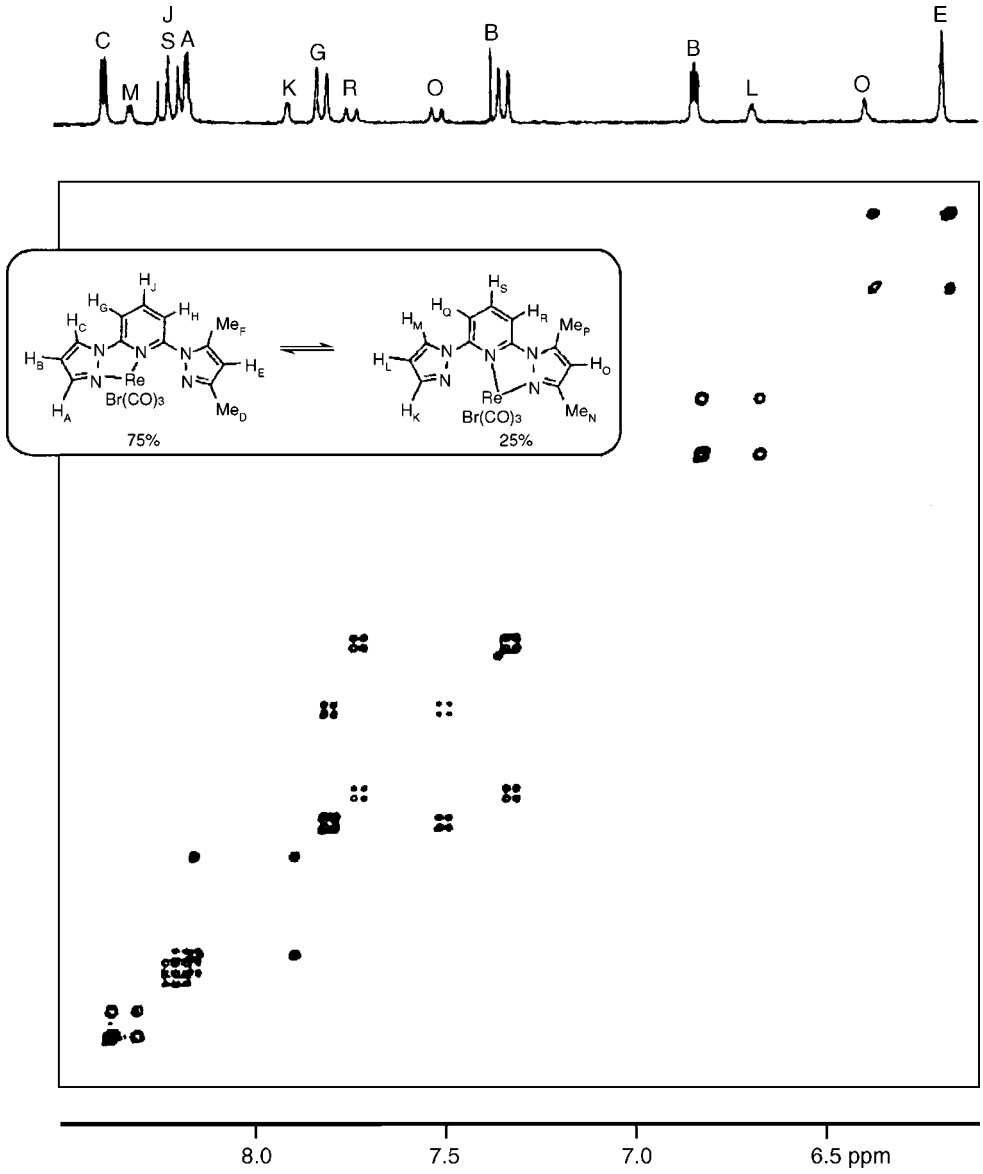

Figure 19.38 Proton two-dimensional exchange spectrum of the organometallic fluxional compound $[ReBr(CO)_3(Me_2\text{-bppy})]$, where bppy denotes 2,6-bis(pyrazol-1-yl)pyridine (see inset). The mixing interval was $\tau_m = 0.1$ s. The off-diagonal peaks may be interpreted in terms of an exchange of the metal atom between two pairs of nitrogen binding sites, as shown in the inset. Adapted from E. W. Abel, *et al.*, *J. Chem. Soc. Dalton Trans.*, 1079 (1994). (Copyright, the Royal Society of Chemistry.)

19.7.3 Motional regimes

Two-dimensional exchange spectroscopy allows chemical exchange processes to be identified and quantitated in the slow exchange regime $T_1^{-1} < k << |\Omega_\Delta/2|$:

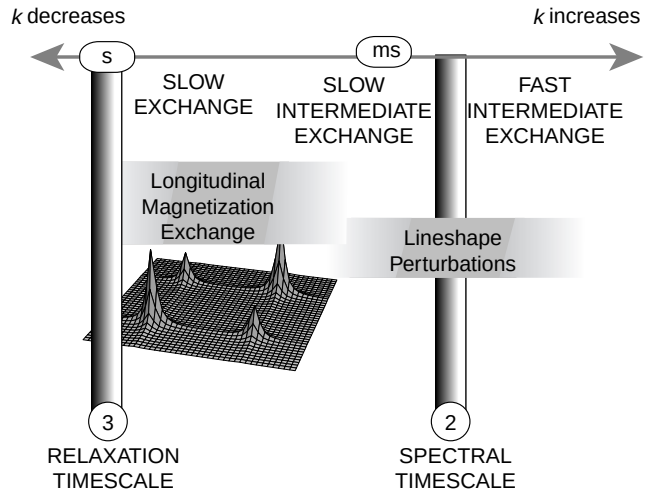

Figure 19.39
Two-dimensional magnetization exchange located on the time-scale diagram.

The two-dimensional exchange experiment does not work if the exchange is much slower than T_1^{-1}, since the spin populations equilibrate completely during the mixing interval, and the 'frequency labelling' of the longitudinal magnetization components is lost.

If the exchange is fast enough to approach the spectral time-scale, the intepretation of the two-dimensional exchange experiment is less straightforward, since the two-dimensional peaks are also broadened and distorted.

19.8 Diffusion

The study of molecular diffusion by NMR is a large and important subject. Only a few superficial remarks will be made here.

One of the basic pulse sequences used to study molecular diffusion is shown in Figure 5.9. This is a three-pulse *stimulated echo* sequence, with pulsed field gradients applied between the first two pulses and after the third one. This pulse sequence has a close relationship with the NOESY sequence in Figure 19.30, and it functions in a similar way. Instead of chemical shift evolution between the first two $\pi/2$ pulses, there is evolution of transverse magnetization in the presence of a field gradient. Instead of chemical exchange during the mixing interval τ_m, there is molecular diffusion. In both experiments, magnetization is stored in the longitudinal form during the relatively long mixing interval, to allow the exchange or motional process to take place.

Suppose that the gradient pulses are applied along the x-axis. It may be shown that the amplitude of the NMR signal after the stimulated echo sequence is proportional to

$$a(T) = a(0)\exp\{-D_x\kappa^2 T\} \tag{19.10}$$

where T is the effective time interval between the two gradient pulses (in general, this takes into account their finite duration), D_x is the diffusion coefficient of the molecules in the x-direction, and κ is a measure of the strength of the gradient pulses, given by

$$\kappa = \gamma\sigma_{\mathrm{G}}\mathrm{G}_{\max}\tau_{\mathrm{G}}$$

where $G_{\max}$ is the maximum gradient strength, τ_G is the gradient pulse duration, and the factor σ_G takes into account the rounded shape of the gradient pulse:

$$\sigma_{\mathrm{G}} = G_{\max}^{-1}\int_0^{\tau_{\mathrm{G}}} G(t)\,\mathrm{d}t$$

The signal, therefore, decays as a function of the interval between the gradient pulses, and the rate constant of this decay may be used to estimate the diffusion constant.

If the experiment is repeated with gradient pulses in the three different directions, it is possible to estimate the three diffusion constants $\{D_x, D_y, D_z\}$ individually. In an isotropic medium, all three diffusion constants are the same, but in an anisotropic medium, such as many body tissues, they are not. For example, the diffusion of water is easier along the length of a narrow channel rather than perpendicular to it:

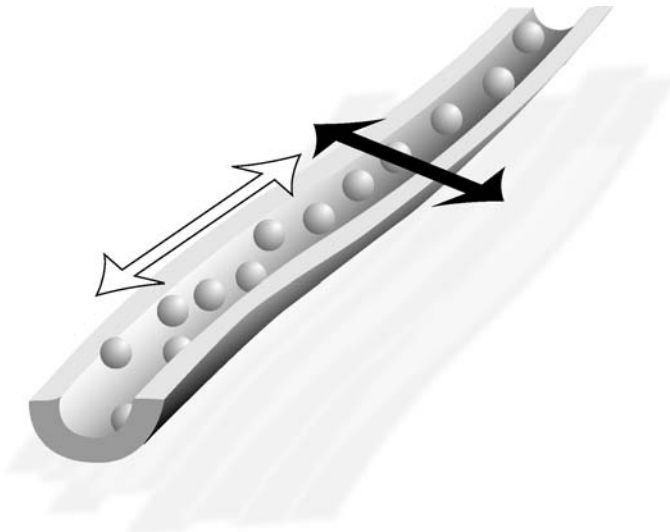

Figure 19.40
The diffusion of water in a fibrous or channel-like system is anisotropic: diffusion is faster along the channel (white) than diffusion perpendicular to the channel (black).

By studying the directions of fastest diffusion for neighbouring volume elements in an NMR image, it is possible to trace out the pathways of nerves and similar channel-like structures in the human body. This technique is called *diffusion tensor imaging*. An experimental result is shown in Plate 4.

Notes

1. In some cases, motional processes that are significantly slower than T_1 may be studied by exploiting *long-lived spin states*. For example, see S. Cavadini, J. Dittmer, S. Antonijevic and G. Bodenhausen, *J. Am. Chem. Soc.* **127**, 15 744–15 748 (2005).

2. The spin–spin *distance* also varies during vibrational or librational motion. However, the oscillation of the distance tends to *increase* the value of the dipole–dipole coupling constant. The observed *decrease* in the dipole–dipole coupling constants is due to the angular libration, which more than compensates the opposite effect of the bond length oscillations. To calculate the motionally averaged dipolar coupling, one must average the *full form* of the dipolar interaction (Equation 9.3).A motional average of the r^{-3} term alone gives incorrect results. The commonly encountered expression $b \sim \langle r^{-3} \rangle$, where the angular brackets denote motional averaging, is *incorrect* in general.

3. Relaxation calculations in liquids that do not employ librationally corrected dipole–dipole coupling constants may lead to an overestimate of the internal molecular mobility and flexibility.

4. The crossover point between the two exchange regimes is close, but not identical, to the *coalesence point*, at which the two peaks merge into one. Coalescence is defined by the point at which the second derivative of $\mathrm{Re}\{S(\Omega)\}$ with respect to Ω vanishes, at the mean frequency of the two peaks $\Omega = \overline{\Omega}$. If λ is ignored, coalescence occurs at the rate constant $k = \Omega_{\Delta}/(2\sqrt{2})$.

5. When performing such fits, one should be aware that the chemical shifts may be temperature dependent, as well as the exchange rate constant.

6. I neglect here the distinction between the concentration and the kinetic activity of a substance.

7. At first sight, it is surprising that NMR may be performed at all on superconductors, which are known to exclude the magnetic field (this is called the *Meissner effect*). NMR studies are possible because of the finite *penetration depth* of the magnetic field into the interior of a superconductor. If a superconducting sample is sufficiently finely divided, then NMR signals may be picked up from most of the sample volume.

8. The r.f. phases specified in Table 19.1 employ a π phase shift for the second pulse. This choice of phases leads to consistently positive diagonal peaks and cross-peaks in two-dimensional exchange spectra.

9. The pulse sequence phases are consistent with the 'sign-corrected' version of the States procedure discussed in Section 5.9.4.

Further Reading

- For a review of chemical exchange effects in NMR, see A. D. Bain, *Prog. NMR Spectrosc.* **43**, 63–103 (2003).
- For reviews of solid-state NMR, including magic-angle-spinning, see M. J. Duer, *Introduction to Solid-State NMR Spectroscopy*, Blackwell Science, 2004; K. Schmidt-Rohr, H. W. Spiess, *Multidimensional Solid-State NMR and Polymers*, Academic Press, London, 1994; M. Mehring, *High Resolution NMR in Solids*, 2nd edition, Springer, Berlin, 1982.
- For a review of sideband suppression and separation methods in magic-angle-spinning NMR, see O. N. Antzutkin, *Prog. NMR Spectrosc.* **35**, 203–266 (1999).
- For diffusion and flow measurements by NMR, see C. S. Johnson Jr, *Prog. NMR Spectrosc.* **34**, 203–256 (1999), and the articles in the *Encyclopedia of Nuclear Magnetic Resonance*, D. M. Grant and R. K. Harris (eds), Wiley, 1996, by K. J. Packer (vol. 3, pp. 1615–1626) and C. S. Johnson Jr, (vol. 3, pp. 1626–1644).
- See *Concepts in Magnetic Resonance, Part A*, **28** (2), (2006) for a series of explanatory articles on diffusion tensor imaging.

Exercises

19.1 Consider an idealized symmetrical two-site exchange process, with kinetics described by the Arrhenius equation over a wide range in temperature. The pre-exponential constant is $A = 10^{14}\,\mathrm{s}^{-1}$ and the activation energy is $E_{\mathrm{act}} = 57\,\mathrm{kJ\,mol}^{-1}$. The exchange process causes a change in the ^{13}C chemical shift at a certain molecular site to change by 50 ppm, while the ^{1}H chemical shift at a different molecular site changes by 5 ppm. All the parameters are assumed to be temperature independent.

(i) At what magnetic field is the crossover in the ^{13}C lineshapes observed if the sample temperature is $T = 300\,\mathrm{K}$?

(ii) At what magnetic field is the crossover in the ^{1}H lineshapes observed if the sample temperature is $T = 300\,\mathrm{K}$?

(iii) At what temperature is the crossover in the ^{1}H lineshapes observed if the proton Larmor frequency is $\omega^0/2\pi = -200\,\mathrm{MHz}$?

(iv) Over which range in temperatures does one expect two-dimensional exchange spectroscopy to be useful for studying the exchange process? Assume that T_1 is of the order of several seconds.

(v) Around which temperature does one expect the exchange process to become a mechanism for proton spin–lattice relaxation if the magnetic field is $B^0 = 11\,\mathrm{T}$?

20 Relaxation

20.1 Types of Relaxation

If the sample is allowed to be undisturbed for a long time in the magnetic field, it reaches a state of *thermal equilibrium*. As discussed in Section 11.3, this implies (i) that all coherences are absent and (ii) that the populations are given by the Boltzmann distribution, at the temperature of the molecular environment.

R.f. pulses disturb the equilibrium of the spin system. The populations after a pulse usually deviate from their thermal equilibrium values and, in many cases, coherences are created. For example, a π pulse inverts the population distribution, whereas a $\pi/2$ pulse equalizes spin state population and generates coherences.

Relaxation is the process by which equilibrium is regained, through interaction of the spin system with the thermal molecular environment.

Relaxation processes may be divided into two types. *Spin–lattice relaxation* is concerned with the movement of spin populations back to their Boltzmann distribution values. *Spin–spin relaxation* is concerned with the decay of coherences. Spin–lattice relaxation is also known as *longitudinal relaxation*; spin–spin relaxation is also known as *transverse relaxation*.

In an ensemble of isolated spins-1/2, there are only two time constants for the relaxation processes: these are the *spin–lattice relaxation time constant* T_1 for the equilibration of populations and the *transverse relaxation time constant* T_2 for the decay of single-quantum coherences.

In systems with coupled spins, relaxation is a more subtle and varied phenomenon, and one needs many more time constants to characterize it, as discussed below.

The study of nuclear spin relaxation is important for several reasons, including the following:

1. Many motional processes in molecules may be studied by nuclear spin relaxation.

2. Nuclear spin relaxation is sensitive to non-secular spin interactions (see Section 8.5.2). The study of relaxation can reveal these 'hidden' spin interactions, which have little effect on the ordinary NMR spectrum. A very important example is the through-space dipole–dipole coupling in isotropic liquids. As discussed in Section 9.3, the secular dipole–dipole couplings average to zero in isotropic liquids, and have almost no effect on the ordinary NMR spectrum. The study of spin relaxation reveals the non-secular parts of the dipole–dipole coupling, thus allowing these couplings to be used for the determination of molecular structure in biomolecules, through the so-called NOESY and ROESY experiments, as discussed below.

20.2 Relaxation Mechanisms

For spins-1/2, relaxation is caused by fluctuating magnetic fields at the sites of the nuclear spins, caused by thermal motion of the molecules.

Spin Dynamics: Basics of Nuclear Magnetic Resonance, Second Edition Malcolm H. Levitt

For example, consider the direct dipole–dipole coupling between two nuclear spins in the same molecule. As the molecule tumbles, the magnitude and direction of the magnetic field exerted by one spin on the other changes:

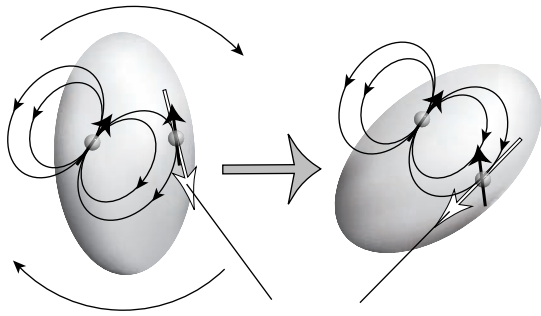

Figure 20.1
Modulation of the local dipolar field by molecular rotation.

Another source of local fields is the *CSA*. As discussed in Section 9.1, these fields are caused by molecular electron currents induced by the external magnetic field. As the molecules tumble in a liquid, the direction and magnitude of these local fields also change:

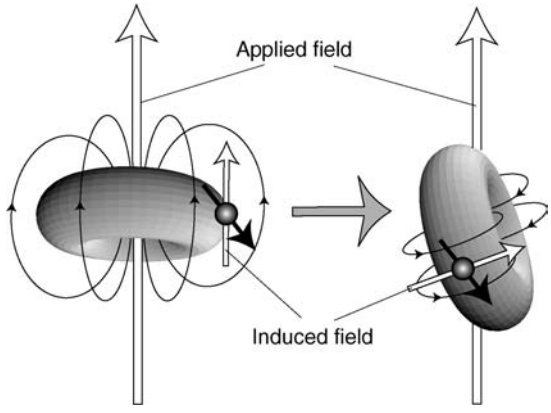

Figure 20.2
Modulation of the chemical shift interaction by molecular rotation.

If one adds these small local fields to the large static field from the magnet, one gets a total field that fluctuates slightly in direction and magnitude as the molecules rotate:

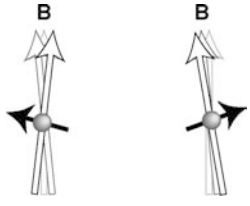

Figure 20.3
Wobbling of the total local field.

As discussed qualitatively in Section 2.6, this 'wobbling' of the local magnetic field is very slight, but is sufficient to cause spin–lattice relaxation.

For spins-1/2, the usual order of importance of relaxation mechanisms is as follows:

$$\text{dipole–dipole} > \text{CSA} > \text{spin–rotation}$$

The CSA becomes increasingly important at high magnetic fields, where it starts to compete effectively with the dipole–dipole mechanism. The spin–rotation mechanism is usually unimportant, except for small molecules in gases or non-viscous liquids.

For spins > 1/2, the usual order of importance of relaxation mechanisms is as follows:

$$\text{quadrupole} >> \text{dipole–dipole} > \text{CSA} > \text{spin–rotation}$$

In most cases, the electric quadrupole relaxation mechanism clearly dominates the relaxation of spins > 1/2.

In most experimental cases, a single relaxation mechanism dominates, but others may also be significant. When several mechanisms are present at the same time, there is the possibility of *cross-correlation* effects, as discussed in Section 20.8.

20.3 Random Field Relaxation

As an introduction to the subject of relaxation, consider a set of non-coupled spins-1/2 exposed to two fields: a large static field B^0 along the z-axis and a small magnetic field $B_x(t)$ along the x-axis. Suppose that each spin experiences the same longitudinal field B^0, but that the transverse fields $B_x(t)$ are different for each spin, and also fluctuate in time:

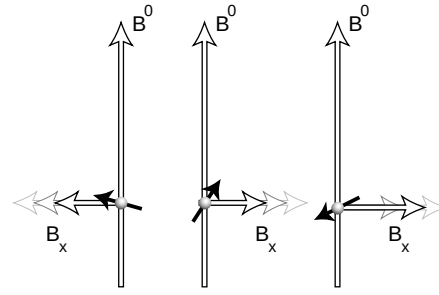

Figure 20.4
The sum of the external field and a fluctuating transverse field.

The value of the transverse field B_x for two different spins has the following appearance when plotted against time:

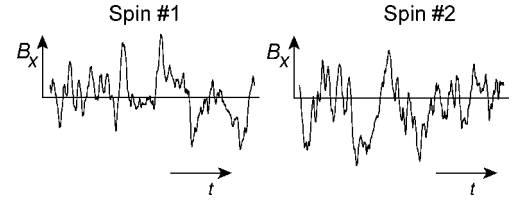

Figure 20.5
Fluctuations of the transverse field at two different spins.

The fluctuations of the fields at the two spins are unrelated to each other in detail, but they have the same general time-scale and the same general amplitude.

20.3.1 Autocorrelation functions and correlation times

In the simplest model, one assumes that the fluctuating transverse fields have the following properties:

1. The fluctuating fields have *zero average*:

$$\langle B_x(t) \rangle = 0$$

For each spin, the field switches between the negative and positive x-axis, so that the average field along the x-axis is zero. In this equation, the angular brackets imply either an average over a long time for a single spin, or an average over many spins at any particular moment; one assumes that these two types of average are the same (this is called the *ergodic hypothesis*).

2. One needs a way of defining the *magnitude* of the fluctuating fields. The average value of the field will not do, because it is zero for all spins, as indicated above. Instead, one uses the *mean square fluctuating field* defined by

$$\langle B_x^2(t) \rangle \neq 0$$

The square field B_x^2 is plotted below as a function of time for two spins:

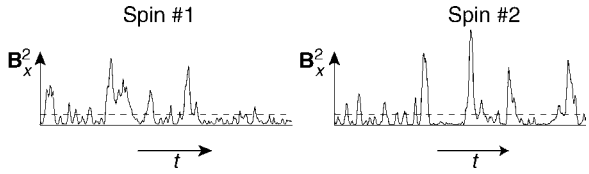

Figure 20.6
Fluctuations of the square transverse field at two different spins.

Since the square of the field is always positive, the mean square field is not zero, and is the same for all spins. The value of $\langle B_x^2(t) \rangle$ is indicated by a dashed line in the plots.

3. One also needs a way of defining *how rapidly* the field fluctuates. This is done by using the *autocorrelation function* of the field, which is defined as follows:

$$\mathbb{G}(\tau) = \langle B_x(t) B_x(t+\tau) \rangle \neq 0 \qquad (20.1)$$

Here, τ is a time interval, whose meaning is examined below. A rapidly fluctuating field has an autocorrelation function that decays quickly with respect to τ:

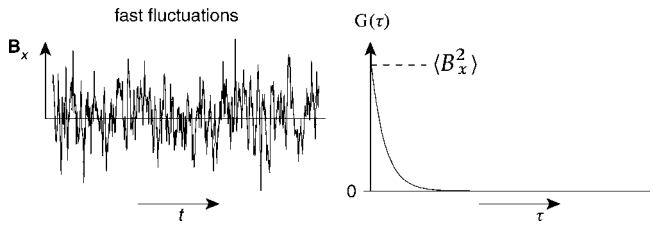

Figure 20.7
Autocorrelation function of a rapidly fluctuating field.

A slowly fluctuating field, on the other hand, has an autocorrelation function that decays slowly with respect to τ:

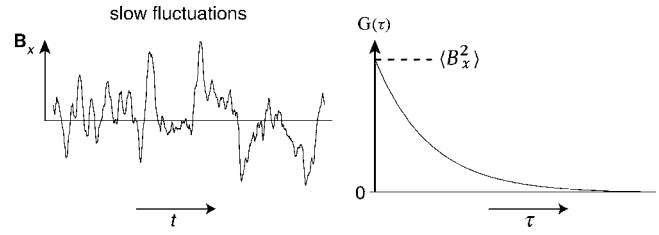

Figure 20.8
Autocorrelation function of a slowly fluctuating field.

By definition, the autocorrelation function at $\tau = 0$ is equal to the mean square field:

$$\mathbb{G}(0) = \left\langle B_x^2(t) \right\rangle$$

As discussed below, the decay rate and form of the autocorrelation function $\mathbb{G}(\tau)$ turns out to be very important for the spin relaxation.

4. The definition of the autocorrelation function, Equation 20.1, is independent of the time point t. This is called the *stationary* assumption.

5. The fluctuating fields are assumed to be *spin independent*. This means that the field experienced by a particular spin depends neither on the orientation of that spin, nor on the orientations of other spins in the vicinity. The fields are assumed to emanate from some source external to the spin system, which is itself ignorant of the states of the spins on which it acts. This is clearly an incorrect assumption for relaxation mechanisms such as the dipole–dipole coupling, in which the fields depend explicitly on the states of neighbouring spins. We must expect the treatment to be only qualitative in this case. In fact, the assumption of spin-independent random fields is not strictly valid for *any* true relaxation mechanism, as discussed in Section 20.3.6.

The physical meaning of the autocorrelation function is now examined in more detail. The general idea is to compare the field at any one time point t with its value at a later time point $t + \tau$.

If the interval τ is small compared with the time-scale of the fluctuations, then the values of the field at the two time points tend to be similar: if $B_x(t)$ is positive, then $B_x(t + \tau)$ also tends to be positive; while if $B_x(t)$ is negative, then $B_x(t + \tau)$ is usually also negative. In both cases, the product of $B_x(t)$ and $B_x(t + \tau)$ is positive, and is close to the value $\left\langle B_x^2(t) \right\rangle$. This is illustrated below for two choices of the initial time point t:

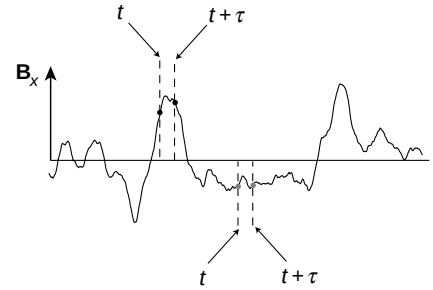

Figure 20.9
Comparison of the fields at close time intervals.

The values of B_x indicated by the black dots have the same sign. The same is true for the values of B_x indicated by the grey dots.

If the interval τ is long compared with the time-scale of the fluctuations, then the system loses its 'memory'. There is no longer any consistent relationship between the value of the function at times separated by τ.

This is illustrated below:

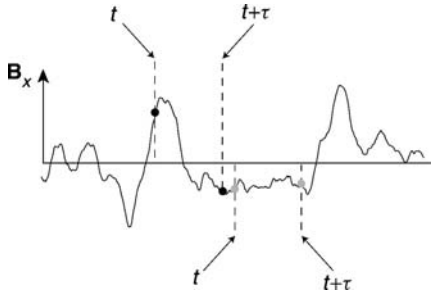

Figure 20.10
Comparison of the fields at long time intervals.

The values of B_x indicated by the black dots have opposite sign, whereas the values of B_x indicated by the grey dots have the same sign. When the product $B_x(t)B_x(t+\tau)$ is averaged over the ensemble, the result will be close to zero.

In general, the autocorrelation function $\mathbb{G}(\tau)$ tends to be large for small values of τ and tends to zero for large values of τ. Often, one *assumes* a simple exponential form for the autocorrelation function:

$$\mathbb{G}(\tau) = \left\langle B_x^2 \right\rangle \mathrm{e}^{-|\tau|/\tau_c} \tag{20.2}$$

This has the correct qualitative form, but it is difficult to justify on the basis of a deeper theory.
The parameter τ_c is called the *correlation time* of the fluctuations. Rapid fluctuations have a small value of τ_c, whereas slow fluctuations have a large value of τ_c. For rotating molecules in a liquid, τ_c is in the range of tens of picoseconds to several nanoseconds.

Qualitatively, the correlation time indicates how long it takes before the random field changes sign.

In practice, the correlation time depends on the physical parameters of the system, such as the temperature. Generally, correlation times are *decreased* by *warming* the sample, since an increase in temperature corresponds to more rapid molecular motion. Conversely, correlation times are *increased* by *cooling* the sample.

20.3.2 Spectral density

An important role is played in relaxation theory by the *spectral density* $\mathbb{J}(\omega)$, which is defined as twice the Fourier transform of the autocorrelation function:[1]

$$\mathbb{J}(\omega) = 2\int_0^\infty \mathbb{G}(\tau)\exp\{-\mathrm{i}\omega\tau\}\,\mathrm{d}\tau \tag{20.3}$$

For a fluctuating field along the x-axis, with an exponentially decaying autocorrelation function given by Equation 20.2, the spectral density is given by

$$\mathbb{J}(\omega) = 2\left\langle B_x^2 \right\rangle \mathcal{A}(\omega; 0, {\tau_c}^{-1})$$

where $\mathcal{A}$ is the absorption Lorentzian, given in Equation 5.14. Explicitly, the spectral density may be written as follows:

$$\mathbb{J}(\omega) = 2\left\langle B_x^2 \right\rangle \frac{\tau_c}{1+\omega^2\tau_c^2} \tag{20.4}$$

If the transverse field fluctuates rapidly, then the correlation time is short and the spectral density function is broad:

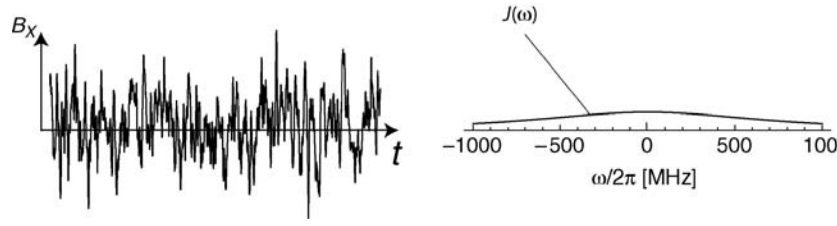

Figure 20.11
Spectral density function of a rapidly fluctuating field ($\tau_c = 0.2$ns).

If the transverse field fluctuates slowly, then the correlation time is long and the spectral density function is narrow:

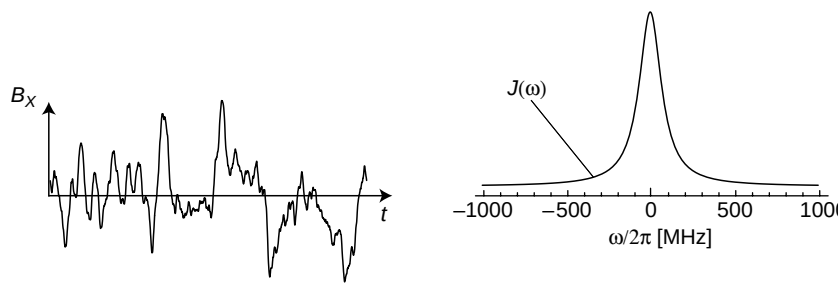

Figure 20.12
Spectral density function of a slowly fluctuating field ($\tau_c = 2.0$ns).

The area under the spectral density function is independent of τ_c, and is given in the present model by $2\langle B_x^2 \rangle$, i.e. twice the mean square amplitude of the fluctuating field.

20.3.3 Normalized spectral density

It is common to work with a *normalized spectral density*, denoted here $\mathcal{J}(\omega)$, which is just the last part of Equation 20.4, i.e.

$$\mathcal{J}(\omega) = \mathcal{A}(\omega; 0, {\tau_c}^{-1}) = \frac{\tau_c}{1 + \omega^2 \tau_c^2} \tag{20.5}$$

For a random field along the x-axis, the spectral density function is given by

$$\mathbb{J}(\omega) = 2 \left\langle B_x^2 \right\rangle \mathcal{J}(\omega)$$

From now on, I will use the term 'spectral density' to imply 'normalized spectral density', which is common practice in the NMR literature.

20.3.4 Transition probabilities

The fluctuating transverse field induces *transitions* between the spin energy eigenstates $|\alpha\rangle$ and $|\beta\rangle$. Suppose that a spin is in the energy state $|\alpha\rangle$ at time t. At a later time $t + \tau$, the spin will be in a different state $|\alpha'\rangle$, because of the action of the fluctuating field. The new state $|\alpha'\rangle$ is generally a superposition of states $|\alpha\rangle$ and $|\beta\rangle$, which implies that a subsequent measurement may produce a result appropriate to the state $|\beta\rangle$. The *transition probability per unit time* from state $|\alpha\rangle$ to state $|\beta\rangle$ is defined for small values of τ through the following equation:

$$W_{\boxed{-}} = \tau^{-1}\overline{|\langle\beta|\alpha'\rangle|^2}$$

where the overbar defines an ensemble average. The notation $W_{\boxed{-}}$ indicates that the spin angular momentum along the z-axis *decreases* upon the transition $|\alpha\rangle \rightarrow |\beta\rangle$.

Similarly, the transition probability per unit time from state $|\beta\rangle$ to state $|\alpha\rangle$ is defined through the following equation:

$$W_{\boxed{+}} = \tau^{-1}\overline{|\langle\alpha|\beta'\rangle|^2}$$

where the overbar defines an ensemble average, and it is assumed that the system starts out in state $|\beta\rangle$ but assumes a new state $|\beta'\rangle$ after an interval τ. The notation $W_{\boxed{+}}$ indicates that the spin angular momentum along the z-axis increases upon the transition $|\beta\rangle \rightarrow |\alpha\rangle$.

The 'transition probability per unit time', denoted W, is often loosely referred to as the 'transition probability'.

In this book, the relaxation-induced transition probabilities between energy eigenstates are denoted on energy level diagrams using *dashed arrows*:

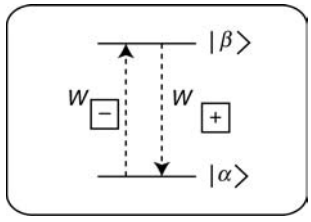

Figure 20.13
Transition probabilities in two directions.

This notation should not be confused with the solid grey arrows used for coherences; as described in Section 11.2, coherences do *not* imply transitions between energy eigenstates, whereas transition probability arrows do.

The subscripts $\boxed{+}$ and $\boxed{-}$ used in the notation for transition probabilities refer to the change in the angular momentum along the z-axis, not to the change in energy. For spins with positive γ, the transition arrow for $W_{\boxed{+}}$ points *down*.

It is possible to derive the transition probabilities for the random field model from first principles (see *Further Reading*). I will state the result without proof:

$$W_{\boxed{-}} = W_{\boxed{+}} = \frac{1}{2}\gamma^2 \left\langle B_x^2 \right\rangle \mathcal{J}(\omega^0) \tag{20.6}$$

The transition probabilities in the two directions are predicted to be equal, and are proportional to the spectral density of the random field at the Larmor frequency ω^0:

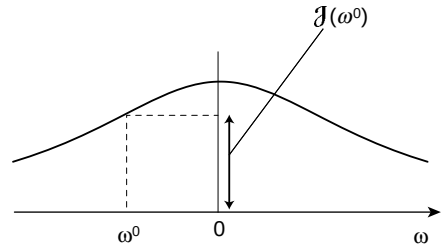

Figure 20.14
For a fluctuating random field, the transition probabilities are proportional to the spectral density at the Larmor frequency ω^0.

20.3.5 Thermally corrected transition probabilities

The equation for transition probabilities, Equation 20.6, is clearly incorrect in detail. Obviously, a simple model in which the fields fluctuate along a single axis is unrealistic. More realistic relaxation models must take into account the fluctuation of the fields in all three directions, and the dependence of the fields on the polarizations of other nuclear spins.

Furthermore, Equation 20.6 is fundamentally incorrect for a deeper reason. The equation predicts that spins have an equal probability of making a transition from a low energy state to a high energy state, as from a high energy state to a low energy state. If this were true, the spin system would eventually adopt an equilibrium position with equal numbers of spins in the two states. In practice, this does not happen: the equilibrium state of the spin ensemble corresponds to a Boltzmann distribution of populations, with the lower energy state more populated than the upper energy state (see Section 11.3).

Consider the case with $\gamma > 0$, so that $|\alpha\rangle$ is lower in energy than $|\beta\rangle$. The Boltzmann distribution is only stable if the probability $W_{\boxed{-}}$ for transitions from $|\alpha\rangle$ to $|\beta\rangle$ is smaller than the probability $W_{\boxed{+}}$ for transitions from $|\beta\rangle$ to $|\alpha\rangle$. In equilibrium, the flow of population in the two directions must be equal:

$$\rho^{\text{eq}}_{\boxed{\alpha}} W_{\boxed{-}} = \rho^{\text{eq}}_{\boxed{\beta}} W_{\boxed{+}}$$

Here, $\rho^{\text{eq}}_{\boxed{\alpha}}$ and $\rho^{\text{eq}}_{\boxed{\beta}}$ are the thermal equilibrium populations given in Section 11.3. Since $\rho^{\text{eq}}_{\boxed{\alpha}} > \rho^{\text{eq}}_{\boxed{\beta}}$ and $W_{\boxed{-}} < W_{\boxed{+}}$, the equilibrium spin system remains in dynamic balance:

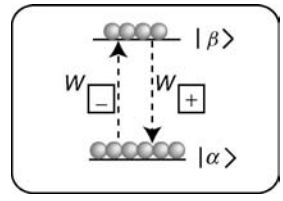

Figure 20.15
The dynamic balance at thermal equilibrium.

In practice, the difference in thermal equilibrium populations is very small (around 10^{-4} or less), so the difference in the two transition probabilities is also of this order of magnitude. Although this difference is small, the existence of thermal equilibrium spin magnetization depends upon it.

Equation 20.6 may be 'fixed' in order to take into account this small imbalance in the transition probabilities. A more accurate version of Equation 20.6 is given by

$$W_{\boxed{-}} = W(1 - \frac{1}{2}\mathbb{B})$$
$$W_{\boxed{+}} = W(1 + \frac{1}{2}\mathbb{B}) \tag{20.7}$$

where the mean transition probability W is

$$W = \frac{1}{2}\gamma^2 \left\langle B_x^2 \right\rangle \mathcal{J}(\omega^0)$$

and $\mathbb{B}$ is the usual Boltzmann factor:

$$\mathbb{B} = \frac{\hbar\gamma B^0}{k_B T}$$

Here, k_B is the Boltzmann constant and T is the temperature of the molecular environment. The 'thermally corrected' transition probabilities given in Equation 20.7 reproduce the correct equilibrium position.

Why does the random field model break down in such a fundamental way? The weak point in the model is the assumption of spin-independent random fields. This assumption sounds plausible, but it fails in a real molecular situation because the energies of the nuclear spins contribute to the total energy of each molecule. In order to raise the energy of the nuclear spin system, energy must be withdrawn from the other degrees of freedom in the molecule, and this has an entropic cost. As a result, processes that raise the energy of the nuclear spin system are slightly less likely than those that decrease the nuclear spin energy. Since the random fields have a molecular origin, they *must* be correlated with the nuclear spin states.

Basically, the motion of the molecules depends slightly on the nuclear spin states, and an accurate relaxation model must take these tiny correlations into account. In practice, this is done by 'fudging' the relaxation equations, on the lines of Equation 20.7. It is difficult to justify this procedure on fundamental grounds, but empirically it is found to give correct results.

The small imbalance in the transition probabilites corresponds to the 'biased wandering motion' of the spin polarizations, introduced in Section 2.6.

20.3.6 Spin–lattice relaxation

Now let us examine how the spin state populations move around under these transition processes.

The kinetic equation for the population of the $|\alpha\rangle$ state is

$$\frac{\mathrm{d}}{\mathrm{d}t}\rho_{\boxed{\alpha}} = -W_{\boxed{-}}\rho_{\boxed{\alpha}} + W_{\boxed{+}}\rho_{\boxed{\beta}}$$

The first term on the right-hand side describes the flow of population out of state $|\alpha\rangle$, through $|\alpha\rangle \rightarrow |\beta\rangle$ transitions, and the second term on the right-hand side describes the flow of population into the state $|\alpha\rangle$, through $|\beta\rangle \rightarrow |\alpha\rangle$ transitions.

Similarly, the kinetic equation for the population of the $|\beta\rangle$ state is

$$\frac{\mathrm{d}}{\mathrm{d}t}\rho_{\boxed{\beta}} = +W_{\boxed{-}}\rho_{\boxed{\alpha}} - W_{\boxed{+}}\rho_{\boxed{\beta}}$$

The z-component of the spin magnetization vector is proportional to the difference in the spin state populations, as described in Section 11.5:

$$M_z = 2\mathbb{B}^{-1}(\rho_{\boxed{\alpha}} - \rho_{\boxed{\beta}}) \tag{20.8}$$

It follows that the z-component of the normalized magnetization vector has the following equation of motion:

$$\begin{aligned}\frac{\mathrm{d}}{\mathrm{d}t}M_z &= 2\mathbb{B}^{-1}\left(\frac{\mathrm{d}}{\mathrm{d}t}\rho_{\boxed{\alpha}} - \frac{\mathrm{d}}{\mathrm{d}t}\rho_{\boxed{\beta}}\right)\\ &= 4\mathbb{B}^{-1}(-W_{\boxed{-}}\rho_{\boxed{\alpha}} + W_{\boxed{+}}\rho_{\boxed{\beta}})\\ &= -2W(M_z - 1)\end{aligned}$$

The last line follows by using $\rho_{\boxed{\alpha}} + \rho_{\boxed{\beta}} = 1$, and Equations 20.7 and 20.8.

The equation of motion may be integrated to get

$$M_z(\tau) = (M_z(0) - 1)\,\mathrm{e}^{-2W\tau} + 1$$

which is exactly the same as that given in Equation 11.45, provided the spin–lattice relaxation rate constant is set equal to

$$T_1{}^{-1} = 2W \tag{20.9}$$

The spin–lattice relaxation rate constant is equal to twice the mean transition probability per unit time between the states.

For the model of a fluctuating random field along the x-axis, this implies the following expression for the spin–lattice relaxation rate constant:

$$T_1{}^{-1} = \gamma^2 \left\langle B_x^2 \right\rangle \mathcal{J}(\omega^0) = \gamma^2 \left\langle B_x^2 \right\rangle \frac{\tau_c}{1 + (\omega^0\tau_c)^2}$$

If we plot the spin–lattice relaxation time constant against the correlation time τ_c, we get the following curve:

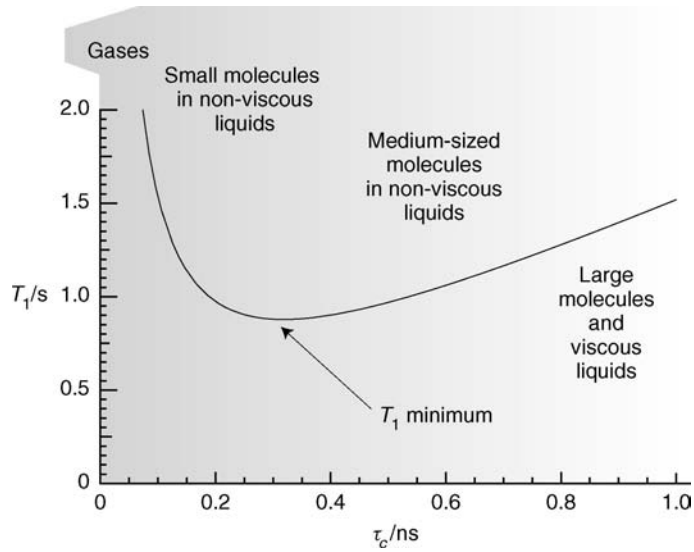

Figure 20.16
The spin–lattice relaxation time constant as a function of correlation time for random field fluctuations. Typical ranges of correlation time are shown.

(This curve is calculated for protons in a static field of 11.74 T, with a fluctuating random field of mean square amplitude $\langle B_x^2 \rangle = 10^{-8}\,\mathrm{T}^2$.) There is a certain correlation time τ_c for which relaxation is most efficient. In the example above, the T_1 minimum occurs at $\tau_c \cong 0.32$ ns.

Figure 20.16 shows typical ranges of correlation times around room temperature. Molecules in gases have the lowest correlation times, followed by small molecules in non-viscous liquids. Large molecules, or molecules in viscous liquids, have correlation times of several nanoseconds at room temperature.

It is a fortuitous circumstance that the most common experimental situation in solution NMR, namely medium-size molecules in non-viscous solutions near room temperature, falls close to the T_1 minimum. The small values of T_1 permit more rapid averaging of NMR signals, and hence a relatively high signal-to-noise ratio within a given experimental time (see Section 5.2).

The physical reason for the T_1 minimum may be seen from the spectral density plots. If we plot the spectral density against frequency for a set of correlation times τ_c, one sees that the spectral density at a certain frequency ω^0 first rises when τ_c is increased from a very small value. The following plots show the spectral density at the proton Larmor frequency $\omega^0/2\pi = -500$ MHz:

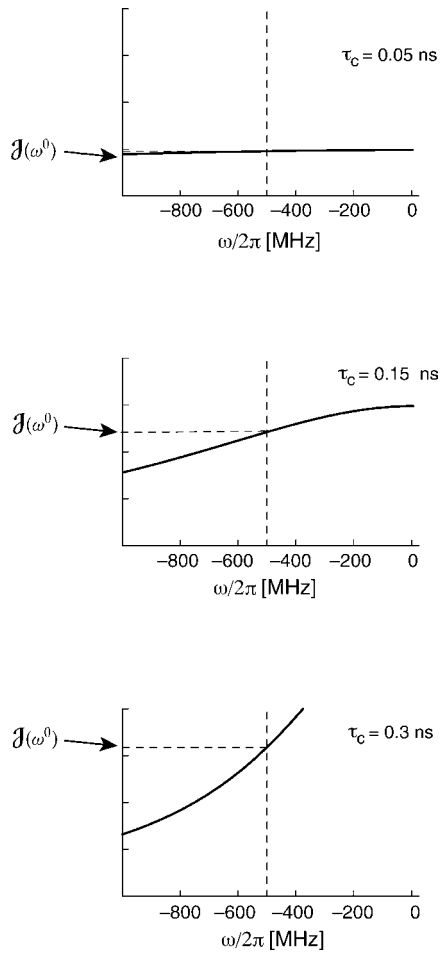

Figure 20.17
Spectral density as a function of correlation time, for fluctuations faster than the T_1 minimum.

The spectral density falls again as τ_c is increased beyond the optimum value, as shown below:

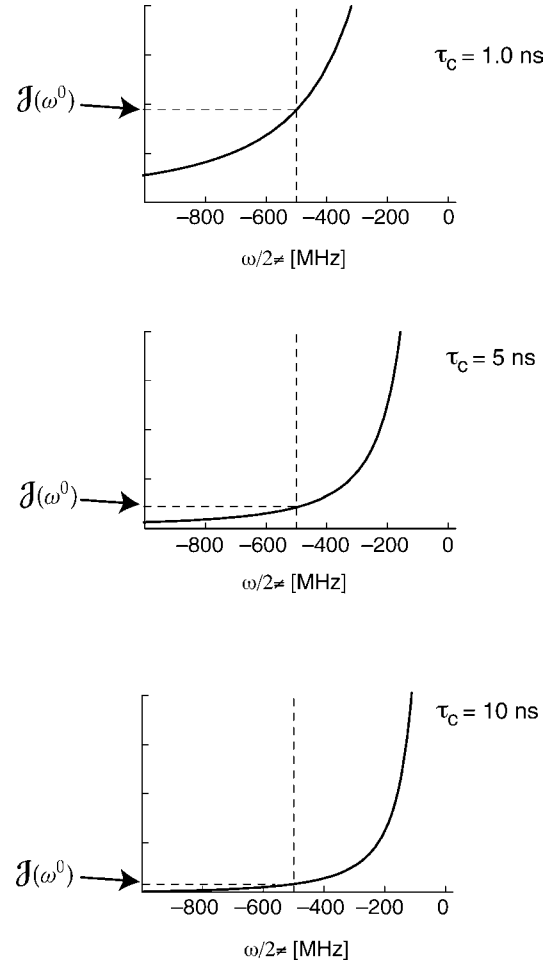

Figure 20.18
Spectral density as a function of correlation time, for fluctuations slower than the T_1 minimum.

At short correlation times τ_c, the spectrum of the fluctuations is very broad, so that the value of $\mathcal{J}$ at any particular frequency is small. At long correlation times, the spectral density function is sharply peaked around $\omega = 0$, so the value of $\mathcal{J}$ at any high frequency is again small. Relaxation is most efficient at an intermediate value of τ_c, where the spectral density function is neither too broad nor too narrow.

In practice, the spin–lattice relaxation time constant T_1 depends on temperature. This is because the random field fluctuations originate in the molecular environment, and the correlation time τ_c is temperature dependent. Warming the sample makes the fluctuations faster, reducing the correlation time, whereas cooling the sample slows down the fluctuations, lengthening the correlation time. The effect of temperature on T_1 depends on the location of τ_c with respect to the T_1 minimum. For systems with *long* correlation times (typically, viscous solutions or large molecules), warming the sample generally *reduces* the spin–lattice relaxation time constant T_1:

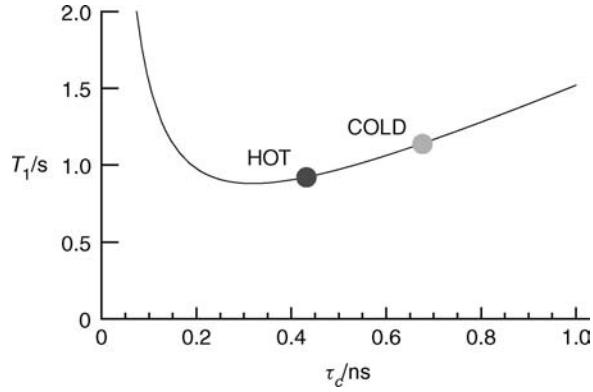

Figure 20.19
For systems with a long correlation time, warming the sample reduces T_1.

For systems with *short* correlation times (typically, small molecules in non-viscous solutions), warming the sample generally *increases* the spin–lattice relaxation time constant T_1:

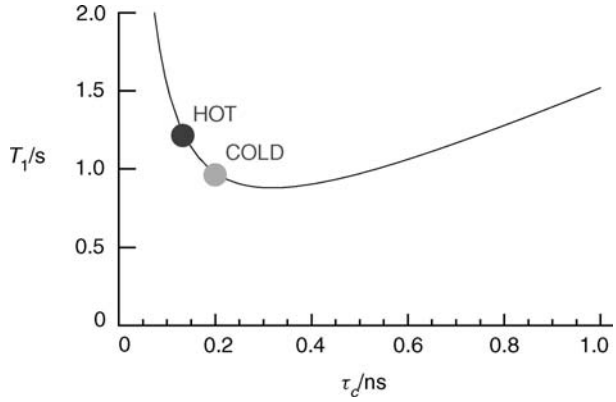

Figure 20.20
For systems with a long correlation time, warming the sample increases T_1.

The value of T_1 is also field-dependent, since the Larmor frequency ω^0 is proportional to the field B^0.

Although these results are quantitative only for a simplified model of relaxation, the general conclusions are qualitatively valid in realistic cases.

20.4 Dipole–Dipole Relaxation

For spins-1/2, the most important relaxation mechanism is usually the through-space dipolar coupling between the spins. The secular part of the coupling averages to zero in isotropic liquids, but the non-secular parts are still capable of causing relaxation.[2]

20.4.1 Rotational correlation time

In a liquid, the magnetic fields exerted by spins on each other are modulated by the random molecular tumbling. The correlation time of the random fields τ_c corresponds to the *rotational correlation time* of the molecules. The rotational correlation time is given (roughly) by the average time taken for the molecules to rotate by 1 rad.[3] Generally speaking, small molecules have short rotational correlation times, whereas large molecules have long rotational correlation times:

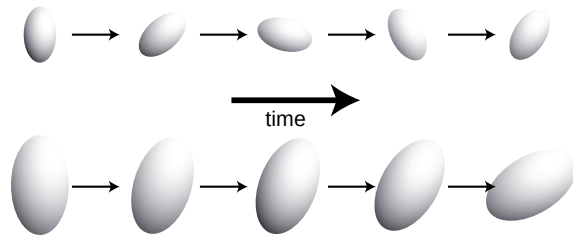

Figure 20.21
In the same time interval, a small molecule rotates more than a large molecule.

The rotational correlation time is also influenced by the viscosity of the liquid (increasing viscosity increases the rotational correlation time) and by temperature (increasing temperature reduces the rotational correlation time).

20.4.2 Transition probabilities

Consider an ensemble of weakly coupled homonuclear AX spin systems, each consisting of a spin I_1 coupled to a spin I_2. There are four energy eigenstates, and hence 12 different transition probabilities, in general. There are eight single-quantum transitions, each with different probabilities:

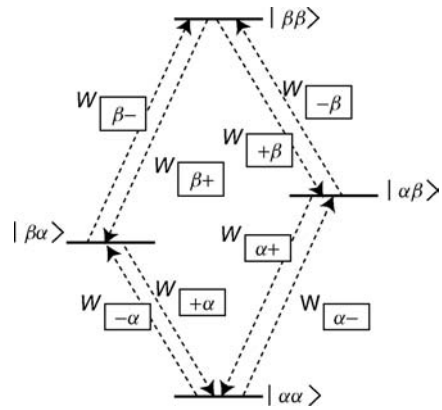

Figure 20.22
Single-quantum transition probabilities in a homonuclear AX system.

There are four double- and zero-quantum transitions, which also have different probabilities.

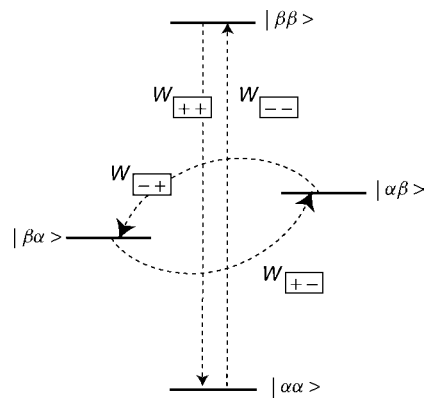

Figure 20.23
Double- and zero-quantum transition probabilities in a homonuclear AX system.

The notation resembles that used for coherences, but recall that coherences do *not* involve transitions between states, whereas spin–lattice relaxation processes do.

Suppose that each molecule only contains two spins of the same type and that the *only* relaxation mechanism is the intramolecular dipole–dipole interaction of these spins with each other. In this case, the following relationships exist between the transition probabilities (see *Further Reading*):

$$\begin{aligned} W_{\boxed{+\alpha}} = W_{\boxed{+\beta}} = W_{\boxed{\alpha+}} = W_{\boxed{\beta+}} &= W_1(1+\tfrac{1}{2}\mathbb{B}) \\ W_{\boxed{-\alpha}} = W_{\boxed{-\beta}} = W_{\boxed{\alpha-}} = W_{\boxed{\beta-}} &= W_1(1-\tfrac{1}{2}\mathbb{B}) \\ W_{\boxed{++}} &= W_2(1+\mathbb{B}) \\ W_{\boxed{--}} &= W_2(1-\mathbb{B}) \\ W_{\boxed{+-}} = W_{\boxed{-+}} &= W_0 \end{aligned} \tag{20.10}$$

Here, W_1 is the *single-quantum transition probability*. Detailed calculation (see *Further Reading*) provides the following result:

$$W_1 = \frac{3}{20} b^2 \mathcal{J}(\omega^0) \tag{20.11}$$

where the quantity $\mathcal{J}(\omega^0)$ is the spectral density of the dipole–dipole couplings at the Larmor frequency ω^0:

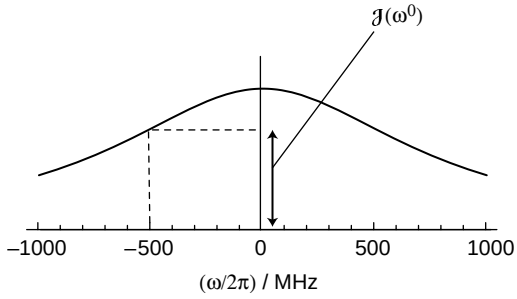

Figure 20.24
Dipole–dipole spectral density at the Larmor frequency $\omega = \omega^0$.

(This and the following plots are shown for protons in a field $B^0 = 11.74\,\mathrm{T}$ and a rotational correlation time $\tau_c = 0.2\,\mathrm{ns}$.) If vibrational motions are ignored, then the dipole–dipole coupling constant is given by

$$b = -\frac{\mu_0}{4\pi}\frac{\hbar\gamma^2}{r^3}$$

where the distance between the spins is denoted r. In practice, the value of the dipole–dipole coupling constant is somewhat smaller than this estimate, because of rapid vibrational and librational motions (see Section 19.4).

The *double-quantum transition probability* W_2 is given by

$$W_2 = \frac{3}{5} b^2 \mathcal{J}(2\omega^0) \tag{20.12}$$

where $\mathcal{J}(2\omega^0)$ is the spectral density at twice the Larmor frequency:

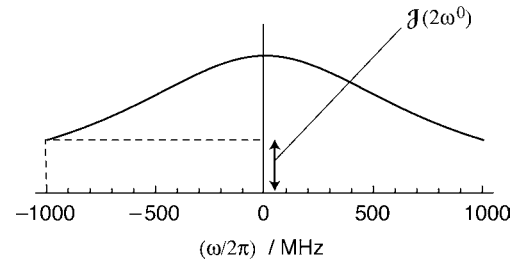

Figure 20.25
Dipole–dipole spectral density at twice the Larmor frequency $\omega = 2\omega^0$.

The *zero-quantum transition probability* W_0 is given by

$$W_0 = \frac{1}{10} b^2 \mathcal{J}(0) \tag{20.13}$$

where $\mathcal{J}(0)$ is the spectral density at zero frequency:

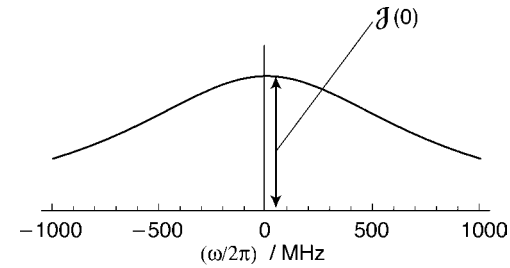

Figure 20.26
Dipole-dipole spectral density at zero frequency $\omega = 0$.

The factors $\mathbb{B}$ in Equation 20.10 provide thermal corrections of the transition probabilities, as in Section 20.3.5. These factors ensure the correct thermal equilibrium state of the AX ensemble, as described in Section 15.7.

All of the transition probabilities depend on the square of the dipole–dipole coupling, and hence on the *inverse sixth power of the internuclear distance*:

$$W \propto r^{-6} \tag{20.14}$$

This very important relationship summarizes the principle behind the determination of molecular structure by NMR in isotropic liquids.

These equations predict that, for *short* rotational correlation times (typically, small molecules in non-viscous solutions), the transition probabilities have the following relationship:

$$W_2 > W_1 > W_0 \qquad \text{(short } \tau_c\text{)}$$

For short τ_c, the spectral density function $\mathcal{J}(\omega)$ is almost independent of ω, and the numerical factors in Equations 20.11–20.13 govern the relative magnitude of the transition probabilities.

For long rotational correlation times, on the other hand (typically, for large molecules or for viscous solutions), the transition probabilities have the following relationship:

$$W_0 > W_1 > W_2 \qquad \text{(long } \tau_c\text{)}$$

In this case, the peaked form of $\mathcal{J}(\omega)$ around $\omega = 0$ governs the magnitude of the transition probabilities.

The importance of the spectral density at *twice* the Larmor frequency is striking and demands a physical explanation. What's going on?

The basic reason for the $2\omega^0$ terms is the geometry of the dipolar local field. To see this, consider a molecule containing two spins, I_1 and I_2. Suppose that the molecule is oriented so that the vector joining the two spins is in the plane of the paper, and suppose that the angular momentum of spin I_1 is also in the same plane. The angular momentum of spin I_2 is assumed to be perpendicular to the plane of the paper. We view the dipolar magnetic field emanating from spin I_1, and the local field experienced by spin I_2:

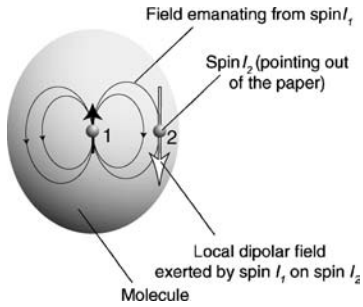

Figure 20.27
Local fields in a molecule.

Suppose, now, that the molecule rotates in the plane of the paper. Keep the polarization of spin I_1 fixed and follow carefully the motion of the local field at spin I_2 (indicated by the white arrow):

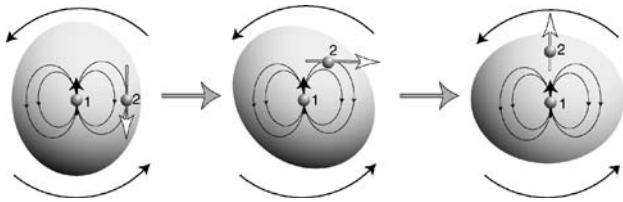

Figure 20.28
Rotation of the local field as the molecule rotates, keeping the spin polarization fixed.

Although the molecule rotates by $\pi/4$ between snapshots, the local dipolar field rotates by roughly $\pi/2$ each time. This implies that, to a good approximation, molecular rotation at the frequency ω modulates the dipolar field at the frequency 2ω. The fluctuation frequency of the dipole–dipole couplings is effectively doubled by this effect. *The $\mathcal{J}(2\omega^0)$ term in the dipole–dipole spectral density is mainly produced by molecular rotations at the Larmor frequency ω^0.*

Now let's take into account the precession of the spins in the magnetic field. Assume that the static magnetic field is coming out of the plane of the paper, and allow spin I_1 to precess around the magnetic field (in the negative sense, assuming $\gamma > 0$). Initially, we keep the molecule fixed and then see what effect the precession of spin I_1 has on the local field at spin I_2:

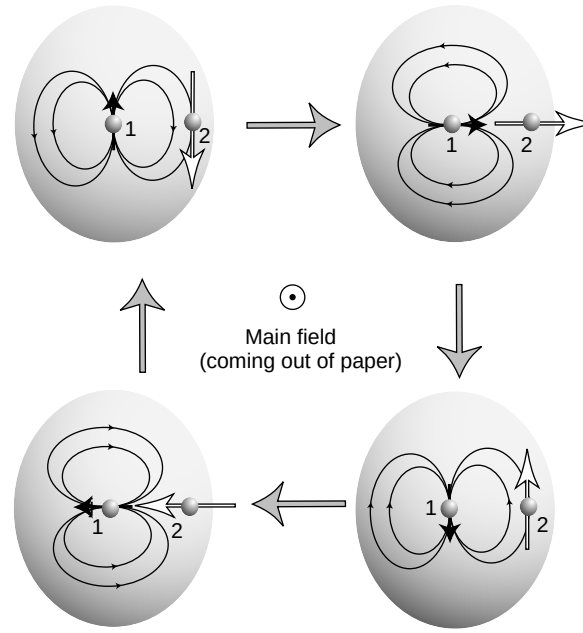

Figure 20.29
Rotation of the local field as spin I_1 precesses, keeping the molecule fixed.

(The snapshots are taken at intervals separated by one-quarter of a Larmor period.) Notice that although spin I_1 precesses in the *negative* sense around the main field, the local field at spin I_2 rotates in the *positive* sense, i.e. at the frequency $-\omega^0$. As discussed in Section 8.4.2, a field rotating in the opposite sense to the Larmor precession is ineffective in inducing spin transitions. Figure 20.29 implies that the precession of the spins in the field does not *by itself* induce transitions of neighbouring spins (at least in this molecular orientation). Molecular motion is necessary for spin–lattice relaxation through dipole–dipole couplings.

Now combine the modulation of the local fields by spin precession with the molecular motion at the Larmor frequency (which is associated with the $\mathcal{J}(2\omega^0)$ term, as discussed above). If the above diagram is repeated, while allowing the molecule to rotate at the same time as the spin precesses, we get the picture shown in Figure 20.30. This shows that a combination of spin precession and molecular motion can generate a local field at spin I_2 that rotates at the Larmor frequency ω^0. This is the correct frequency, and the correct sense of rotation, for transitions of spin I_2 to be induced by the dipolar coupling to spin I_1.

Intramolecular dipole–dipole relaxation is therefore caused by a complicated combination of spin precession and molecular rotation.

In practice, the modulation by the dipolar couplings involves all possible orientations of the spins and the molecules. Detailed analysis gives rise to the numerical factors in Equations 20.11–20.13 that take into account all of these effects.

20.4.3 Solomon equations

The equation of motion of an individual state population may be derived by taking into account the transition probabilities to the other states. For example, the population of state $|\alpha\alpha\rangle$ is depleted by the transition into state $|\beta\alpha\rangle$ (probability per unit time = $W_{\boxed{-\alpha}}$), the transition into state $|\beta\beta\rangle$ (probability per unit time = $W_{\boxed{--}}$), and the transition into state $|\alpha\beta\rangle$ (probability per unit time = $W_{\boxed{\alpha-}}$). At the same time, the population of state $|\alpha\alpha\rangle$ is replenished by the transition from state $|\beta\alpha\rangle$ (probability per unit time = $W_{\boxed{+\alpha}}$), the transition

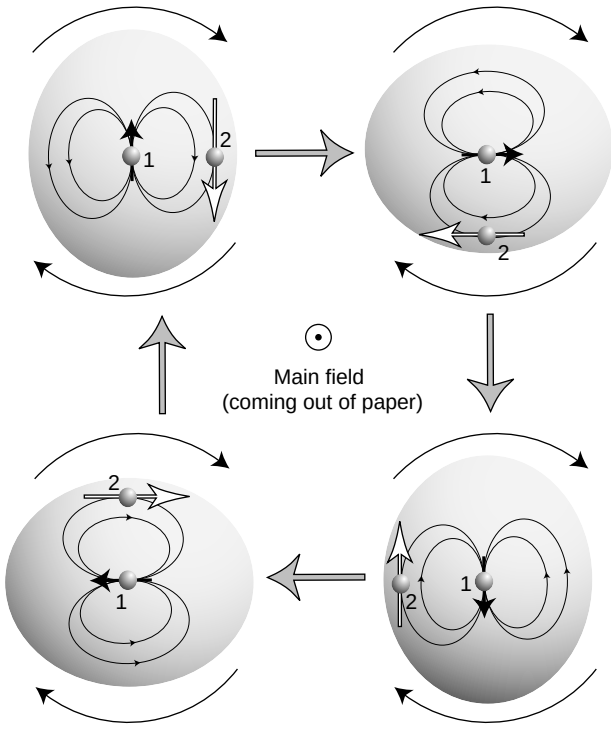

Figure 20.30
The combined effects of molecular rotation and spin precession.

from state $|\beta\beta\rangle$ (probability per unit time = $W_{\boxed{++}}$), and the transition from state $|\alpha\beta\rangle$ (probability per unit time = $W_{\boxed{\alpha+}}$). The kinetic equation for the population of state $|\alpha\alpha\rangle$ is therefore

$$\frac{\mathrm{d}}{\mathrm{d}t}\rho_{\boxed{\alpha\alpha}} = -W_{\boxed{-\alpha}}\rho_{\boxed{\alpha\alpha}} - W_{\boxed{--}}\rho_{\boxed{\alpha\alpha}} - W_{\boxed{\alpha-}}\rho_{\boxed{\alpha\alpha}} + W_{\boxed{+\alpha}}\rho_{\boxed{\beta\alpha}} + W_{\boxed{++}}\rho_{\boxed{\beta\beta}} + W_{\boxed{\alpha+}}\rho_{\boxed{\alpha\beta}}$$

The individual transition probabilities are given by Equation 20.10. Similar equations may be written down for the kinetic equations of the other three populations.

It is convenient to convert the kinetic equations for the populations into kinetic equations for the longitudinal magnetizations of the two types of spin. The longitudinal magnetizations of the two spins I_1 and I_2 are given by

$$\langle \hat{I}_{1z} \rangle = \frac{1}{2}\rho_{\boxed{\alpha\alpha}} - \frac{1}{2}\rho_{\boxed{\beta\alpha}} + \frac{1}{2}\rho_{\boxed{\alpha\beta}} - \frac{1}{2}\rho_{\boxed{\beta\beta}}$$

$$\langle \hat{I}_{2z} \rangle = \frac{1}{2}\rho_{\boxed{\alpha\alpha}} + \frac{1}{2}\rho_{\boxed{\beta\alpha}} - \frac{1}{2}\rho_{\boxed{\alpha\beta}} - \frac{1}{2}\rho_{\boxed{\beta\beta}}$$

As shown in Appendix A.15, these equations may be rewritten in terms of the *Solomon equations* for the relaxation of the two-spin system:[4]

$$\frac{\mathrm{d}}{\mathrm{d}t}\begin{pmatrix} \langle \hat{I}_{1z} \rangle \\ \langle \hat{I}_{2z} \rangle \end{pmatrix} = \begin{pmatrix} -R_{\mathrm{auto}} & R_{\mathrm{cross}} \\ R_{\mathrm{cross}} & -R_{\mathrm{auto}} \end{pmatrix} \begin{pmatrix} \langle \hat{I}_{1z} \rangle - \langle \hat{I}_{1z} \rangle^{\mathrm{eq}} \\ \langle \hat{I}_{2z} \rangle - \langle \hat{I}_{2z} \rangle^{\mathrm{eq}} \end{pmatrix} \tag{20.15}$$

The terms $\langle \hat{I}_{1z} \rangle^{eq}$ and $\langle \hat{I}_{2z} \rangle^{eq}$ in Equation 20.15 are the thermal equilibrium expectation values of the angular momentum operators, and are given by

$$\langle \hat{I}_{1z} \rangle^{eq} = \langle \hat{I}_{2z} \rangle^{eq} = \frac{1}{4}\mathbb{B}$$

as given in Section 15.7.

R_{auto} is called the *leakage rate constant* or *auto-relaxation rate constant*, and is given by

$$R_{auto} = W_0 + 2W_1 + W_2 \tag{20.16}$$

or in terms of the spectral densities as

$$R_{auto} = \frac{1}{10} b^2 \left\{ \mathcal{J}(0) + 3\mathcal{J}(\omega^0) + 6\mathcal{J}(2\omega^0) \right\}$$

The auto-relaxation rate constant has the following dependence on the rotational correlation time τ_c:

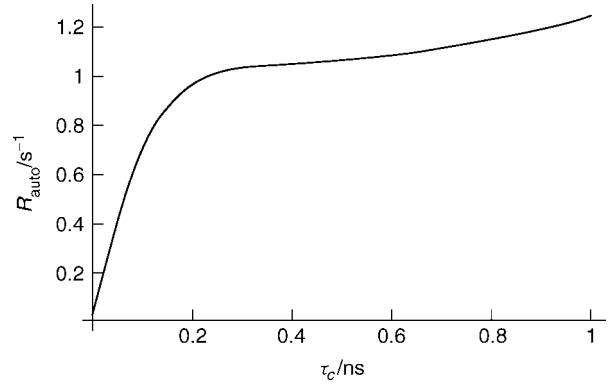

Figure 20.31
Variation of the auto-relaxation rate constant with correlation time.

(Calculated for two protons separated by 0.2 nm, in a field of 11.74 T.)

The term R_{cross} is called the *cross-relaxation rate constant*, and is given by[4]

$$R_{cross} = W_0 - W_2 \tag{20.17}$$

or in terms of the spectral densities as

$$R_{cross} = \frac{1}{10} b^2 \left\{ \mathcal{J}(0) - 6\mathcal{J}(2\omega^0) \right\}$$

The cross-relaxation rate constant R_{cross} has a strong dependence on the rotational correlation time and changes sign as τ_c is increased:

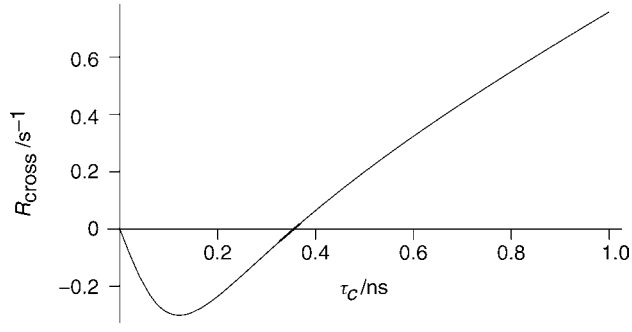

Figure 20.32
Variation of the cross-relaxation rate constant with correlation time.

(Calculated for two protons separated by 0.2 nm, in a field of 11.74 T.) The cross-relaxation rate constant R_{cross} is negative for short correlation times (small molecules in non-viscous solution), but is positive for long correlation times (large molecules, or for molecules in viscous solutions).

The cross-relaxation rate constant vanishes at the *critical correlation time*, given by

$$\tau_c^{\text{crit}} = |\frac{\sqrt{5}}{2\omega^0}| \tag{20.18}$$

Many smallish and medium-sized molecules are often close to this condition. Large molecules, on the other hand, usually have $\tau_c >> \tau_c^{\text{crit}}$, and have large (positive) cross-relaxation rate constants R_{cross}.

Cross-relaxation is an essential component of the important NOESY experiment, as discussed in Section 20.6.

20.4.4 Longitudinal relaxation

Using the Solomon equations, one can figure out how the spin system relaxes, starting from an arbitrary configuration of spin state populations.

As a first example, let's calculate the relaxation of the *sum* z-angular momentum of the two spins, i.e. $\langle \hat{I}_z \rangle = \langle \hat{I}_{1z} \rangle + \langle \hat{I}_{2z} \rangle$. From the Solomon equations, the equation of motion of the sum z-angular momentum is given by

$$\begin{aligned}\frac{\mathrm{d}}{\mathrm{d}t}\langle \hat{I}_z \rangle &= \frac{\mathrm{d}}{\mathrm{d}t}\langle \hat{I}_{1z} \rangle + \frac{\mathrm{d}}{\mathrm{d}t}\langle \hat{I}_{2z} \rangle \\ &= -R_{\text{auto}}(\langle \hat{I}_{1z} \rangle - \frac{1}{4}\mathbb{B}) + R_{\text{cross}}(\langle \hat{I}_{2z} \rangle - \frac{1}{4}\mathbb{B}) \\ &\quad + R_{\text{cross}}(\langle \hat{I}_{1z} \rangle - \frac{1}{4}\mathbb{B}) - R_{\text{auto}}(\langle \hat{I}_{2z} \rangle - \frac{1}{4}\mathbb{B})\end{aligned}$$

If intramolecular dipole–dipole couplings are the only relaxation mechanism, then we get

$$\frac{\mathrm{d}}{\mathrm{d}t}\langle \hat{I}_z \rangle = -R_{\text{sum}}(\langle \hat{I}_z \rangle - \langle \hat{I}_z \rangle^{\text{eq}}) \tag{20.19}$$

where the relaxation rate constant for the sum magnetization is

$$R_{\text{sum}} = R_{\text{auto}} - R_{\text{cross}} = 2W_1 + 2W_2 \tag{20.20}$$

Equation 20.19 may be integrated to obtain the trajectory of the sum longitudinal magnetization. If two time points t_a and t_b are separated by an interval $\tau = t_b - t_a$ (in which no r.f. fields are applied), then the sum longitudinal magnetization at the later time point t_b is given by

$$\langle \hat{I}_z \rangle(t_b) = \left(\langle \hat{I}_z \rangle(t_a) - \langle \hat{I}_z \rangle^{\text{eq}}\right) \exp\{-R_{\text{sum}}\tau\} + \langle \hat{I}_z \rangle^{\text{eq}}$$

where R_{sum} is given by Equation 20.20. This describes the usual exponential recovery of the sum longitudinal magnetization, as described in Section 11.9.2. The spin–lattice relaxation rate constant for the two-spin system is therefore given by

$$T_1{}^{-1} = R_{\text{sum}} = 2W_1 + 2W_2$$

or in terms of spectral densities as

$$T_1{}^{-1} = \frac{3}{10}b^2\left\{\mathcal{J}(\omega^0) + 4\mathcal{J}(2\omega^0)\right\} \tag{20.21}$$

This simple exponential relaxation behaviour only applies to the relaxation of the *sum* of the longitudinal spin magnetizations. The motion of the *individual* z-magnetization components is more complicated, as described in Section 20.6.

The relaxation time constant T_1 displays the usual minimum as a function of the correlation time, as shown by the following plot (calculated for two protons separated by 0.2 nm, in a field of 11.74 T):

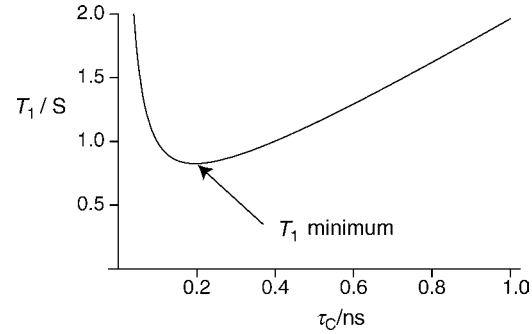

Figure 20.33
Variation of the spin–lattice relaxation time constant with correlation time, for intramolecular dipole–dipole relaxation.

It might appear that Equation 20.21 allows one to estimate the distance between the spins, through a measurement of the spin–lattice relaxation time constant T_1. However, this does not prove to be realistic. First, most molecules contain more than two spins, in which case the expression for T_1 consists of a superposition of many dipole–dipole couplings, and the contributions from individual spin pairs are difficult to disentangle. Second, there are many other relaxation mechanisms, and there is no simple way of distinguishing the dipole–dipole contribution from the others. In summary, the spin–lattice relaxation constant proves to be a poor source of information on molecular geometry, except in extremely simple cases.

20.4.5 Transverse relaxation

The transverse relaxation rate constant $T_2{}^{-1}$ takes the following value in the case of intramolecular dipole–dipole relaxation:

$$T_2{}^{-1} = \frac{3}{20} b^2 \left\{ 3\mathcal{J}(0) + 5\mathcal{J}(\omega^0) + 2\mathcal{J}(2\omega^0) \right\} \tag{20.22}$$

The relaxation time constants T_1 and T_2 are compared in Figure 20.34:

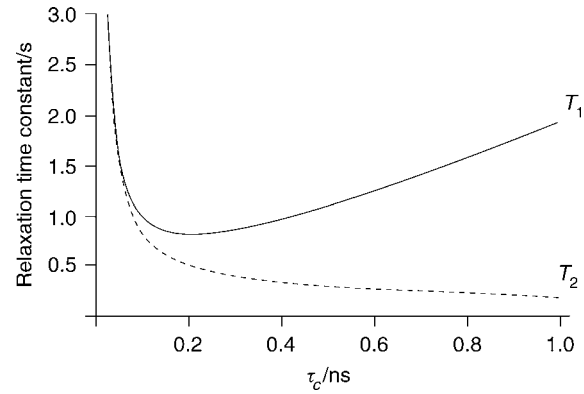

Figure 20.34
Variation of T_1 and T_2 with correlation time, for intramolecular dipole-dipole relaxation.

At very short rotational correlation times, the values of T_1 and T_2 are equal. This is called the *extreme narrowing limit*. As the correlation time is increased, T_1 passes through a minimum and then increases. The transverse relaxation time constant T_2, on the other hand, continues to decrease.

In practice, this means that the NMR peaks get progressively broader as the molecular mass is increased.

For many years, this behaviour was believed to set a fundamental limit on the size of molecule that may be studied by solution NMR. However, the development of the TROSY method (see Section 20.8.4) allows one to overcome the increase in linewidth at large rotational correlation times, at least in favourable cases.

20.5 Steady-State Nuclear Overhauser Effect

The Solomon equations predict a surprising effect: application of a weak r.f. field at the Larmor frequency of one of the spins, for a sufficiently long time, has a strong effect on the longitudinal magnetization of the non-irradiated spins, and, in some cases, even *enhances* the magnetization of those spins.

This is called the *steady-state nuclear Overhauser effect*, or *steady-state NOE* (the original Overhauser effect applied to electrons and nuclei).

In modern NMR, the steady-state NOE is mainly exploited in heteronuclear spin systems, where the enhancement of magnetization can be useful and dramatic. The INADEQUATE pulse sequence, described in Section 16.2, is an example. Therefore, we will treat this effect in the case of an ensemble of heteronuclear AX systems, with a spin species I of gyromagnetic ratio γ_I, coupled to a species S with gyromagnetic ratio γ_S, with $|\gamma_I| > |\gamma_S|$. For example, I could represent protons and S could represent ^{13}C nuclei.

A detailed treatment of dipole–dipole relaxation in the heteronuclear case leads to the following expressions for the transition probabilities:

$$\begin{aligned}
W_{\boxed{+\alpha}} &= W_{\boxed{+\beta}} = W_{1I}(1 + \tfrac{1}{2}\mathbb{B}_I) & W_{\boxed{++}} &= W_2(1 + \tfrac{1}{2}\mathbb{B}_I + \tfrac{1}{2}\mathbb{B}_S) \\
W_{\boxed{-\alpha}} &= W_{\boxed{-\beta}} = W_{1I}(1 - \tfrac{1}{2}\mathbb{B}_I) & W_{\boxed{--}} &= W_2(1 - \tfrac{1}{2}\mathbb{B}_I - \tfrac{1}{2}\mathbb{B}_S) \\
W_{\boxed{\alpha+}} &= W_{\boxed{\beta+}} = W_{1S}(1 + \tfrac{1}{2}\mathbb{B}_S) & W_{\boxed{+-}} &= W_0(1 + \tfrac{1}{2}\mathbb{B}_I - \tfrac{1}{2}\mathbb{B}_S) \\
W_{\boxed{\alpha-}} &= W_{\boxed{\beta-}} = W_{1S}(1 - \tfrac{1}{2}\mathbb{B}_S) & W_{\boxed{-+}} &= W_0(1 - \tfrac{1}{2}\mathbb{B}_I + \tfrac{1}{2}\mathbb{B}_S)
\end{aligned} \tag{20.23}$$

The Boltzmann factors $\mathbb{B}_I$ and $\mathbb{B}_S$ are required in order to reproduce the correct thermal equilibrium state (see Section 16.3):

$$\hat{\rho}^{\text{eq}} = \frac{1}{4}\hat{1} + \frac{1}{4}\mathbb{B}_I\hat{I}_z + \frac{1}{4}\mathbb{B}_S\hat{S}_z \tag{20.24}$$

Since $\mathbb{B}_I/\mathbb{B}_S = \gamma_I/\gamma_S$, the thermal equilibrium polarization of the I-spins is larger than that of the S-spins, by a factor γ_I/γ_S.

The single-quantum transition probabilities are given by

$$W_{1I} = \frac{3}{20}b_{IS}^2\mathcal{J}(\omega_I^0) \qquad W_{1S} = \frac{3}{20}b_{IS}^2\mathcal{J}(\omega_S^0)$$

while the double- and zero-quantum transition probabilities are equal to

$$W_2 = \frac{3}{5}b_{IS}^2\mathcal{J}(\omega_I^0 + \omega_S^0) \qquad W_0 = \frac{1}{10}b_{IS}^2\mathcal{J}(\omega_I^0 - \omega_S^0)$$

where the dipole–dipole coupling constant is given in Equation 9.32.

In the heteronuclear case, the spectral density of the dipole–dipole coupling is sampled at four different frequencies:

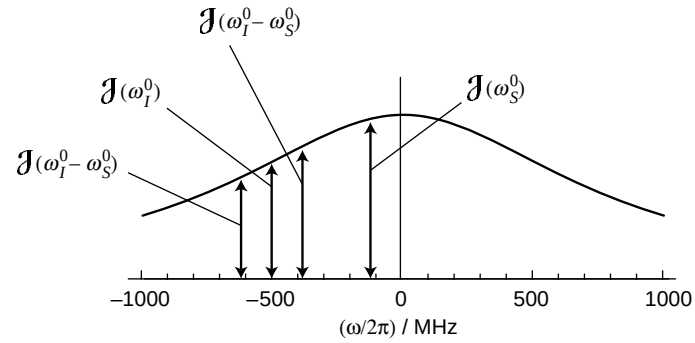

Figure 20.35
Spectral densities in a heteronuclear spin pair.

(This plot is shown for $I = {}^1\mathrm{H}$ and $S = {}^{13}\mathrm{C}$, in a field of $B^0 = 11.74\,\mathrm{T}$.)

Now assume that a continuous r.f. field is applied at the I-spin Larmor frequency, inducing transitions across two pairs of energy levels:

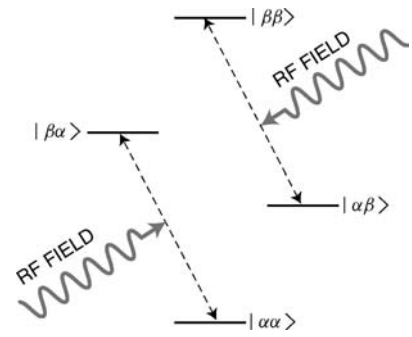

Figure 20.36
Irradiation of two pairs of transitions in a steady-state NOE experiment.

Assume that, after sufficient time, the r.f. field equalizes the populations across the irradiated transitions, so that one may write

$$\rho^{\mathrm{ss}}_{\boxed{\alpha\alpha}} = \rho^{\mathrm{ss}}_{\boxed{\beta\alpha}} = A$$
$$\rho^{\mathrm{ss}}_{\boxed{\alpha\beta}} = \rho^{\mathrm{ss}}_{\boxed{\beta\beta}} = B \qquad (20.25)$$

where A and B are as yet unknown. The superscript 'ss' stands for 'steady state', implying that, after sufficiently long r.f. irradiation, the populations settle into steady-state values, which do not change any more, as long as the r.f. field is left on.

The fact that the populations equalize after a sufficiently long interval of resonant irradiation is called *saturation*. It is presented here as an assumption, but it may be justified theoretically, for sufficiently strong r.f. fields, by using a more sophisticated analysis of the combined effects of r.f. irradiation and relaxation.

Equation 20.25 allows us to deduce the steady-state populations A and B by simple kinetic arguments. In the steady state, the flux into the pair of populations $\rho_{\boxed{\alpha\alpha}}$ and $\rho_{\boxed{\beta\alpha}}$ is equal to the flux out. Similarly, the flux into the pair of populations $\rho_{\boxed{\alpha\beta}}$ and $\rho_{\boxed{\beta\beta}}$ is equal to the flux out.

The flux *into* the $\{\rho_{\boxed{\alpha\alpha}}, \rho_{\boxed{\beta\alpha}}\}$ pair is given by

$$\text{flux in} = (W_{\boxed{\beta+}} + W_{\boxed{++}} + W_{\boxed{-+}} + W_{\boxed{\alpha+}})B$$

as may be seen from the following diagram:

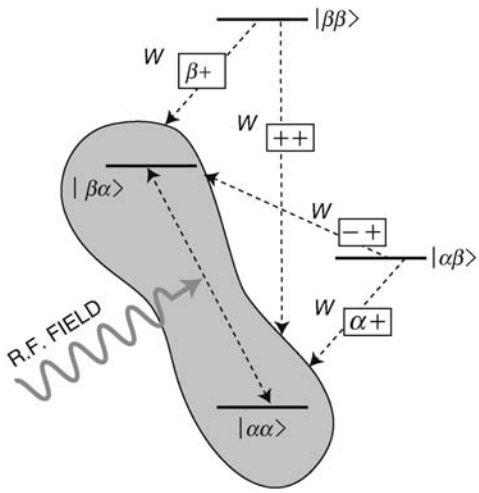

Figure 20.37
Population flux into one pair of states in a steady-state NOE experiment.

Similarly, the flux *out* of the $\{\rho_{\boxed{\alpha\alpha}}, \rho_{\boxed{\beta\alpha}}\}$ pair is given by

$$\text{flux out} = (W_{\boxed{\beta-}} + W_{\boxed{--}} + W_{\boxed{+-}} + W_{\boxed{\alpha-}})A$$

as shown below:

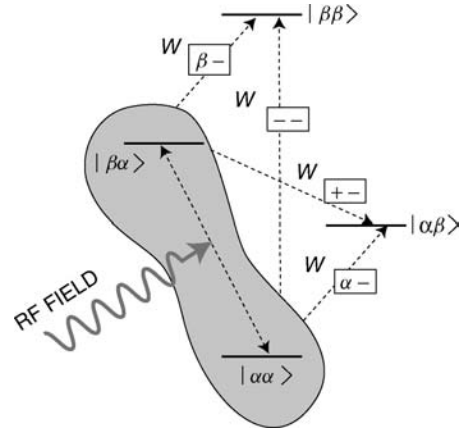

Figure 20.38
Population flux out of a pair of states in a steady-state NOE experiment.

At the steady state:

$$\text{flux in} = \text{flux out} \tag{20.26}$$

In addition, the sum of all populations is equal to one:

$$2A + 2B = 1 \tag{20.27}$$

Equations 20.26 and 20.27 may be solved and the transition probabilities in Equation 20.23 substituted in. By using the fact that $\mathbb{B}_I$ and $\mathbb{B}_S$ are very small, we get after some manipulations:

$$\rho^{\text{ss}}_{\boxed{\alpha\alpha}} = \rho^{\text{ss}}_{\boxed{\beta\alpha}} \cong \frac{1}{4}\left(1 + \epsilon_{\text{NOE}}\frac{1}{2}\mathbb{B}_S\right)$$

$$\rho^{\text{ss}}_{\boxed{\alpha\beta}} = \rho^{\text{ss}}_{\boxed{\beta\beta}} \cong \frac{1}{4}\left(1 - \epsilon_{\text{NOE}}\frac{1}{2}\mathbb{B}_S\right)$$

where the *NOE enhancement factor* ϵ_{NOE} is given by[5]

$$\epsilon_{\text{NOE}} = 1 + \frac{\gamma_I}{\gamma_S}\frac{W_2 - W_0}{W_0 + 2W_{1S} + W_2} \tag{20.28}$$

The steady-state spin density operator is

$$\hat{\rho}^{\text{ss}} = \frac{1}{4}\widehat{1} + \epsilon_{\text{NOE}}\frac{1}{4}\mathbb{B}_S\hat{S}_z$$

By comparing with Equation 20.24, one sees that the S-spin magnetization is enhanced by a factor ϵ_{NOE}, compared with its thermal equilibrium value.

The NOE enhancement factor depends on the correlation time, and hence the motion of the molecules. In the limit of very rapid molecular motion (small values of τ_c), the enhancement factor is given by

$$\epsilon_{\text{NOE}}(\text{fast motion}) = 1 + \frac{\gamma_I}{2\gamma_S}$$

This factor is equal to 2.99 for the case $I = {}^1\text{H}$ and $S = {}^{13}\text{C}$, and -3.93 for the case $I = {}^1\text{H}$ and $S = {}^{15}\text{N}$, implying that the ^{15}N magnetization changes sign when the ^{1}H spins are saturated.

The enhancement factor is reduced if the molecular motion is slow. In the limit of slow molecular motion (very large values of τ_c), the enhancement factor is given by

$$\epsilon_{\text{NOE}}(\text{very slow motion}) = \frac{(\gamma_I^2 - \gamma_S^2)(3\gamma_I^2 + 5\gamma_I\gamma_S - 10\gamma_S^2)}{3\gamma_I^4 + \gamma_I^2\gamma_S^2 - 10\gamma_I\gamma_S^3 + 10\gamma_S^4}$$

This factor is equal to 1.153 for the case $I = {}^1\text{H}$ and $S = {}^{13}\text{C}$, and 0.783 for the case $I = {}^1\text{H}$ and $S = {}^{15}\text{N}$. For very slow molecular motion, the ^{13}C magnetization is only slightly enhanced by ^{1}H irradiation, and for the case of ^{15}N the magnetization is reduced by ^{1}H irradiation. The following plot shows the variation of ϵ_{NOE} with τ_c, for $I = {}^1\text{H}$ and $S = {}^{13}\text{C}$ or ^{15}N in a field of $B^0 = 11.74\,\text{T}$:

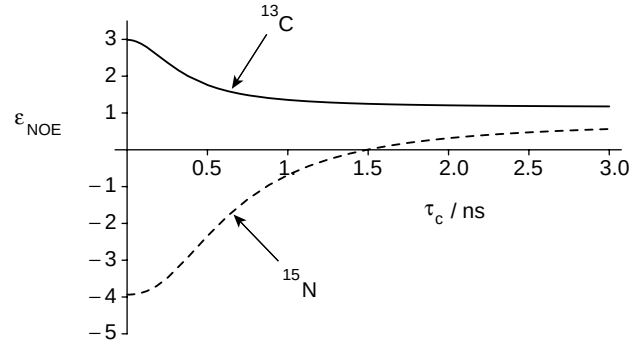

Figure 20.39
Variation of steady-state NOE as a function of correlation time, for ^{13}C–^{1}H and ^{15}N–^{1}H pairs.

Note that the sign of the steady-state ^{15}N magnetization changes sign as the molecular motion is slowed down.

In practice, the spin relaxation is not purely due to the heteronuclear dipole–dipole interaction. The presence of additional relaxation mechanisms further reduces the steady-state magnetization.

The steady-state NOE gives smaller theoretical enhancements than the INEPT method (see Section 16.3), and is sensitive to the details of the relaxation mechanisms and the molecular motion. Nevertheless, the technique is useful for positive-γ nuclei, such as ^{13}C, where it is more simple and reliable than the INEPT method, and has the advantage of not requiring a resolved J-coupling. For negative-γ nuclei, such as ^{15}N, on the other hand, saturation of the protons often destroys the ^{15}N magnetization rather than enhancing it.

20.6 NOESY

The cross-relaxation phenomenon is used in the NOESY experiment, which is one of the most widely used NMR methods for determining the structures of molecules in solution.

NOESY stands for *Nuclear Overhauser Effect Spectroscopy*.[6]

20.6.1 NOESY pulse sequence

The basic NOESY pulse sequence is precisely the same as that used in two-dimensional exchange spectroscopy, described in Section 19.7. The pulse sequence diagram is repeated here:

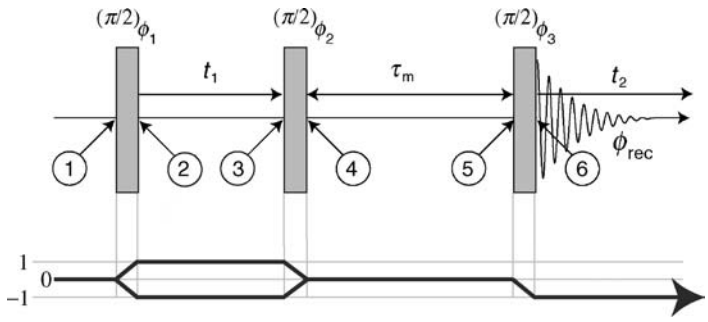

Figure 20.40
NOESY pulse sequence.

The phase cycle[7] is specified in Table 19.1.

20.6.2 NOESY signal

Consider an ensemble of homonuclear two-spin systems, in which the spins have chemical shift frequencies Ω_1^0 and Ω_2^0. The spins within each pair are assumed to be close in space, but have no J-coupling with each other.

The density operator may be calculated from time point ① to time point ④ as follows:

$$\begin{aligned}
\hat{\rho}_{①} &= \hat{I}_{1z} + \hat{I}_{2z} \\
&\Big\downarrow (\pi/2)_x \\
\hat{\rho}_{②} &= -\hat{I}_{1y} - \hat{I}_{2y} \\
&\Big\downarrow t_1 \\
\hat{\rho}_{③} &= \left(-\hat{I}_{1y}\cos(\Omega_1^0 t_1) + \hat{I}_{1x}\sin(\Omega_1^0 t_1)\right)\ \exp\{-\lambda t_1\} \\
&\quad + \left(-\hat{I}_{2y}\cos(\Omega_2^0 t_1) + \hat{I}_{2x}\sin(\Omega_2^0 t_1)\right)\ \exp\{-\lambda t_1\} \\
&\Big\downarrow (\pi/2)_{\bar{x}} \\
\hat{\rho}_{④} &= \left(\hat{I}_{1z}\cos(\Omega_1^0 t_1) + \hat{I}_{1x}\sin(\Omega_1^0 t_1)\right)\ \exp\{-\lambda t_1\} \\
&\quad + \left(\hat{I}_{2z}\cos(\Omega_2^0 t_1) + \hat{I}_{2x}\sin(\Omega_2^0 t_1)\right)\ \exp\{-\lambda t_1\}
\end{aligned} \tag{20.29}$$

(The phases of the pulses correspond to the first row of Table 19.1, with $\Psi = 0$.) The decay rate constant of the transverse magnetization is given by $\lambda = {T_2}^{-1}$.

The phase cycle has the effect of suppressing signals that do not originate in longitudinal magnetization between time points ④ and ⑤. The transverse terms in Equation 20.29 may therefore be ignored:

$$\hat{\rho}_{④} = \left(\hat{I}_{1z}\cos(\Omega_1^0 t_1) + \hat{I}_{2z}\cos(\Omega_2^0 t_1)\right)\ \exp\{-\lambda t_1\} + \ldots$$

The magnetization components evolve in the mixing interval τ_m according to the following simplified form of the Solomon equations, in which the thermal equilibrium terms are dropped:

$$\frac{\mathrm{d}}{\mathrm{d}t}\begin{pmatrix}\langle\hat{I}_{1z}\rangle \\ \langle\hat{I}_{2z}\rangle\end{pmatrix} = \begin{pmatrix}-R_{\text{auto}} & R_{\text{cross}} \\ R_{\text{cross}} & -R_{\text{auto}}\end{pmatrix}\begin{pmatrix}\langle\hat{I}_{1z}\rangle \\ \langle\hat{I}_{2z}\rangle\end{pmatrix} \tag{20.30}$$

This step is justifiable, since the magnetization exchange takes place in the middle of a pulse sequence that involves phase cycling. The thermal equilibrium terms give rise to constant signals that are removed by the phase cycling procedure.[8]

The equation of motion of the magnetization components is solved in Appendix A.16. The density operator components are transformed as follows during the mixing interval τ_m of the NOESY pulse sequence:

$$\begin{aligned}
\hat{I}_{1z} &\xrightarrow{\tau_m} a_{1\to1}(\tau_m)\hat{I}_{1z} + a_{1\to2}(\tau_m)\hat{I}_{2z} \\
\hat{I}_{2z} &\longrightarrow a_{2\to1}(\tau_m)\hat{I}_{1z} + a_{2\to2}(\tau_m)\hat{I}_{2z}
\end{aligned} \tag{20.31}$$

where the transfer amplitudes are given by Equation A.100:

$$\begin{aligned}
a_{1\to1}(\tau_m) = a_{2\to2}(\tau_m) &= \cosh(R_{\text{cross}}\tau_m)\exp\{-R_{\text{auto}}\tau_m\} \\
a_{1\to2}(\tau_m) = a_{2\to1}(\tau_m) &= \sinh(R_{\text{cross}}\tau_m)\exp\{-R_{\text{auto}}\tau_m\}
\end{aligned} \tag{20.32}$$

The longitudinal part of the density operator at time point ⑤ is therefore given by

$$\begin{aligned}\hat{\rho}_{⑤} = &\hat{I}_{1z}\, a_{1\to1}(\tau_m)\cos(\Omega_1^0 t_1)\exp\{-\lambda t_1\}\\ &+\hat{I}_{1z}\, a_{2\to1}(\tau_m)\cos(\Omega_2^0 t_1)\exp\{-\lambda t_1\}\\ &+\hat{I}_{2z}\, a_{2\to2}(\tau_m)\cos(\Omega_2^0 t_1)\exp\{-\lambda t_1\}\\ &+\hat{I}_{2z}\, a_{1\to2}(\tau_m)\cos(\Omega_1^0 t_1)\exp\{-\lambda t_1\}+\ldots\end{aligned}$$

The last $(\pi/2)_x$ pulse gives

$$\begin{aligned}\hat{\rho}_{⑥} = &-\hat{I}_{1y}\, a_{1\to1}(\tau_m)\cos(\Omega_1^0 t_1)\exp\{-\lambda t_1\}\\ &-\hat{I}_{1y}\, a_{2\to1}(\tau_m)\cos(\Omega_2^0 t_1)\exp\{-\lambda t_1\}\\ &-\hat{I}_{2y}\, a_{2\to2}(\tau_m)\cos(\Omega_2^0 t_1)\exp\{-\lambda t_1\}\\ &-\hat{I}_{2y}\, a_{1\to2}(\tau_m)\cos(\Omega_1^0 t_1)\exp\{-\lambda t_1\}+\ldots\end{aligned}$$

The two-dimensional signal is therefore

$$\begin{aligned}s^{\cos}(t_1,t_2) = &\, a_{1\to1}(\tau_m)\cos(\Omega_1^0 t_1)\exp\{i\Omega_1^0 t_2-\lambda(t_1+t_2)\}\\ &+a_{2\to1}(\tau_m)\cos(\Omega_2^0 t_1)\exp\{i\Omega_2^0 t_2-\lambda(t_1+t_2)\}\\ &+a_{1\to2}(\tau_m)\cos(\Omega_1^0 t_1)\exp\{i\Omega_2^0 t_2-\lambda(t_1+t_2)\}\\ &+a_{2\to2}(\tau_m)\cos(\Omega_2^0 t_1)\exp\{i\Omega_1^0 t_2-\lambda(t_1+t_2)\}\end{aligned}\qquad(20.33)$$

where the amplitudes of the diagonal- and cross-signals are

$$\begin{aligned}a_{\text{diag}} &= a_{1\to1}=a_{2\to2}=\cosh(R_{\text{cross}}\tau_m)\exp\{-R_{\text{auto}}\tau_m\}\\ a_{\text{cross}} &= a_{1\to2}=a_{2\to1}=\sinh(R_{\text{cross}}\tau_m)\exp\{-R_{\text{auto}}\tau_m\}\end{aligned}\qquad(20.34)$$

The superscript 'cos' in Equation 20.33 indicates the 'cosine' two-dimensional experiment in the States procedure ($\Psi = 0$ in Table 19.1).

Repetition of the calculation for the 'sine' component of the States two-dimensional signal ($\Psi = -\pi/2$ in Table 19.1) gives

$$\begin{aligned}s^{\sin}(t_1,t_2) = &\, a_{1\to1}(\tau_m)\sin(\Omega_1^0 t_1)\exp\{i\Omega_1^0 t_2-\lambda(t_1+t_2)\}\\ &+a_{2\to1}(\tau_m)\sin(\Omega_2^0 t_1)\exp\{i\Omega_2^0 t_2-\lambda(t_1+t_2)\}\\ &+a_{1\to2}(\tau_m)\sin(\Omega_1^0 t_1)\exp\{i\Omega_2^0 t_2-\lambda(t_1+t_2)\}\\ &+a_{2\to2}(\tau_m)\sin(\Omega_2^0 t_1)\exp\{i\Omega_1^0 t_2-\lambda(t_1+t_2)\}\end{aligned}\qquad(20.35)$$

All signal components have the correct cosine and sine modulations in the two States experiments, so the procedure in Section 5.9.4 may be followed to obtain a two-dimensional spectrum with pure absorption lineshapes for all components:

$$
\begin{aligned}
S(\Omega_1, \Omega_2) = {} & a_{\text{diag}}(\tau_m)\mathcal{A}(\Omega_1, \Omega_2;\ \Omega_1^0, \lambda, \Omega_1^0, \lambda) \\
& + a_{\text{diag}}(\tau_m)\mathcal{A}(\Omega_1, \Omega_2;\ \Omega_2^0, \lambda, \Omega_2^0, \lambda) \\
& + a_{\text{cross}}(\tau_m)\mathcal{A}(\Omega_1, \Omega_2;\ \Omega_1^0, \lambda, \Omega_2^0, \lambda) \\
& + a_{\text{cross}}(\tau_m)\mathcal{A}(\Omega_1, \Omega_2;\ \Omega_2^0, \lambda, \Omega_1^0, \lambda)
\end{aligned} \tag{20.36}
$$

The spectrum contains two diagonal peaks, with amplitudes given by a_{diag}, and two cross-peaks, with amplitudes given by a_{cross} (Equation 20.34).

One should note the origin of the spectral peaks in Equation 20.36. The diagonal peak at frequency coordinates $(\Omega_1, \Omega_2) = (\Omega_1^0, \Omega_1^0)$ and the cross-peak at frequency coordinates $(\Omega_1, \Omega_2) = (\Omega_1^0, \Omega_2^0)$ originate in the $\hat{I}_{1z}$ part of the initial density operator $\hat{\rho}_{①}$. These peaks, therefore, are totally independent of the state of the spins I_2 at the beginning of the pulse sequence. Similarly, the diagonal peak at frequency coordinates $(\Omega_1, \Omega_2) = (\Omega_2^0, \Omega_2^0)$ and the cross-peak at frequency coordinates $(\Omega_1, \Omega_2) = (\Omega_2^0, \Omega_1^0)$ are independent of the state of the spins I_1 at the beginning of the pulse sequence.

20.6.3 NOESY spectra

The relative signs of the cross-peaks in a NOESY spectrum depend on the rotational correlation time.

1. *Long rotational correlation time.* If the rotational correlation time of the molecules is long ($\tau_c > \tau_c^{\text{crit}}$), then the sense of the magnetization transfer during the mixing interval is *positive*. The process may be visualized as follows:

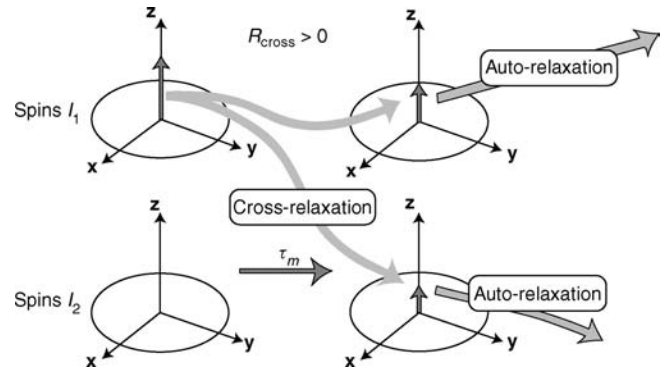

Figure 20.41
Visualization of the magnetization transfer process, for a long rotational correlation time.

The magnetization of spins I_1 is converted into magnetization of spins I_2, at the same time as it decays with rate constant R_{auto}. At long times, the two sets of spins reach a state of *internal equilibrium*, in which the magnetizations of the two species become equal and decay together.

This resembles the act of magnetizing a piece of iron by bringing it close to another piece of magnetic material.

In this regime, the diagonal- and cross-peak amplitudes vary as a function of τ_m as follows:

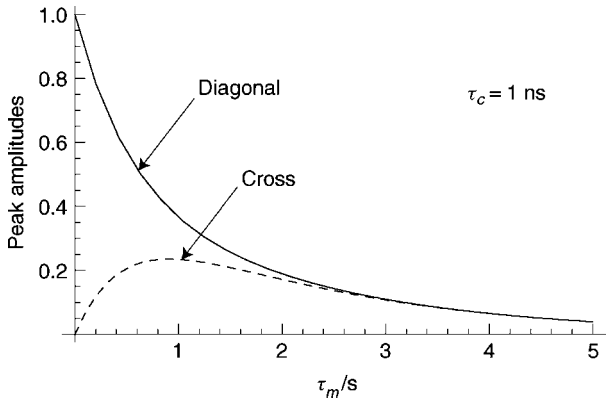

Figure 20.42
NOESY peak amplitudes for a long rotational correlation time.

These simulations are for an ensemble of proton pairs separated by 0.2 nm in a field of 11.74 T, with a rotational correlation time $\tau_c = 1$ ns.

The diagonal and cross-peaks in the two-dimensional spectrum have the *same* sign in the long correlation time regime:

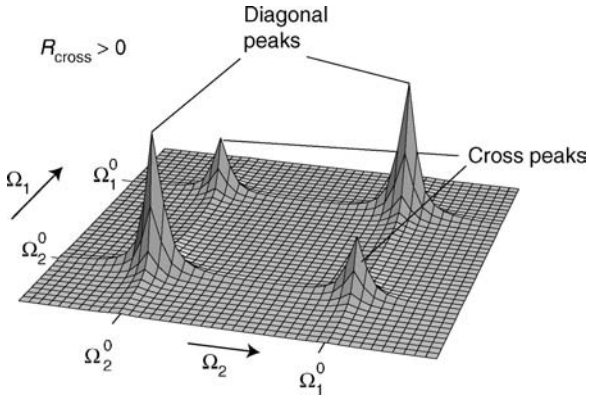

Figure 20.43
Form of the NOESY spectrum in the case of a long rotational correlation time.

2. *Short rotational correlation time*. If the rotational correlation time of the molecules is short ($\tau_c < \tau_c^{crit}$), then the sense of the magnetization transfer during the mixing interval is *negative*, which may be visualized as follows:

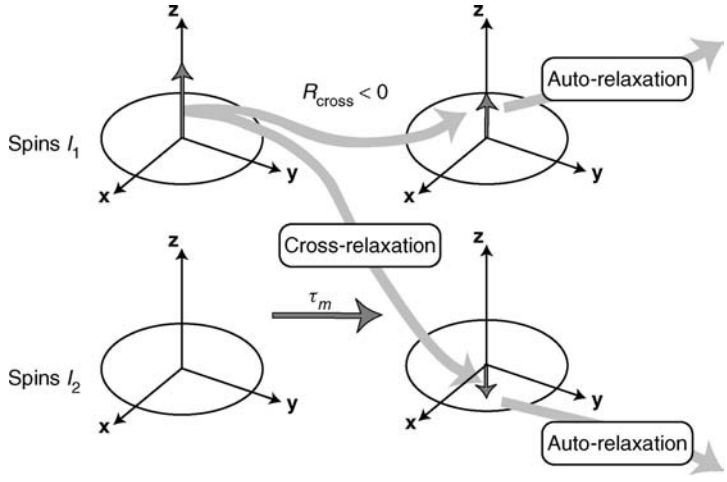

Figure 20.44
Visualization of the magnetization transfer process, for a short rotational correlation time.

The magnetization of spins I_1 is changed in sign on conversion into magnetization of spins I_2. In this regime, the diagonal- and cross-peak amplitudes vary as a function of τ_m as follows:

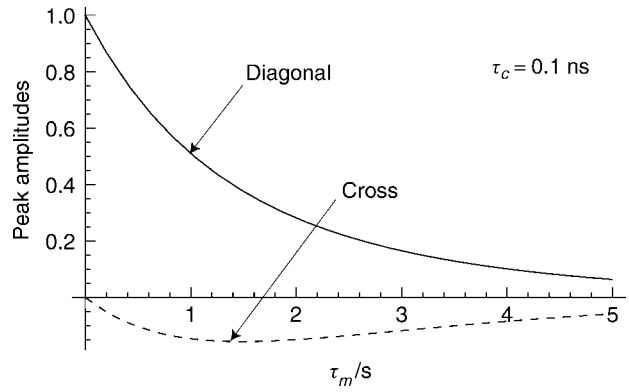

Figure 20.45
NOESY peak amplitudes for a short rotational correlation time.

These simulations are for an ensemble of proton pairs separated by 0.2 nm in a field of 11.74 T, with a rotational correlation time $\tau_c = 0.1$ ns.

The diagonal and cross-peaks in the two-dimensional spectrum have *opposite* sign in the short correlation time regime:

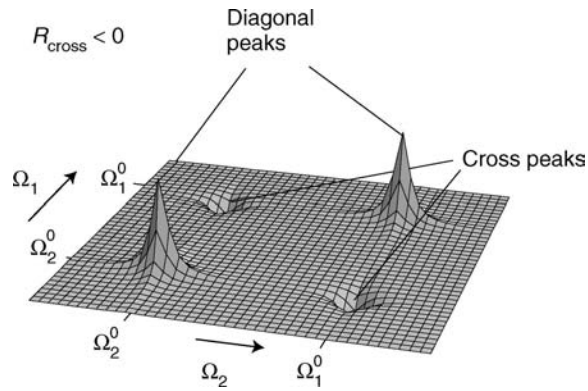

Figure 20.46
Form of the NOESY spectrum in the case of a short rotational correlation time.

3. *Critical rotational correlation time*. The cross-peaks disappear for the critical rotational correlation time τ_c^{crit} (Equation 20.18).

20.6.4 NOESY and chemical exchange

The NOESY and two-dimensional exchange experiments are identical. In general, this experiment does not distinguish between magnetization transfer through dipole–dipole spin interactions (cross-relaxation) and magnetization transfer due to chemical exchange processes (see Section 19.7). A partial distinction between these processes is obtained for small molecules, where cross-relaxation gives negative cross-peaks, whereas chemical exchange gives positive cross-peaks.

20.6.5 Molecular structure determination

At short values of mixing interval τ_m, the cross-peak amplitudes are given approximately by

$$a_{cross}(\tau_m) \cong R_{cross}\tau_m$$

The cross-relaxation rate constant is proportional to the square of the dipole–dipole interaction and, hence, to the inverse sixth power of the distance between the spins:

$$a_{cross}(\tau_m) \sim r^{-6} \quad (20.37)$$

This equation accounts for the importance of NOESY in structural biology. By taking a NOESY spectrum of a biomolecule, and measuring the cross-peak amplitudes, one may estimate simultaneously a large number of internuclear distances and, hence, build up a picture of the molecular structure.

Kurt Wüthrich was awarded the Nobel Prize in 1992, in part for the development of NOESY into a powerful tool for the determination of biomolecular structures.

It is difficult to determine *absolute* internuclear distances by NOESY, since the proportionality constant in Equation 20.37 is difficult to determine. However, this does not matter too much in practice, since the distance scale may be calibrated using proton pairs separated by known distances in rigid parts of the molecule.

Figure 20.47 shows an experimental NOESY spectrum of a protein in isotropic solution. The spectrum displays a large number of cross-peaks, each of which may be analysed to obtain a single structural constraint – an estimated distance between one pair of nuclear sites. Usually, a computer is used to construct a molecular structural model in which all of the NOESY distance constaints are satisfied simultaneously, in the ideal case. An example of a solution-state biomolecular structure, solved with the assistance of NOESY, is shown in Plate 5.

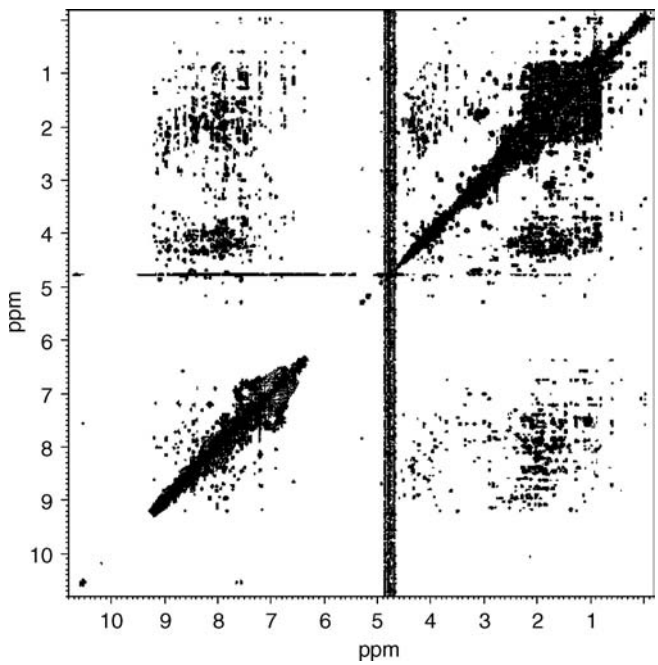

Figure 20.47
Experimental ^{1}H NOESY spectrum of a medium-sized biomolecule in solution (the C-terminal domain of rat ERp29 protein). The protein contains 120 amino acid residues. A special pulse technique was used to suppress the water proton resonance. For details, see G. Otting, E. Liepinsh and K. Wüthrich, *J. Am. Chem. Soc.* **114**, 7093–7095 (1992). Thanks to E. Liepinsh and G. Otting for providing this spectrum.

20.7 ROESY

20.7.1 Transverse cross-relaxation

Much has now been said about the through-space cross-relaxation of *longitudinal* magnetization components. What about *transverse* magnetization? Can transverse magnetization components also cross-relax?

The answer is yes, provided precautions are taken to arrest the mutual precession of spins at different chemical sites.

To see what this means, consider the precessing transverse magnetizations of two different sets of spins, I_1 and I_2. View the precession from a frame rotating at the average Larmor frequency of the spins I_1. From this frame, the transverse magnetization of spins I_1 appears to be static, whereas the transverse magnetization of spins I_2 precesses in the positive direction, if $\Omega_2^0 > \Omega_1^0$:

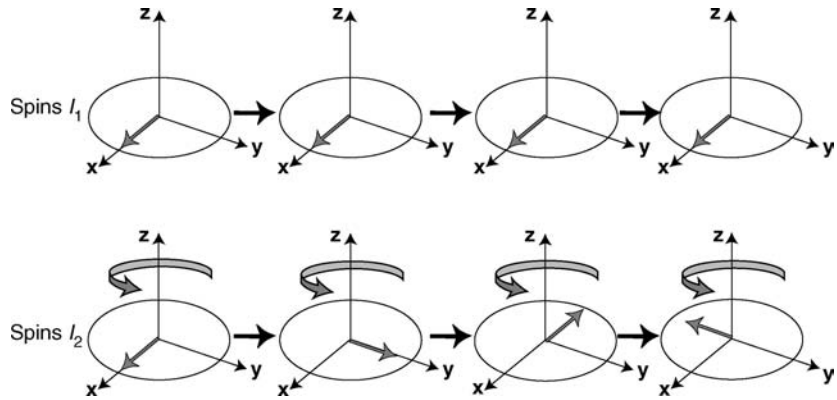

Figure 20.48 Transverse magnetization vectors in the rotating frame, for the case $\omega_{\text{ref}} = \omega_1^0$.

Now suppose that there is a *transverse cross-relaxation process* that allows the transverse magnetizations of the two species to communicate with each other. If the transverse cross-relaxation rate constant is positive, then the transferred magnetization has the same sign as the source magnetization.

Suppose that initially, spins I_1 have magnetization along the x-axis, whereas spins I_2 have no magnetization. The diagram below shows the course of events schematically:

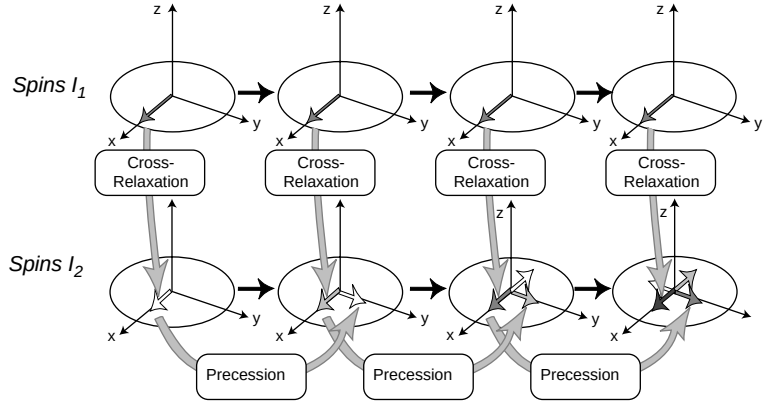

Figure 20.49 The cross-relaxation of transverse magnetization is suppressed by differential spin precession.

In the leftmost diagram, a small amount of magnetization is transferred from spins I_1 to I_2, appearing along the x-axis (short white arrow). In the next frame, some more magnetization is transferred along the x-axis (light grey arrow). However, in the preceding interval, the initially transferred magnetization (white arrow) has precessed, and is now oriented along the y-axis. The process is repeated in the next two frames: In the last frame, there are four transferred magnetization components, but they are all out of phase with each other and cancel exactly.

Because of the mutual precession, the transferred magnetization does not build up. Transverse cross-relaxation is effectively *decoupled* by the mutual spin precession.

It is only possible to observe transverse cross-relaxation without intervention if the participating spins have exactly the same precession frequency.

20.7.2 Spin locking

The mutual precession of spins with different chemical shifts may be suppressed by using *spin locking*, as described in Section 12.3. A strong, resonant r.f. field, applied with the same phase as the transverse magnetization, inhibits the differential precession:

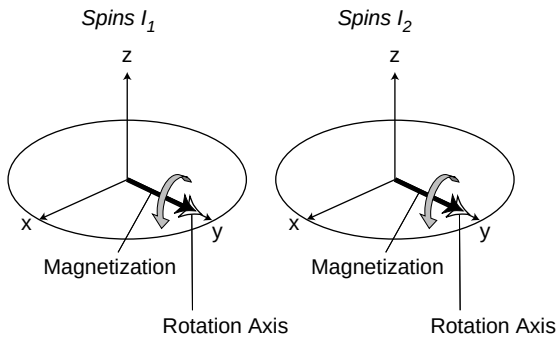

Figure 20.50
Suppression of the differential precession by the strong r.f. field.

The differential precession is suppressed effectively by the r.f. field, providing that the nutation frequency is strong compared to both chemical shift offset frequencies:

$$|\omega_{\text{nut}}| >> |\Omega_1^0|, |\Omega_2^0|$$

where the nutation frequency is as usual proportional to the r.f. field strength:

$$\omega_{\text{nut}} = \left| \frac{1}{2} \gamma B_{\text{RF}} \sin \theta_{\text{RF}} \right|$$

20.7.3 Transverse Solomon equations

The r.f. field inhibits the mutual precession of the spins and allows magnetization transfer to take place. The spin-locked magnetization components may then communicate through cross-relaxation processes. This

process is described by the *transverse Solomon equations*, which are analogous to the simplified longitudinal Solomon equations given in Equation 20.30:

$$\frac{\mathrm{d}}{\mathrm{d}t}\begin{pmatrix}\langle\hat{I}_{1y}\rangle\\ \langle\hat{I}_{2y}\rangle\end{pmatrix} = \begin{pmatrix}-R^{\mathrm{T}}_{\mathrm{auto}} & R^{\mathrm{T}}_{\mathrm{cross}}\\ R^{\mathrm{T}}_{\mathrm{cross}} & -R^{\mathrm{T}}_{\mathrm{auto}}\end{pmatrix}\begin{pmatrix}\langle\hat{I}_{1y}\rangle\\ \langle\hat{I}_{2y}\rangle\end{pmatrix} \tag{20.38}$$

The superscript 'T' indicates 'transverse'.

The transverse relaxation rate constants are somewhat different from the longitudinal ones. For intramolecular dipole–dipole relaxation between two spins, the transverse auto-relaxation rate constant is given by

$$R^{\mathrm{T}}_{\mathrm{auto}} = \frac{1}{20}b^2\left\{5\mathcal{J}(0) + 9\mathcal{J}(\omega^0) + 6\mathcal{J}(2\omega^0)\right\} \tag{20.39}$$

and the transverse cross-relaxation rate constant is given by[4]

$$R^{\mathrm{T}}_{\mathrm{cross}} = -\frac{1}{10}b^2\left\{2\mathcal{J}(0) + 3\mathcal{J}(\omega^0)\right\} \tag{20.40}$$

The longitudinal and transverse auto-relaxation rate constants are the same for fast molecular motion, but the transverse relaxation is faster if the molecular tumbling is slow (see Figure 20.51, which is calculated for two protons separated by 0.2 nm, in a field of 11.74 T.)

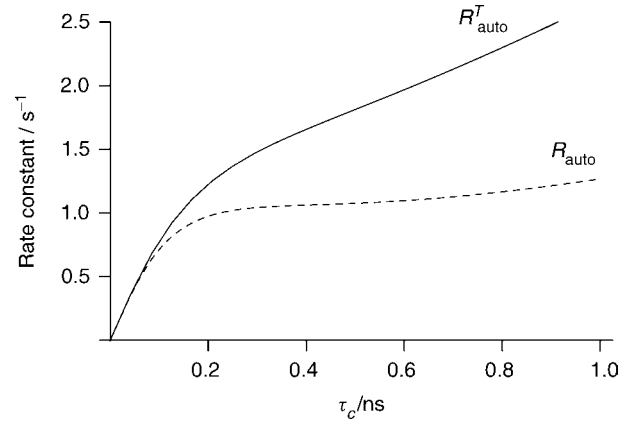

Figure 20.51
Transverse and longitudinal auto-relaxation rate constants, as a function of rotational correlation time.

The longitudinal and transverse cross-relaxation rate constants are also the same for rapid molecular tumbling, but behave quite differently as the rotational correlation time is increased. As discussed in Section 20.6, the longitudinal cross-relaxation rate constant changes sign as a function of τ_c. The transverse cross-relaxation rate constant, on the other hand, is always negative:[4]

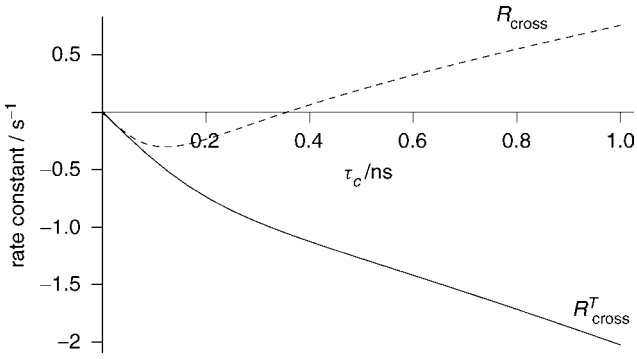

Figure 20.52
Transverse and longitudinal cross-relaxation rate constants, as a function of rotational correlation time.

Since there is no sign change in $R^{\mathrm{T}}_{\mathrm{cross}}$, it is easier to observe transverse cross-relaxation than longitudinal cross-relaxation, for the case of medium-sized molecules tumbling near the critical correlation time ($\tau_{\mathrm{c}} \sim \tau_{\mathrm{c}}^{\mathrm{crit}}$).

For *slowly* tumbling molecules ($\tau_{\mathrm{c}} >> \tau_{\mathrm{c}}^{\mathrm{crit}}$), on the other hand, transverse cross-relaxation is *less* easy to observe than longitudinal cross-relaxation, because of the large value of R^T_{auto}, which causes the transverse magnetization to decay quickly.

20.7.4 ROESY spectra

Transverse cross-relaxation is usually exploited by the two-dimensional experiment known as ROESY (which stands for *Rotating Frame Overhauser Effect Spectroscopy*[9]).

A basic ROESY pulse sequence is shown below:

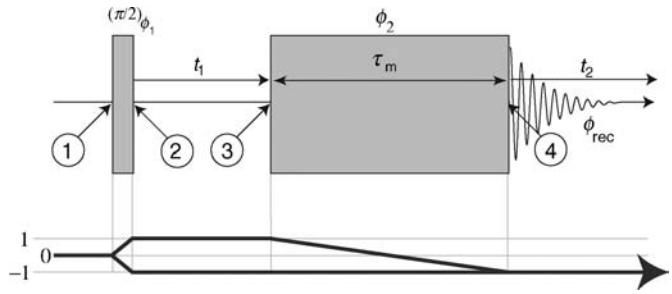

Figure 20.53
ROESY pulse sequence.

An initial $\pi/2$ pulse with phase ϕ_1 is followed by a variable evolution interval t_1 and a long mixing interval of continuous r.f. irradiation, of constant duration τ_{m} and phase ϕ_2. The signal is detected in the subsequent t_2 interval, using a receiver phase ϕ_{rec}.

A simple phase cycle for the ROESY experiment is given in Table 20.1. This includes a phase Ψ used in the States scheme for generating two-dimensional absorption lineshapes.

Table 20.1 A two-step phase cycle ($\mathfrak{n} = 2$) appropriate for the ROESY experiment. The phase Ψ is used in the States scheme for generating pure absorption two-dimensional lineshapes, with discrimination of positive and negative Ω_1-frequencies (see Section 5.9.4). For the 'cosine' data set, $\Psi = 0$. For the 'sine' data set, $\Psi = -\pi/2$.

Cycle counter $\mathfrak{m}$	ϕ_1	ϕ_2	ϕ_{rec}
0	Ψ	$\pi/2$	0
1	$\Psi + \pi$	$\pi/2$	π

Calculation of the spin-density operator for an ensemble of homonuclear spin pairs runs as follows up to time point ③, for the case $\Psi = 0$:

$$
\begin{aligned}
\hat{\rho}_{①} &= \hat{I}_{1z} + \hat{I}_{2z} \\
&\Big\downarrow (\pi/2)_x \\
\hat{\rho}_{②} &= -\hat{I}_{1y} - \hat{I}_{2y} \\
&\Big\downarrow t_1 \\
\hat{\rho}_{③} &= \left(-\hat{I}_{1y}\cos(\Omega_1^0 t_1) + \hat{I}_{1x}\sin(\Omega_1^0 t_1)\right)\ \exp\{-\lambda t_1\} \\
&\quad + \left(-\hat{I}_{2y}\cos(\Omega_2^0 t_1) + \hat{I}_{2x}\sin(\Omega_2^0 t_1)\right)\ \exp\{-\lambda t_1\}
\end{aligned}
\tag{20.41}
$$

The strong r.f. field is applied with phase $\phi_2 = \pi/2$, which spin-locks the y-components of the spin angular momenta. The x-components nutate rapidly around the spin-locking field, and are usually effectively destroyed by the inhomogeneity in the r.f. field. There are variants of the ROESY pulse sequence that destroy these components in a more sophisticated and exact way (see *Further Reading*).

The $\hat{I}_{1y}$ and $\hat{I}_{2y}$ components evolve according to the transverse Solomon equations, Equation 20.38. These equations may be solved using the technique described in Appendix A.16. The result is

$$
\begin{aligned}
\hat{\rho}_{④} = &-\hat{I}_{1y}\cos(\Omega_1^0 t_1)\cosh(R^{\text{T}}_{\text{cross}}\tau_{\text{m}})\exp\{-\lambda t_1 - R^{\text{T}}_{\text{auto}}\tau_{\text{m}}\} \\
&-\hat{I}_{1y}\cos(\Omega_2^0 t_1)\sinh(R^{\text{T}}_{\text{cross}}\tau_{\text{m}})\exp\{-\lambda t_1 - R^{\text{T}}_{\text{auto}}\tau_{\text{m}}\} \\
&-\hat{I}_{2y}\cos(\Omega_2^0 t_1)\cosh(R^{\text{T}}_{\text{cross}}\tau_{\text{m}})\exp\{-\lambda t_1 - R^{\text{T}}_{\text{auto}}\tau_{\text{m}}\} \\
&-\hat{I}_{2y}\cos(\Omega_2^0 t_1)\sinh(R^{\text{T}}_{\text{cross}}\tau_{\text{m}})\exp\{-\lambda t_1 - R^{\text{T}}_{\text{auto}}\tau_{\text{m}}\} + \ldots
\end{aligned}
$$

The resulting two-dimensional signal, for the case of $\Psi = 0$, is given by

$$
\begin{aligned}
s^{\cos}(t_1, t_2) = {} & a_{\text{diag}}(\tau_m)\cos(\Omega_1^0 t_1)\exp\{i\Omega_1^0 t_2 - \lambda(t_1 + t_2)\} \\
& + a_{\text{diag}}(\tau_m)\cos(\Omega_2^0 t_1)\exp\{i\Omega_2^0 t_2 - \lambda(t_1 + t_2)\} \\
& + a_{\text{cross}}(\tau_m)\cos(\Omega_1^0 t_1)\exp\{i\Omega_2^0 t_2 - \lambda(t_1 + t_2)\} \\
& + a_{\text{cross}}(\tau_m)\cos(\Omega_2^0 t_1)\exp\{i\Omega_1^0 t_2 - \lambda(t_1 + t_2)\}
\end{aligned}
$$

where the amplitudes of the diagonal- and cross-signals are

$$
\begin{aligned}
a_{\text{diag}}(\tau_m) &= \cosh(R^T_{\text{cross}}\tau_m)\exp\{-R^T_{\text{auto}}\tau_m\} \\
a_{\text{cross}}(\tau_m) &= \sinh(R^T_{\text{cross}}\tau_m)\exp\{-R^T_{\text{auto}}\tau_m\}
\end{aligned}
\qquad (20.42)
$$

The peak amplitudes are exactly the same as in NOESY (Equation 20.34), but with the substitution of R_{cross} and R_{auto} by R^T_{cross} and R^T_{auto} respectively. Since R^T_{cross} is negative, ROESY cross-peaks always have the opposite sign to the diagonal peaks:

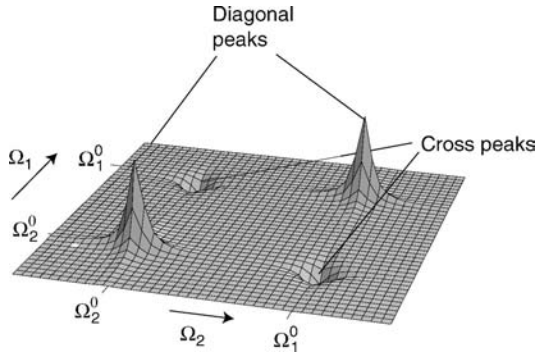

Figure 20.54
Form of the ROESY spectrum. The cross-peaks are always negative, independent of the correlation time.

Figure 20.55 shows simulations of NOESY and ROESY peak amplitudes, as a function of mixing interval τ_m, for a series of rotational correlation times τ_c. Note that the ROESY cross-peaks are always negative, and are larger than the NOESY cross-peaks for short values of τ_c. The NOESY cross-peaks vanish at the critical correlation time $\tau_c^{\text{crit}} = 0.36$ ns. However, NOESY cross-peaks are larger when τ_c is long.

ROESY is widely used as a method for structure determination of small- to medium-sized molecules in solution (typically up to around 3000 atomic mass units).

20.7.5 ROESY and chemical exchange

ROESY enables a relatively clear distinction between cross-relaxation and chemical exchange. Cross-relaxation always gives rise to negative cross-peaks in a ROESY experiment, whereas chemical exchange

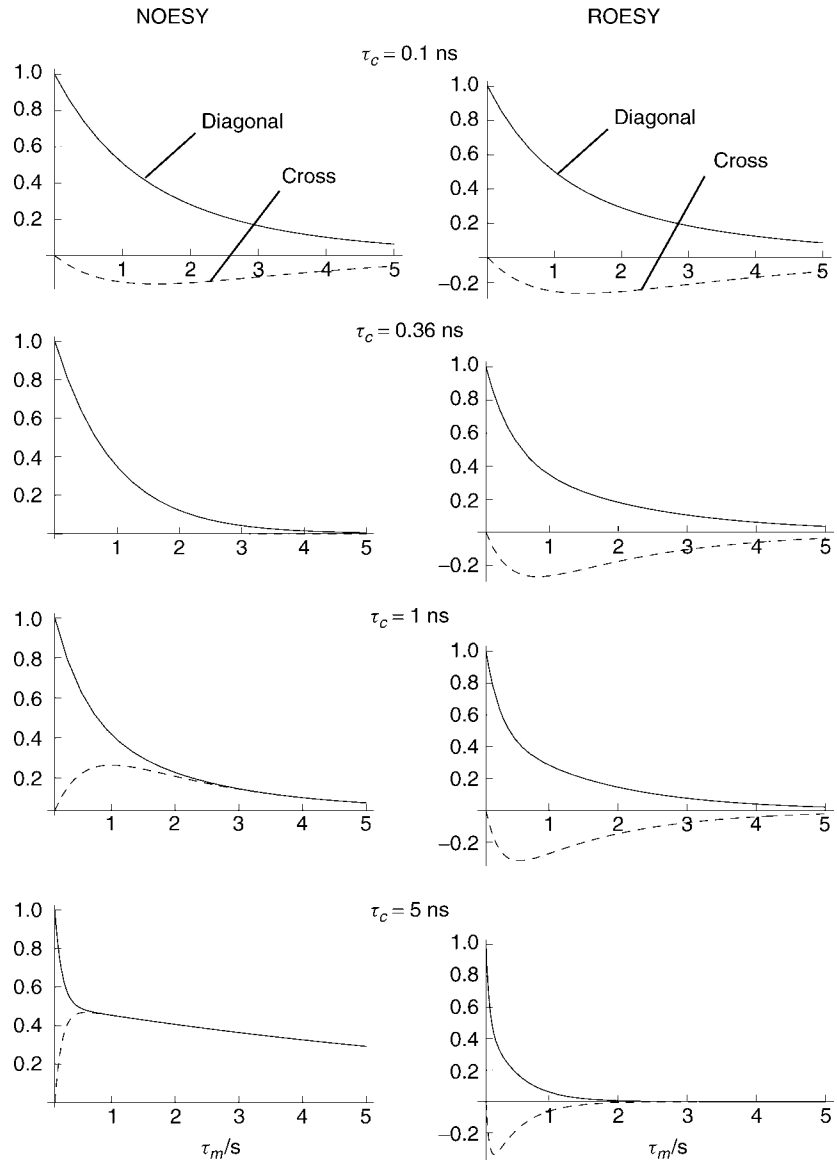

Figure 20.55
Comparison of diagonal-peak and cross-peak amplitudes for NOESY and ROESY for a set of rotational correlation times. All simulations are for the case of two protons separated by 0.2 nm in a field of 11.74 T.

always gives rise to positive cross-peaks in the same experiment. This distinction is not obtained so cleanly in the NOESY experiment (see Section 20.6.4).

20.7.6 ROESY and TOCSY

The ROESY pulse sequence is very similar to the TOCSY pulse sequence (see Section 18.14). Indeed, in general, TOCSY effects (magnetization transfer through *J*-couplings) are observed in the ROESY experiment, and ROESY effects (magnetization transfer through cross-relaxation) are observed in TOCSY experiments. A series of modified pulse sequences have been developed that give relatively 'clean' TOCSY and ROESY

effects, compensated for pulse imperfections and off-resonance effects during the spin-locking pulse (see *Further Reading*).

20.8 Cross-Correlated Relaxation

20.8.1 Cross-correlation

Consider three random processes, *A*, *B* and *C*, that vary as a function of time. Suppose that they also have the same autocorrelation function. A plot of the three random processes against time might have the following appearance:

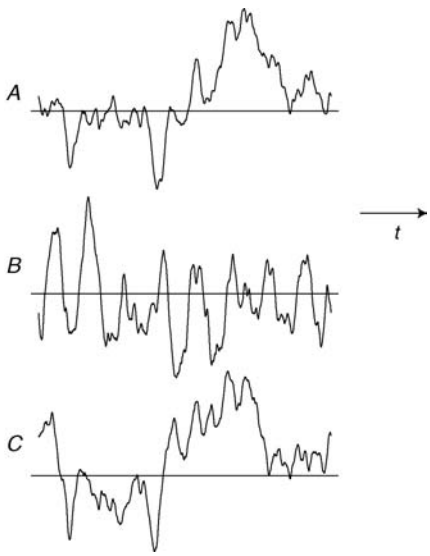

Figure 20.56
Three random processes.

In all cases, the value of the function at a particular time is unpredictable. Despite this, there is a relationship between two of the functions, as is seen clearly when they are superimposed:

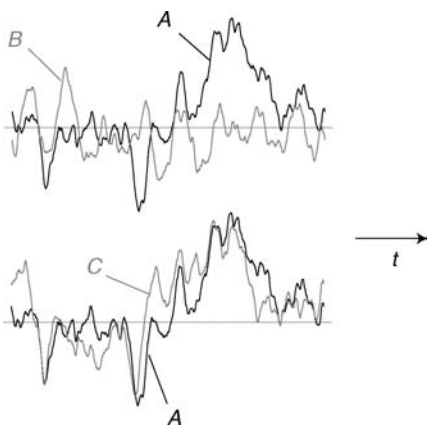

Figure 20.57
Overlay of the random processes, making the cross-correlation of *A* and *C* clear.

There is no particular relationship between A and B, whereas there is a distinct tendency for C and A to follow each other.

This tendency may be expressed mathematically in terms of the *cross-correlation* of the two processes, defined as

$$\mathbb{K}_{AB}(\tau) = \langle A(t)B(t+\tau)\rangle \tag{20.43}$$

This is analogous to the autocorrelation function of a single process, defined in Equation 20.1.

In the examples shown above, the processes A and B are *uncorrelated* (meaning that the cross-correlation function is zero), whereas the processes A and C are *correlated* (meaning that the cross-correlation function is finite).

The existence of cross-correlation implies a common physical mechanism underlying both processes. Here is an example: the intensity of the northern lights (aurora borealis) fluctuates unpredictably. The same is true for the number of dark spots on the surface of the sun. Nevertheless, these two apparently unrelated processes are strongly correlated. This is because a common physical mechanism underlies both. Immense storms on the surface of the sun reduce locally the temperature of the surface (causing dark spots) and also eject particles into space, which generate the aurora as they impact the upper atmosphere of the Earth.

20.8.2 Cross-correlation of spin interactions

Typically, a nuclear spin experiences many different sources of local magnetic fields, which fluctuate as the molecule rotates in a liquid. Neighbouring nuclear spins generate magnetic fields – this comprises the dipole–dipole relaxation mechanism, described above. In addition, local magnetic fields are generated by induced electron currents, leading to spin relaxation through chemical shift anisotropy.

All of these local fields have a molecular origin. They are all modulated by the rotation of the molecule. There is, therefore, a common physical link between all molecular relaxation mechanisms, which implies a degree of correlation.

For example, consider a molecule containing three protons, arranged in a line. The central proton is relaxed by the dipole–dipole couplings to the two outer protons. If the molecule is rigid, all three dipole–dipole couplings change in synchrony when the molecule rotates, and are therefore strongly correlated:

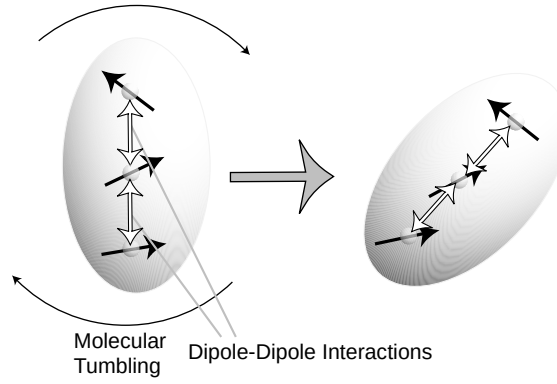

Figure 20.58
Cross-correlation of two dipole–dipole interactions.

Another example is when a nuclear spin experiences a local field from a different nuclear spin as well as a local field from the surrounding electrons. When the molecule rotates, both the nuclear spins and the electrons move at the same time. As a result, the fluctuations of dipole–dipole couplings and CSA also tend to be correlated.

Cross-correlation of different relaxation mechanisms is therefore a ubiquitous phenomenon in rigid molecules and is responsible for many interesting and useful effects. In general, cross-correlated relaxation breaks the symmetry of relaxation equations such as Equations 20.10 and 20.23. In the presence of cross-correlation, it is no longer true that transition probabilities such as $W_{\boxed{+\alpha}}$ and $W_{\boxed{+\beta}}$ are equal. Similarly, the transverse relaxation time constants of coherences such as $\rho_{\boxed{\alpha-}}$ and $\rho_{\boxed{\beta-}}$ are not, in general, equal in the presence of cross-correlated relaxation.

20.8.3 Dipole–dipole cross-correlation and angular estimations

In a rigid molecule, two different dipole–dipole interactions are, in general, cross-correlated, because there is a fixed geometrical relationship between them. For example, consider two different ^{13}C–^{1}H interactions in a $^{13}C_2$-labelled molecule, in which each labelled carbon atom is bonded to one proton. The two ^{13}C–^{1}H interactions are cross-correlated. The relevant cross-correlation function $\mathbb{K}_{CH,CH}$ depends on the *angle* $\theta_{CH,CH}$ between the two ^{13}C–^{1}H vectors, according to

$$\mathbb{K}_{CH,CH} \sim \frac{1}{2}\left(3\cos^2\theta_{CH,CH} - 1\right)$$

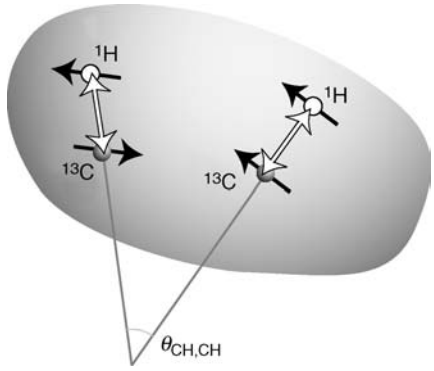

Figure 20.59
The angle between two ^{13}C–^{1}H vectors.

If the two vectors are *parallel or antiparallel* ($\theta_{CH,CH} = 0$ or π), then the cross-correlation function is *positive*, since the two dipole–dipole couplings track each other exactly as the molecule rotates.

If the two vectors are *perpendicular* ($\theta_{CH,CH} = \pi/2$), then the cross-correlation function is *negative*, implying that the two dipole–dipole couplings are *anticorrelated*. If the molecule is oriented so that one ^{13}C–^{1}H vector is parallel to the external field (leading to a positive secular dipolar coupling), then the second ^{13}C–^{1}H vector must be perpendicular to the field (leading to a negative secular dipolar coupling). In this geometry, the two secular dipolar couplings tend to have opposite signs as the molecule rotates.

This type of cross-correlation leads to a variety of effects on the spin dynamics, but perhaps the clearest effects are observed on the linewidths of the $^{13}C_2$ double-quantum coherences.

As an example, consider the two anomers of [1,2-$^{13}C_2$]-glucose, which have the following molecular structure:

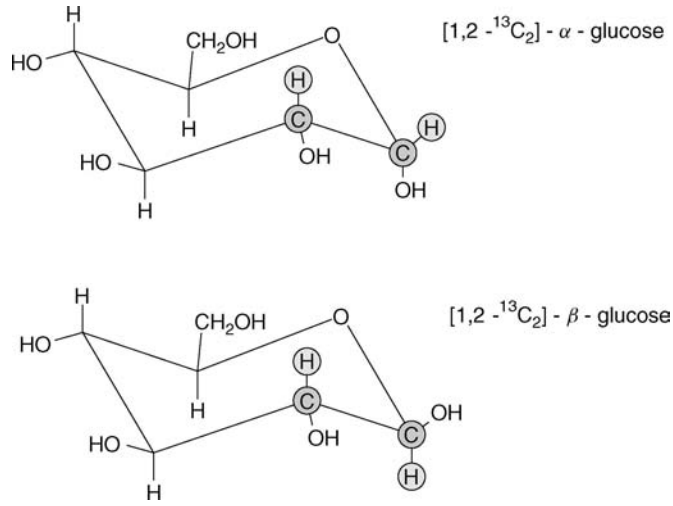

Figure 20.60
The two anomers of [1,2-$^{13}C_2$]-glucose, showing the HCCH four-spin moieties.

The two CH vectors are roughly perpendicular in the α-anomer, whereas they are approximately antiparallel in the β-anomer.

As discussed in Chapter 17, there are four (-2)-quantum $^{13}C_2$ coherences in this four-spin system, denoted $\rho_{\boxed{\alpha--\alpha}}$, $\rho_{\boxed{\alpha--\beta}}$, $\rho_{\boxed{\beta--\alpha}}$ and $\rho_{\boxed{\beta--\beta}}$ (the state labels are arranged as follows: ^{1}H–^{13}C–^{13}C–^{1}H). These coherences may be excited, for example, by using the INADEQUATE pulse sequence (see Section 16.2) and allowed to evolve in the absence of proton decoupling. Two-dimensional spectroscopy may be used to obtain a double-quantum ^{13}C spectrum, which contains four peaks, one for each (-2)-quantum $^{13}C_2$ coherence.

The frequencies of these coherences may be deduced using the arguments given in Section 18.5.3. They are as follows:

$$\Omega_{\boxed{\alpha--\alpha}} = \Omega_2^0 + \Omega_3^0 + \pi J_{12} + \pi J_{13} + \pi J_{24} + \pi J_{34}$$
$$\Omega_{\boxed{\alpha--\beta}} = \Omega_2^0 + \Omega_3^0 + \pi J_{12} + \pi J_{13} - \pi J_{24} - \pi J_{34}$$
$$\Omega_{\boxed{\beta--\alpha}} = \Omega_2^0 + \Omega_3^0 - \pi J_{12} - \pi J_{13} + \pi J_{24} + \pi J_{34}$$
$$\Omega_{\boxed{\beta--\beta}} = \Omega_2^0 + \Omega_3^0 - \pi J_{12} - \pi J_{13} - \pi J_{24} - \pi J_{34}$$

If proton decoupling is not used during the evolution interval, the $^{13}C_2$ double-quantum spectrum has the form of a four-peak multiplet, centred around the sum of the offset frequencies $\Omega_2^0 + \Omega_3^0$.

An experimental example for the β-anomer is shown in Figure 20.61. The different widths of the four peaks are clearly visible. The two central peaks, which are associated with the $\rho_{\boxed{\alpha--\beta}}$ and $\rho_{\boxed{\beta--\alpha}}$ coherences, are narrow, whereas the two outer peaks, which are associated with the coherences $\rho_{\boxed{\alpha--\alpha}}$ and $\rho_{\boxed{\beta--\beta}}$, are broad.

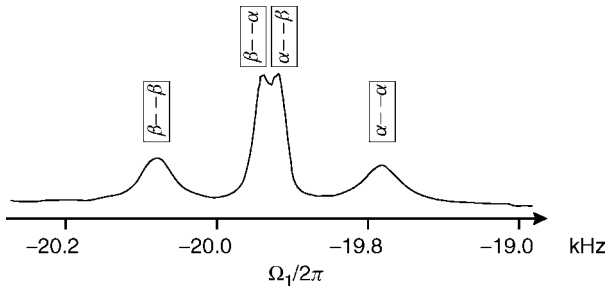

Figure 20.61 Experimental 2Q spectrum of [1,2-$^{13}C_2$]-β-glucose in viscous solution. The plot shows a one-dimensional slice through a two-dimensional 2Q spectrum. Adapted from S. Ravindranathan, X. Feng, T. Karlsson and M. H. Levitt, *J. Am. Chem. Soc.*, **122**, 1102–1115 (2000). (Copyright the American Chemical Society).

These peak width variations are due to the cross-correlation of the two ^{13}C–^{1}H dipolar interactions. The relaxation of the double-quantum $^{13}C_2$ coherences depends primarily on the *sum* of the local fields at the two ^{13}C sites. The sum of the local fields depends on the molecular geometry and also on the proton spin states.

Consider, for example, the coherence $\rho_{\boxed{\alpha--\beta}}$, which generates one of the central peaks in the 2Q multiplet. The local fields in the β-anomer, with the protons in states $|\alpha\rangle$ and $|\beta\rangle$, may be visualized as follows:

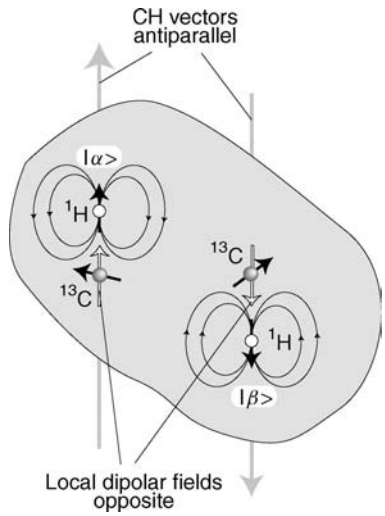

Figure 20.62
Local heteronuclear fields in the case that the two ^{13}C–^{1}H vectors are antiparallel, for opposite proton spin states.

Although each ^{13}C experiences a strong local field from its proton neighbour, the *sum* of the local fields, which is important for 2Q evolution, cancels out in this geometry. This remains true even when the molecule rotates.

The outer peaks, which belong to the $\rho_{\boxed{\alpha--\alpha}}$ and $\rho_{\boxed{\beta--\beta}}$ coherences, are broad because the heteronuclear local fields at the two carbon sites add up constructively, for these proton states, in this molecular geometry:

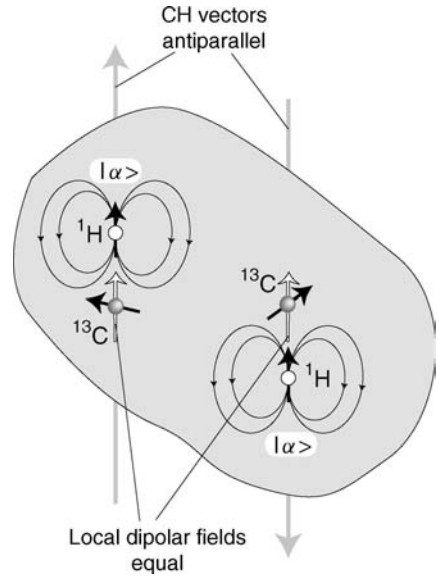

Figure 20.63
Local heteronuclear fields in the case that the two ^{13}C–^{1}H vectors are antiparallel, for equal proton spin states.

An experimental 2Q ^{13}C spectrum for the α-anomer is shown below. The outer peaks are narrower than the inner peaks, which are poorly resolved in this case:

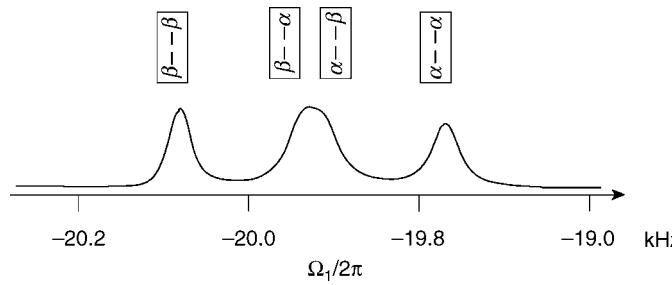

Figure 20.64 Experimental 2Q spectrum of [1,2-$^{13}C_2$]-α-glucose in viscous solution. The plot shows a one-dimensional slice through a two-dimensional 2Q spectrum. Adapted from S. Ravindranathan, X. Feng, T. Karlsson and M. H. Levitt, *J. Am. Chem. Soc.*, **122**, 1102–1115 (2000). (Copyright the American Chemical Society).

This peak width pattern is again easily rationalized by considering the molecular geometry. For the α-anomer, the two ^{13}C–^{1}H vectors are almost perpendicular. The local fields in the α-anomer, with the protons in states $|\alpha\rangle$ and $|\beta\rangle$, are depicted in Figure 20.65. In this case, the local fields at the two carbon sites build up constructively, leading to broad peaks for the coherences $\rho_{\boxed{\alpha--\beta}}$ and $\rho_{\boxed{\beta--\alpha}}$.

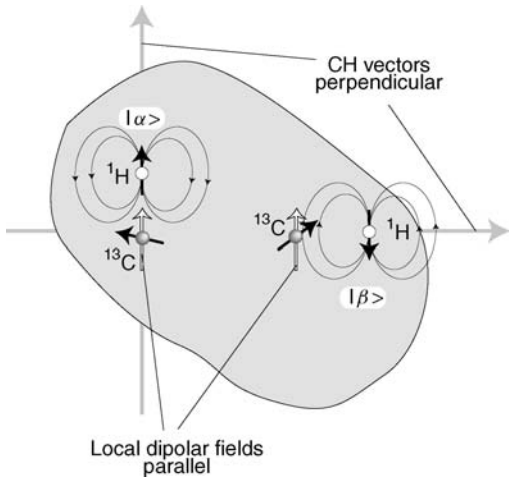

Figure 20.65
Local heteronuclear fields in the case that the two ^{13}C–^{1}H vectors are perpendicular, for opposite proton spin states.

A quantitative study of these linewidth effects allows one to determine the angle $\theta_{CH,CH}$ between the two ^{13}C–^{1}H interactions.

Experiments of this type are exploited in solution NMR for obtaining *angular* information on the molecular structure (see *Further Reading*). A particularly important class of experiments uses cross-correlated relaxation to estimate the angles between ^{13}C–^{1}H and ^{15}N–^{1}H dipole–dipole interactions in labelled proteins, in order to constrain the secondary structure. This complements nicely the *distance* information available from NOESY and ROESY.

20.8.4 TROSY

One of the more remarkable aspects of cross-correlation is found in heteronuclear two-spin systems, e.g. the AX system of a ^{15}N coupled to a neighbouring ^{1}H. Typically, the ^{15}N nuclei are subjected to two sources of local fields, i.e. the magnetic field emanating from the neighbouring proton and the CSA interaction from the induced currents in the surrounding electron clouds. Both of these interactions are generated by sources within the molecule, and are therefore cross-correlated.

If proton decoupling is *not* employed, then the ^{15}N spectrum has two peaks, originating from the $\rho_{\boxed{\alpha-}}$ and $\rho_{\boxed{\beta-}}$ (-1)-quantum ^{15}N coherences. The rotating-frame frequencies of these coherences are

$$\Omega_{\boxed{\alpha-}} = \Omega_S^0 + \pi J_{IS} \qquad \Omega_{\boxed{\beta-}} = \Omega_S^0 - \pi J_{IS}$$

where the ^{15}N spin is denoted S and the ^{1}H spin is denoted I. The relative width of the two single-quantum peaks depends on the cross-correlation between the CSA and the heteronuclear dipole–dipole interaction.

Consider, for example, a ^{15}N–^{1}H moiety in a ^{15}N-labelled protein, such as may be found in the peptide bonds that make up the protein backbone. If the ^{15}N–^{1}H bond in a peptide is along the external magnetic

field, then the induced currents in the electron clouds set up a local magnetic field at the ^{15}N nucleus that is *parallel* to the external field:[10]

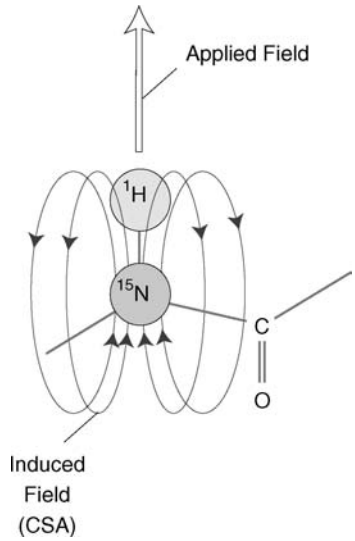

Figure 20.66
Induced field around the ^{15}N site in a ^{15}N-labelled peptide bond, when the NH vector is parallel to the external field.

If the ^{15}N–^{1}H bond is perpendicular to the external magnetic field, then the induced magnetic field at the ^{15}N nucleus tends to *oppose* the external field:

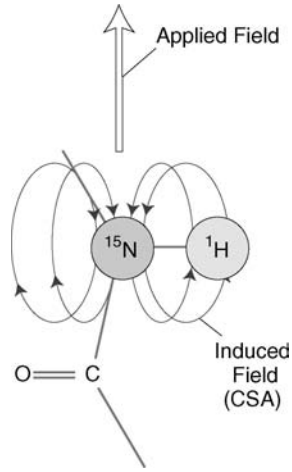

Figure 20.67
Induced field around the ^{15}N site in a ^{15}N-labelled peptide bond, when the NH vector is perpendicular to the external field.

As the molecule rotates, the induced fields at the ^{15}N nucleus are modulated, which leads to relaxation. This is the mechanism of relaxation through CSA.

The induced fields are proportional to the external magnetic field B^0, and the relaxation rate constants are proportional to the square of the local magnetic fields (Equation 20.6). As a result, the CSA relaxation mechanism is proportional to the square of the external magnetic field and becomes competitive with the dipole–dipole relaxation mechanism at the highest commercially-available magnetic field, which is currently around 22.3 T (in 2007).

Now consider what happens if we also take the local field from the ^{1}H into account. If the ^{1}H is in the $|\beta\rangle$ state and the NH vector is parallel to the field, then the local field from the ^{1}H at the site of the ^{15}N nucleus

tends to *oppose* the external field:

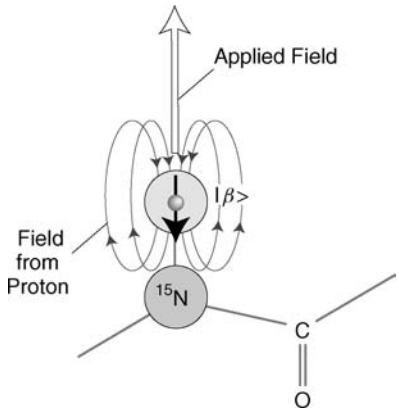

Figure 20.68
Local field generated by the proton in the $|\beta\rangle$ state, when the NH vector is parallel to the external field.

Similarly, if the ^{1}H is in the $|\beta\rangle$ state and the NH vector is perpendicular to the field, then the local field from the ^{1}H at the site of the ^{15}N nucleus tends to be *parallel* to the external field:

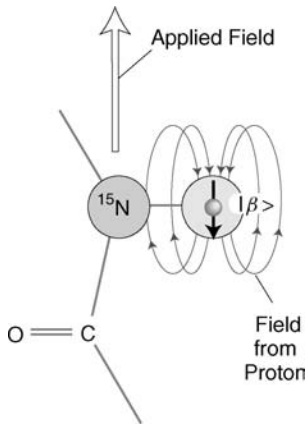

Figure 20.69
Local field generated by the proton in the $|\beta\rangle$ state, when the NH vector is perpendicular to the external field.

To summarize, the local field at the ^{15}N nucleus contains a contribution from the CSA and from the ^{1}H magnetic moment. When the ^{1}H is in the $|\beta\rangle$ state, these two contributions always have opposite sign, whatever the orientation of the molecule. The ^{15}N local field is *reduced* by the interference of the CSA and dipolar interactions, in the case of the $|\beta\rangle$ proton spin state.

Similarly, when the ^{1}H is in the $|\alpha\rangle$ state, these two contributions always have the same sign, whatever the orientation of the molecule. The ^{15}N local field is *increased* by the interference of the CSA and dipolar interactions, in the case of the $|\alpha\rangle$ proton spin state.

As a result, the peak due to the ^{15}N coherence $\rho_{\boxed{\beta-}}$ is *narrowed* by the CSA/dipole–dipole cross-correlation, whereas the peak due to the ^{15}N coherence $\rho_{\boxed{\alpha-}}$ is *broadened* by the CSA/dipole–dipole cross-correlation.

The CSA interaction is proportional to the external field. It is possible, therefore, to adjust the CSA interaction by changing the external field. At a certain value of the field, the CSA and dipole–dipole interactions exactly cancel each other out for the $|\beta\rangle$ proton spin state. The precise value of the optimum field depends on the magnitude and orientation of the chemical shift tensor and may differ from site to site in a biomolecule. For many ^{15}N–^{1}H spin pairs in proteins, the optimal narrowing effects are anticipated to occur in the range 20–25 T, and may now be exploited on the highest currently available magnetic fields.

Significant broadening/narrowing effects are observed even at moderate magnetic fields. The experimental example shown in Figure 20.70 was obtained for a ^{15}N-labelled protein–DNA complex in a field of 17.6 T. Note the assignment of the peaks: the absolute frequency axis for ^{15}N runs from right to left (see Section 3.5), and the one-bond ^{15}N–^{1}H J-coupling is negative, so the peak for $\rho_{\boxed{\alpha-}}$ is to the right of the peak for $\rho_{\boxed{\beta-}}$ (see Section 15.5).

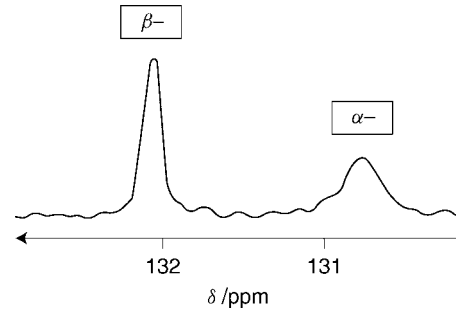

Figure 20.70
^{15}N doublet obtained from one protonated ^{15}N site in a 17 kDa protein–DNA complex without ^{1}H decoupling. Adapted from K. Pervushin, R. Riek, G. Wider and K. Wüthrich, *Proc. Natl. Acad. Sci. USA*, **94**, 12 366–12 371 (1997). Copyright National Academy of Sciences, U.S.A.

The narrowing of one multiplet component by CSA/dipole–dipole cross-correlation is only observed if the spectrum is acquired *without* proton decoupling. If the proton decoupler is turned on, then a single relatively broad peak is observed.

The term TROSY refers to a set of techniques that exploit these differential linewidth effects for enhancing the NMR of large biomolecules (the acronym stands for *Transverse Relaxation Optimized Spectroscopy*).[11] TROSY techniques exploit the following elements: (i) acquisition of the NMR signal without heteronuclear decoupling, in order to resolve the J-coupled multiplets; (ii) careful choice of the external magnetic field so as to achieve optimal line narrowing of some multiplet components through cross-correlation; (iii) careful pulse sequence design so as to make predominant use of the slowly decaying coherences, and to avoid passing the signal through coherences with short lifetimes; (iv) extensive deuteration of the biological molecules so as to reduce all sources of relaxation that are not amenable to cancellation by cross-correlation.

In suitable cases, TROSY allows narrow peaks to be obtained from large macromolecules in solution, under circumstances that would normally give hopelessly broad spectra.[11]

Notes

1. The factor of two in this equation is a consequence of the definition of the Fourier transform in this book, which employs an integral over time from 0 to $+\infty$. In the original relaxation theory, a 'two-sided' Fourier transform was used, in which the integral runs from $-\infty$ to $+\infty$.

2. All the transition probabilities derived in this section are roughly equal to $T_1{}^{-1}$ (give or take some numerical factors). Therefore, it is remarkable that, in the right circumstances, some types of spin order persist for orders of magnitude longer than T_1. See Chapter 14, Note 2.

3. The strict definition of the rotational correlation time τ_c is quite involved. Consider some vector fixed with respect to the molecule. The direction of this vector may be defined using two angles θ and ϕ. As the molecule rotates, the vector rotates with it, so the angles θ and ϕ change. It is possible to calculate some special functions, called *second-rank spherical harmonics*, which depend on θ and ϕ. There are five such functions, which resemble the d-orbitals used in atomic theory, and which are denoted

$Y_{2m}(\theta, \phi)$, where the index m takes values $m = -2, -1, 0, 1, 2$. Since θ and ϕ depend on time, the functions Y_{2m} also depend on time, and it is possible to define autocorrelation functions of the following form:

$$\mathbb{G}_m(\tau) = \left\langle Y_{2m}(0) Y_{2m}(\tau)^* \right\rangle$$

If the molecules tumble isotropically, then all five autocorrelation functions $\mathbb{G}_m$ are the same. In addition, it is usually assumed that the autocorrelation function decays exponentially with respect to τ. The rotational correlation time τ_c is defined as the time constant for this exponential decay.

4. For historical reasons, it is common to employ a Solomon cross-relaxation rate constant denoted σ that is equal to $-R_{\text{cross}}$. I have changed the sign of the cross-relaxation rate constant to bring the definition into line with that used in ordinary kinetics. I suspect that the historical definition of σ, and its curious choice of sign, was flavoured by early NMR experiments on small molecules, for which R_{cross} is negative. Readers who are used to the historical definition may substitute R_{cross} by $-\sigma$ in all expressions.

5. The NOE enhancement factor is often written as $\eta = \epsilon_{\text{NOE}} - 1$, where η is the last term in Equation 20.28. With this definition, $\eta = 0$ indicates no enhancement of the signal, and $\eta = 1$ indicates a doubling of the signal when the dipolar-coupled spin species is saturated.

6. Strictly speaking, the NOE refers to the steady-state enhancement of one spin species when the populations of a second spin species are saturated by a resonant r.f. field (Section 20.5). This is not obviously related to the NOESY experiment, which does not employ saturation. The name arose historically through the so-called *transient NOE* experiment, which was a precursor of NOESY. In this experiment, the populations of the spin states are perturbed by r.f. pulse sequences, and the cross-relaxation followed as a function of time.

7. The NOESY phase cycle specified in Table 19.1 includes a π phase shift for the second pulse and leads to consistently positive diagonal peaks. The cross-peaks are positive for NOESY experiments on slowly tumbling molecules ($R_{\text{cross}} > 0$), and negative for NOESY experiments on rapidly tumbling molecules ($R_{\text{cross}} < 0$). One should be aware that many standard NOESY pulse sequences do not include the π phase shift on the second pulse, and give rise to spectra in which *both* diagonal- and cross-peaks have an inverted sign.

8. For a justification of this, see R. R. Ernst, G. Bodenhausen and A. Wokaun, "*Principles of Nuclear Magnetic Resonance in One and Two Dimensions*", Clarendon Press, Oxford, 1987, p. 287–288.

9. It has become customary to name any experiment that employs an extended period of r.f. irradiation a 'rotating-frame experiment'. This is a curious and misleading practice, since essentially all NMR experiments are easiest to analyse in the rotating reference frame. The original name for the ROESY experiment is CAMELSPIN (which stands for Cross-Relaxation Appropriate for Minimolecules Emulated by Locked Spins), but this title is rarely used now.

10. The discussion of dipole–dipole CSA cross-correlation in a ^{15}N–^{1}H spin pair assumes a uniaxial ^{15}N CSA tensor with $\delta^j_{zz} < \delta^{\text{iso}}_j$, i.e. a negative CSA in deshielding units, and zero biaxiality. Experimentally determined ^{15}N CSA tensors in peptide bonds have approximately uniaxial CSA tensors with the sign and orientation assumed here.

11. K. Pervushin, R. Riek, G. Wider, and K. Wüthrich *Proc. Natl. Acad. Sci. USA*, **94**, 12 366–12 371 (1997) ; K. Wüthrich *Nature Struct. Biol.*, **5**, 492 (1998).

Further Reading

- The classic paper on relaxation in liquids is N. Bloembergen, E. M. Purcell and R. V. Pound, *Phys. Rev.* **73**, 679–712 (1948). It is still a fresh source of physical insights.
- For a thorough review of relaxation in liquids, including key results for many different mechanisms, see J. Kowalewski and L. Mäler, '*Nuclear Spin Relaxation in Liquids: Theory, Experiments and Applications*.' CRC Press, Boca Raton, Florida, 2006.
- For the formal relaxation theory, see A. Abragam, "The Principles of Nuclear Magnetism", Clarendon Press, Oxford, 1961; C. P. Slichter, "Principles of Magnetic Resonance", 3rd Edition Springer, Berlin, 1989 and R. R. Ernst, G. Bodenhausen, and A. Wokaun, "Principles of Nuclear Magnetic Resonance in One and Two Dimensions", Clarendon Press, Oxford, 1987.
- For a summary of theoretical relaxation time constants in liquids, treating a variety of motional models, see J. McConnell, "The Theory of NMR Spin Relaxation in Liquids", Cambridge University Press, Cambridge, 1987.
- For the application of NOESY to biomolecular structure determination, see K. Wüthrich, "NMR of Proteins and Nucleic Acids", Wiley, New York, 1986, and J. Cavanagh, W. J. Fairbrother, A. G. Palmer and N. J. Skelton, "Protein NMR Spectroscopy. Principles and Practice", Academic Press New York, 1996.
- For more detail on ROESY, see the articles in the "Encyclopedia of Nuclear Magnetic Resonance", Wiley, 1996, by A. Bax and S. Grzesiek, (vol. 7, p. 4157) and J. Sleucher, J. Quant, S. J. Glaser and C. Griesinger (vol. 6, p. 4789).
- For the applications of cross-correlated relaxation to biomolecules, see B. Reif, M. Hennig and C. Griesinger, *Science*, **276**, 1230 (1997), and B. Brutscher *Concepts Magn. Reson.*, **12**, 207–228 (2000).
- For parallels between cross-correlated double-quantum experiments in solids and liquids, see S. Ravindranathan, X. Feng, G. Widmalm, and M. H. Levitt, *J. Am. Chem. Soc.*, **122**, 1102–1115 (2000).
- For a comprehensive review of cross-correlation effects, see Anil Kumar, R. Christy Rani Grace and P. K. Madhu, *Prog. NMR Spectrosc.*, **37**, 191–319 (2000).

Exercises

20.1 Consider a molecule with rotational correlation time $\tau_c = 0.3\,\text{ns}$, containing a pair of protons separated by 2 nm. Assume that the relaxation is caused exclusively by intramolecular dipole–dipole couplings.
(i) Plot the relaxation time constants T_1 and T_2 against field B^0, in the range $B^0 = 0$ to $B^0 = 20\,\text{T}$. Comment on the form of the plots.
(ii) Plot the NOESY cross-relaxation rate constant R_{cross} and the ROESY cross-relaxation rate constant R^T_{cross} against the static field B^0, in the range $B^0 = 0$ to $B^0 = 20\,\text{T}$. Is NOESY or ROESY expected to be better at high magnetic field?